WAGENINGEN UNIVERSITY

METEOROLOGY AND AIR QUALITY GROUP

MSC THESIS

Oxygen as a tracer for fossil fuel CO_2 emission sources

Author:
Bernice KUIJPERS

Supervisors:
Prof. Dr. Wouter PETERS
Dr. Ingrid van der LAAN-LUIJKX

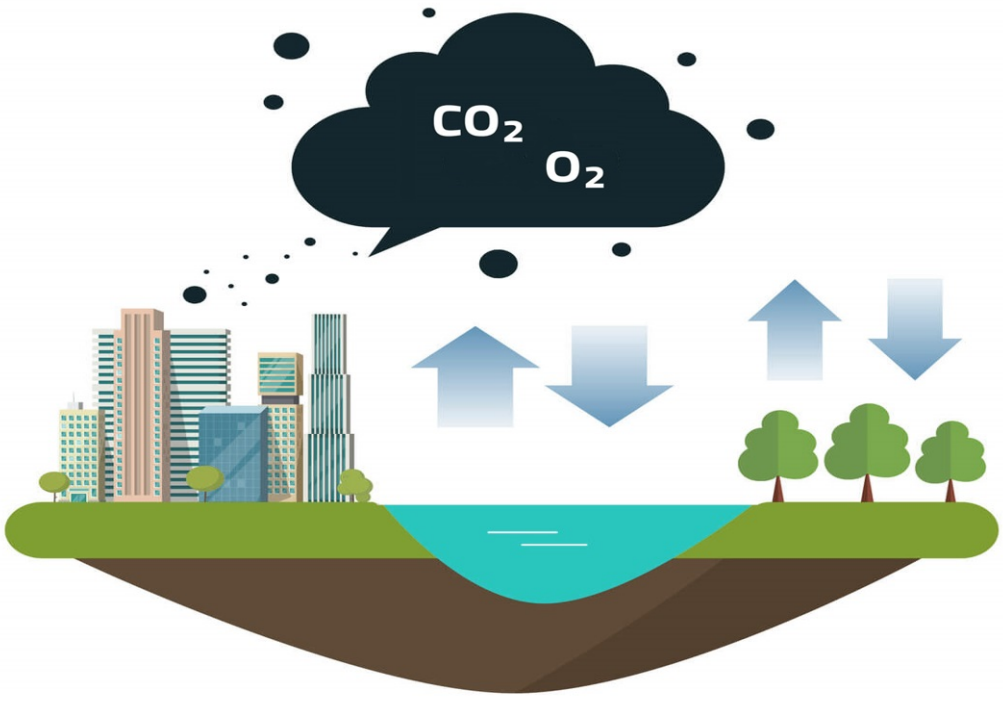

March 15, 2018

Abstract

The combustion processes involved in fossil fuel burning lead to emittance of carbon dioxide and consumption of oxygen. The fact that every fuel type has a specific oxidative ratio, makes oxygen a potential tracer for fossil fuel carbon dioxide. Fluctuations in atmospheric oxygen concentration are modelled using WRF-chem. In order to do so, an average oxidative ratio is calculated per emission category for the Netherlands. To complete the modelling of oxygen, biosphere and ocean exchanges are included. The model outcomes are validated using measurements from Weybourne (UK) and Lutjewad (NL) of October 2014. Even though Weybourne is situated outside the Netherlands, the model reached an index of agreement of 0.75 for that location. Most discrepancies in the simulation of the compound concentrations are found to be due to errors in the meteorological circumstances and wind direction.

Furthermore, study area Rijnmond (NL) is analysed in more detail. The information about the usage of distinct fuel types of various point sources in Rijnmond allowed for a more veracious modelling of oxygen in that area, using the (known) oxidative ratios of point sources within the domain. This results in lower oxidative ratios and higher oxygen concentrations as compared to the simulation done with the average oxidative ratio of the Netherlands. Unfortunately, results at Rijnmond cannot yet be validated due to the absence of oxygen measurements in the area. A measurement campaign as part of the RINGO project (ICOS n.d.) is however planned to start in the near future, which will allow for more insight in the potential of modelling oxygen as a tracer for fossil fuel carbon dioxide in urban areas.

Preface

The report presented here is the result of the work I did for my Master thesis at the Meteorology and Air Quality group at Wageningen University. During my study, my interest in climate and atmospheric composition grew as I learned more about atmospheric science. Whilst looking for a subject for my Master thesis, Wouter Peters introduced me to Ingrid van der Laan-Luijkx, who sparked my interest for atmospheric oxygen leading me to write the following thesis.

I would like to thank both my supervisors for their support and guidance. I want to express my gratitude to Ingrid van der Laan-Luijkx for her day-to-day supervision and the content related discussions I had with her, which really contributed to my learning process. The calm manner in which Ingrid interacts made me feel comfortable and she really contributed to my confidence during my research. Furthermore, I'd like to thank Wouter Peters for his weekly supervision, overall keeping track of my progress, and intermediate feedback. I appreciate being invited to join the RINGO meeting at Groningen University, involving me in the project and increasing my insight in the relevance of my research. Together, my supervisors created an environment in which I was able to develop myself.

I would also like to thank Ingrid Super, for the WRF-chem model setup and the scripts she provided at the start of my research. Furthermore, Michiel van der Molen as well as Kees van den Dries spent considerable time and effort in helping me with my first model runs, which I very much appreciate.

Valuable data in the form of APO fields and the COFFEE dataset were made available by Christian Rödenbeck and Christoph Gerbig, respectively, which greatly contributed to the analysis done in this research. Furthermore, oxygen measurements at Lutjewad were made available by Charlotte van Leeuwen, Elise Broekema, and Harro Meijer, and measurements at Weybourne by Thomas Barningham, Penelope Pickers, and Andrew Manning. Both datasets were crucial in validating the created model.

Finally, I would like to express my gratitude to my friends and fellow students at the Meteorology and Air Quality department, for their scientific and mental support and at times much needed supply of chocolate. Largely because of you, I will look back on my time working on my thesis with much joy and laughter. Thank you.

Contents

List of Figures

List of Tables

1 Introduction

There is a general agreement in the scientific community that humans have a major influence on the recent changes recorded in the climate (Cook et al. 2013). Questions that arise from this are mainly related to how the climate will change in the future and what can and should be done about it. An important contributor to anthropogenic climate change is the emission of greenhouse gases, such as carbon dioxide (CO_2) and methane (CH_4). Emission of these greenhouse gases cause global temperatures to rise, which is expected have adverse effects for humans as well as many other species on Earth (IPCC - Intergovernmental Panel on Climate Change 2013). In order to successfully reduce and verify anthropogenic greenhouse gas emissions, it is important to know what causes increases and decreases in these emissions. For instance, how would emissions change during a cold winter, if house-hold electricity and gas are more smartly managed, or if electric cars instead of petrol cars are driven? To answer these kind of questions, high resolution temporal and spatial information is needed (Pickers 2016). Especially urban areas are important in this, since about 70% of all anthropogenic CO_2 emissions originate from cities (Nicole 2010). Monitoring as well as modelling of urban and regional concentrations of CO_2 and co-emitted species has therefore received a lot of attention (Huszar, Belda, and Halenka 2016; Lopez et al. 2013; Q. J. Zhang et al. 2015). $^{14}CO_2$ can be used as a tracer to separate fossil fuel CO_2 and CO_2 from the biosphere, as CO_2 emitted from fossil fuels does not contain $^{14}CO_2$. Furthermore, ^{13}C:^{12}C ratios in combination with ^{14}C concentrations can be used to separate various fossil fuel sources (Djuricin, Pataki, and Xu 2010; Zondervan and Meijer 1996). Carbon monoxide (CO) can also be used as a tracer to quantify fossil fuel CO_2, due to the co-emittance of CO as fossil fuels are combusted (Lopez et al. 2013). The CO_2 co-emitted species often have a distinct emission ratio for specific source types (Djuricin, Pataki, and Xu 2010; Lopez et al. 2013). The emission ratios thus provide information about the dominant emission sources. Eulerian as well as Gaussian models (and a combination these methods) are being developed as to use emission ratios to provide insight in emission sources (Super et al. 2017). A relatively novel tracer for fossil fuel CO_2 sources is oxygen (O_2). Introducing O_2 as a tracer for fossil fuel CO_2 can potentially contribute to the information these models generate about the emission sources for fossil fuel CO_2. The general aim of this research is to study and

improve the knowledge about the importance of various fossil fuel types in urban areas. This will be attempted by implementing atmospheric O_2 as a tracer in an emission model, validating the model using measurements, and finally studying the modelled results. Before going into more detail about the research objectives in Section 1.3, relevant theory concerning atmospheric O_2 will be discussed and information about the research area and used model will be provided in Section 1.1 and Section 1.2.

1.1 Background theory

1.1.1 Carbon reservoirs

On relatively short (i.e. non-geological) timescales, the global carbon cycle consists of four main carbon reservoirs: the atmosphere, oceans, terrestrial biosphere (including soils), and fossil fuels (Figure 1). In the past 50 years, there has been a significant transfer of carbon from fossil fuels to the atmosphere by human activities. About 44% of the released carbon stays in the atmosphere, as the remaining carbon is taken up by the oceans or the terrestrial biosphere (Figure 2) (Le Quéré et al. 2016).

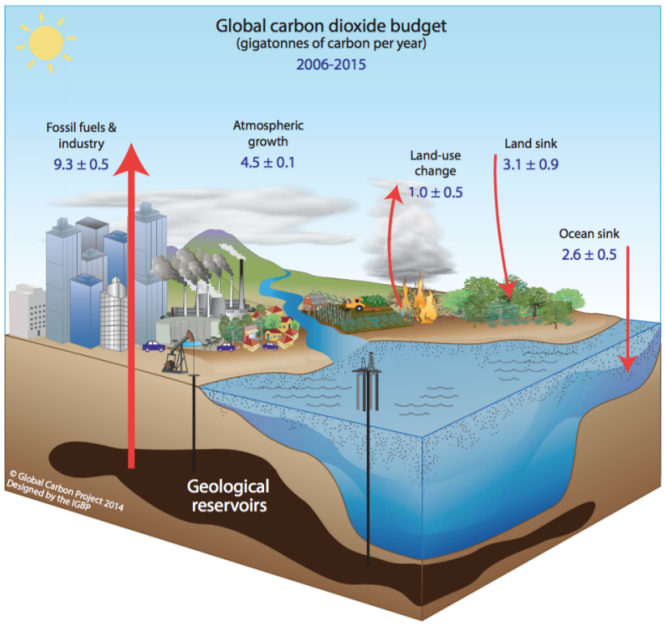

Figure 1: Overview of the global carbon dioxide budget. The carbon reservoirs are shown along with their contribution to the atmospheric carbon in gigatonnes of carbon per year (Le Quéré et al. 2016).

CO_2 interacts with the terrestrial biosphere mainly through photosynthesis and respiration.

As plants photosynthesise, CO_2 is taken up and O_2 is released into the atmosphere. Fossil fuel combustion releases CO_2 into the atmosphere while using O_2 from the atmosphere. The atmospheric O_2 and CO_2 are thus anti-correlated to each other due to photosynthesis and respiration by the terrestrial biosphere and fossil fuel combustion (Figure 3). As opposed to the terrestrial sink and fossil fuel source, however, carbon uptake by the oceans does not directly influence atmospheric O_2 concentrations. Atmospheric carbon is taken up through the solubility of CO_2. This process is known as the solubility pump. The dissolved carbon is taken up by marine organisms which – when they die – sink and transport the carbon to the deeper oceans. This process is known as the biological pump. Due to these processes, along with the physical mixing of the oceans and the change in ocean pH acting as a buffer, the oceans are expected to take up about 26% of the carbon released into the atmosphere (Le Quéré et al., 2016). The main O_2 flux from the oceans results from outgassing, mainly influenced by changes in the oceans heat budget (Randerson et al. 2006).

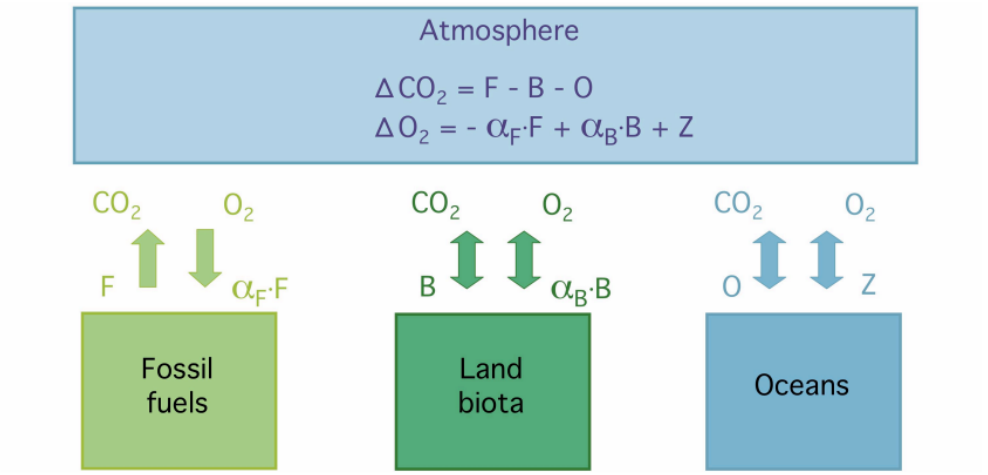

Figure 2: Most important carbon reservoirs and fluxes influencing the atmospheric CO_2 and O_2 concentrations. The changes in atmospheric O_2 and CO_2 are shown in the 'Atmosphere' box. In these formulas F is the CO_2 emission from fossil fuel combustion, B is the net land biosphere sink, O is the net ocean CO_2 sink, and Z is the net air-sea O_2 flux. α_F and α_B are the oxidative ratios for fossil fuel combustion and net biosphere exchange, respectively (I. Van Der Laan-Luijkx 2010).

1.1.2 Oxidative ratios

Because of the processes underlying the anti-correlation described in Section 1.1.1, high precision atmospheric O_2 measurements along with atmospheric CO_2 measurements can be used

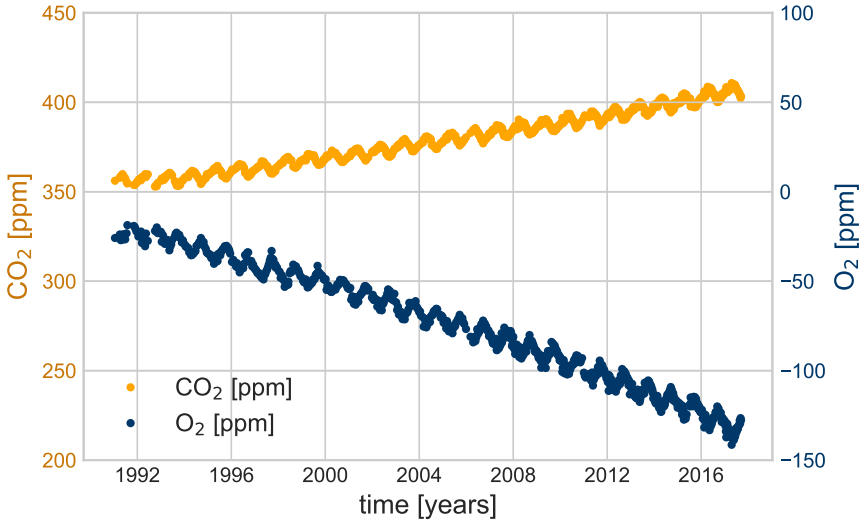

Figure 3: Time series of CO_2 and O_2 measurements conducted at Mauna Loa, Hawaii. Measurements over multiple years show the anticorrelation between atmospheric CO_2 and O_2.

to separate out oceanic and terrestrial carbon fluxes (R. F. Keeling and Shertz 1992). The terrestrial carbon fluxes can be further distinguished by their differences in oxidative ratios. Terrestrial photosynthesis and respiration occurs through the following process (Seibt et al. 2004):

$$CO_2 + H_2O \leftrightarrow CH_2O + O_2. \tag{1}$$

In this process, on average 1.1 moles of O_2 are consumed per mole of CO_2 emitted and vise versa. The average oxidative ratio of the terrestrial biosphere is thus α_B = 1.1 (Severinghaus 1995). This oxidative ratio can vary over spatial and temporal scales, largely dependent on the elements involved in the oxidation process.

For fossil fuel combustion, the oxidative process is described as (R. F. Keeling and A. C. Manning 2014):

$$C_xH_y + (x + \frac{y}{4})O_2 \rightarrow xCO_2 + \frac{y}{2}H_2O. \tag{2}$$

The oxidative ratios for fossil fuel combustion can be distinguished for the three main types of fossil fuel: solids (e.g. coal), liquids (e.g. oil), and gases (e.g. natural gas). The average ratios for these types of fossil fuel are α_F = 1.17, 1.44, and 1.95, respectively (R. F. Keeling 1988). Cement production is also an anthropogenic source of atmospheric CO_2. The processes involved in cement production, however, do not consume oxygen. The oxidative ratio of cement

production is therefore 0. A global average value for the oxidative ratio of fossil fuel combustion of α_F = 1.4 is mainly used (R. F. Keeling 1988). However, due to the differences in the fossil fuel sources used in different countries and over the seasons, this value can vary in space and time.

1.1.3 Expressing atmospheric oxygen

As described above, the atmospheric O_2 concentration is affected by exchange with components in the carbon cycle. Changes in atmospheric O_2 are often expressed as changes in the ratio O_2/N_2 in per meg. This is because the changes in atmospheric oxygen are relatively small compared to its total mole fraction, i.e. 0.20946 (R. F. Keeling, A. C. Manning, et al. 1998). Atmospheric nitrogen (N_2) is much less variable, which means that the O_2/N_2 ratio mainly represents the O_2 concentration and is less sensitive to changes in other atmospheric gases (R. F. Keeling and Shertz 1992). A change of 1 ppm O_2 without changes in other gases causes a change of δ(O_2/N_2) = 6.04 per meg, where an exchange of O_2 for an equal amount of CO_2 causes a change of δ(O_2/N_2) = 4.77 per meg. Changes in O_2/N_2 ratio are expressed as:

$$\delta(O_2/N_2) = \frac{(O_2/N_2)_{\text{sample}}}{(O_2/N_2)_{\text{reference}} - (O_2/N_2)_{\text{reference}}}. \tag{3}$$

To separate the oceanic component from the measured O_2 levels, a tracer called Atmospheric Potential Oxygen (APO) is used. APO is defined as the O_2/N_2 ratio if all methane (CH_4) and carbon monoxide (CO) were oxidised to CO_2 and converted to O_2 through photosynthesis. This means that variations can be caused only by oceanic CO_2 uptake and partly by fossil fuel emissions. Biological processes are thus excluded. APO can be expressed as (Stephens et al. 1998):

$$APO = \delta\frac{O_2}{N_2} - \frac{\alpha_B}{X_{O_2}}CO_2 - \frac{0.9}{X_{O_2}}CH_4 + \frac{0.6}{X_{O_2}}CO, \tag{4}$$

in which X_i is the mole fraction of the molecule i (e.g. 0.20946 for O_2). To model changes in APO due to changes in O_2, N_2, or CO_2, equation 4 can be written as (Stephens et al. 1998):

$$\Delta APO = \frac{\frac{1.0}{X_{O_2}}\Delta O_2 - \frac{1.0}{X_{N_2}}\Delta N_2 + \frac{1.1}{X_{O_2}}\Delta CO_2}{M}, \tag{5}$$

in which M is the total number of moles. Equations 4 and 5 include the influence of CH_4

and CO on APO. If these species are not taken into account, equation 5 can be combined with the global carbon and oxygen budget equations as shown in Figure 2. This results in a global APO budget (Andrew C. Manning and Ralph F. Keeling 2006):

$$\Delta APO = (\alpha_F - \alpha_B)F + \alpha_B O + Z, \tag{6}$$

where F is the atmospheric CO_2 from fossil fuels, O is the atmospheric CO_2 sink due to the ocean, and Z is the net O_2 air-sea exchange (A. C. Manning and R. F. Keeling 2006). If F and Z are known (or can be estimated), the land and ocean carbon sinks can be calculated. A graphical representation of this is shown in Figure 4 (R. F. Keeling and A. C. Manning 2014). Figure 4 also shows the increase in atmospheric CO_2 due to fossil fuel combustion, and the mitigation of these concentrations due to ocean and land uptake.

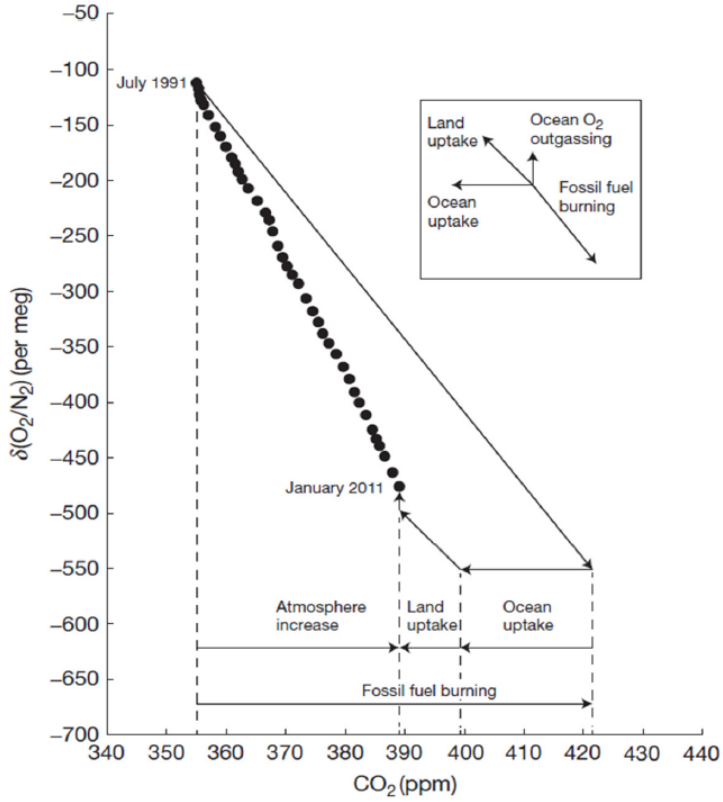

Figure 4: Increase in atmospheric CO_2 and decrease in $\delta(O_2/N_2)$ due to fossil fuel combustion, along with the mitigating effects of uptake by the land and ocean components. The dots represent 6 - monthly averages of $\delta(O_2/N_2)$ and CO_2 from Alert, Canada, La Jolla, California, USA, and Cape Grim, Tasmania, Australia (R. F. Keeling and A. C. Manning 2014).

As mentioned above, APO still includes influence of some fossil fuel combustion. There-

fore, a modified version APO* is suggested, which is only sensitive to air-sea exchange (Sirignano et al. 2010):

$$\Delta APO^* = \Delta APO - (\alpha_F - \alpha_B)F. \tag{7}$$

Because the oxidative ratio for fossil fuel combustion (α_F) varies in space (depending on what kind of fossil fuel is used), I. T. Van Der Laan-Luijkx et al. (2010) performed a modelling study to estimate regional oxidative ratios. The REgional MOdel (REMO) (Chevillard et al. 2002) is an atmospheric transport model which uses hourly CO_2 and O_2 fluxes from the CO_2 release and Oxygen uptake from Fossil Fuel Emissions Estimate (COFFEE) dataset as input (Steinbach et al. 2011). COFFEE combines CO_2 emissions from the Emission Database for Global Atmospheric research (EDGAR) (Olivier and Berdowski 2001) and fossil fuel type specific oxidative ratios from the EN energy statistics (http://www.data.un.org) to model the distribution of the oxidative ratios from fossil fuel combustion.

1.2 Research area and WRF-Chem

The aim of this research is to find the CO_2 emission sources in urban areas by incorporating O_2 as a tracer for urban fossil fuel emissions. To achieve this, the model setup by Super et al. (2017) will be used as a starting point. This setup models CO_2 mole fractions in the Rijnmond area. This area will therefore also be used as the study area in this research. The Rijnmond area is shown in Figure 5. It includes Rotterdam as the major urban area, a large harbour, and an industrial area. To model the mole fractions and oxidative ratios in the study area, the Eulerian model Weather Research and Forecasting (WRF-Chem) V3.2.1 is used (Skamarock et al. 2008). Four domains are defined which have a horizontal resolution of 48x48, 12x12, 4x4, and 1x1 km respectively. Domain 1 covers the largest part of Europe, domain 2 covers the Netherlands, Belgium, Luxembourg, Germany, and part of the UK, domain 3 zooms into the Netherlands, and domain 4 shows the Rijnmond area in more detail (Figure 7).

O_2 measurement campaigns at Rijnmond were planned to start in December 2017. In the end this was not realised, though measurements are planned to start in the near future. Due to the uncertainty in availability of the data, study areas containing Weybourne and Lutjewad were studied as a backup. O_2 measurements have been conducted at Weybourne and Lutjewad for

several years. O_2 data from these stations are thus useful to validate the model. Weybourne is located in North Norfolk on the east coast of the United Kingdom, in model domain 2. Lutjewad is located on the north coast of the Netherlands, in model domain 3. More information about the study areas are given in Section 2.1.

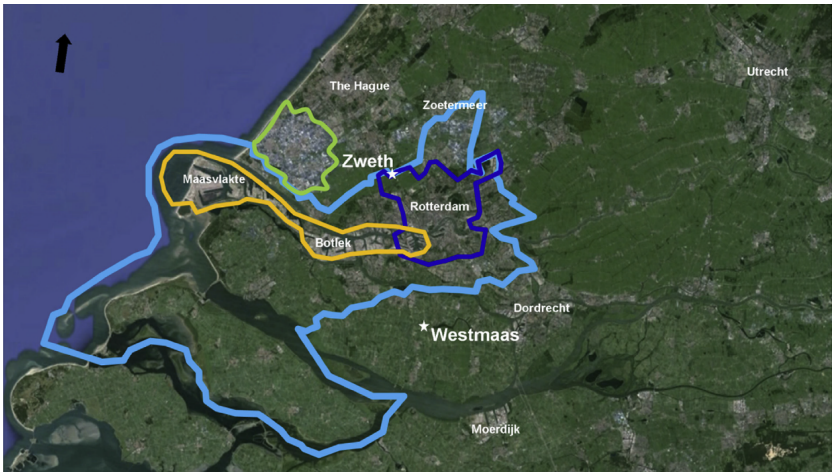

Figure 5: Map of the Rijnmond area (light blue) including the city of Rotterdam (dark blue), the harbour area (yellow), and the glasshouse agricultural sector (green). The prevailing wind direction during October 2014 is indicated by the black arrow (Super et al. 2016).

1.3 Research justification and research objectives

In the past, research has been done on continuously measuring atmospheric O_2 and CO_2 concentrations in order to partition CO_2 emissions from the terrestrial biosphere and oceans, and quantify fossil fuel CO_2 emissions. O_2 measurements can be useful in characterising and monitoring the fossil fuel mix in urban areas based on the different oxidative ratios (R. F. Keeling and A. C. Manning 2014). A combination of atmospheric O_2 measurements and modelling could improve the quantification of CO_2 emissions in cities. O_2 has however not yet been integrated in regional fossil fuel emission models and can be considered an under-exploited tool for quantifying fossil fuel CO_2 emissions in urban areas.

The aim of this research is therefore to incorporate O_2 as a tracer in an atmospheric model to study the importance of the various fossil fuel types within the study area. As a starting point for this research, the urban area Rijnmond will be used. The three main objectives of this research are:

1. Implementing O_2 as a tracer for fossil fuel CO_2 in WRF-Chem.
2. Validating the model outcomes by comparing them with O_2 concentration measurements from the study areas.
3. Using the developed model to investigate the fossil fuel sources of atmospheric CO_2 in Rijnmond.

From these main objectives, the following research questions are defined:

- How do the modelled O_2 concentrations compare to the measured concentrations at the Weybourne and Lutjewad?
- Following from the oxidative ratios found in WRF-Chem, what are the fossil fuel sources of atmospheric CO_2 in Rijnmond, the north of Groningen, and North Norfolk?

O_2 concentrations are modelled using WRF-chem. The methods used to implement O_2 in the model are described in Chapter 2. This chapter therefore mainly deals with the first research objective. In Chapter 2, the approach to calculating oxidative ratios for further analysis is also specified. Chapter 3 gives insight in the model's performance in simulating the wind direction for the chosen case study. In Chapter 4, the importance of the three main sources and sinks (i.e. the ocean, the biosphere, and fossil fuels) in atmospheric O_2 concentration is elaborated on for the three study areas (Rijnmond, the north of Groningen, and North Norfolk). In chapter 4, the second research objective is also addressed by validating the modelled O_2 concentrations using measurements conducted at Lutjewad and Weybourne. Chapters 5 and 6 will focus on oxygen fluctuations due to fossil fuel burning in order to achieve the third research objective. In Chapter 5 the modelled fossil fuel CO_2, fossil fuel O_2, and the fossil fuel oxidative ratios that follow from this are analysed. Furthermore, specific events where high CO_2 concentrations were simulated are analysed in order to find the emission sources responsible. Finally, in Chapter 6, the results of a second strategy in modelling fossil fuel O_2 in Rijnmond are analysed and compared to earlier results, which may in the future be validated using measurements conducted at Zweth.

2 Methods

2.1 Case study

The main study area, Rijnmond (Figure 5), is located in a flat terrain near the west coast of the Netherlands. It includes one of the most industrialized parts of the country, containing an industrial area (Botlek) and one of the largest harbours in the world (Europoort). The area is highly urbanised with more than 1.4 million inhabitants (CBS, 2017) over 807.5 km^2. The bottom-up estimated emissions in Rijnmond are about 35 Mt CO_2 per year (PRTR 2015), where the harbour is identified as the largest CO_2 emitter. The main sources of CO_2 are energy production and industrial processes. These are often point sources, which result in 80% of the total CO_2 emissions (Super et al. 2017). At first instance, the month of October 2014 will be studied, which - according to Super et al. (2017) - is a month with various moments of high CO_2 concentrations. The wind direction (Chapter 3), and various CO_2 emission sources (Chapter 5) will be analysed for the month of October 2014. The emission sources are linked to oxygen uptake. The implementation of this will be described in more detail in Section 2.3.

As mentioned in Section 1.2, regions North Norfolk and the north of Groningen can be used as extra study areas, because of the availability of O_2 observations during the month of October 2014 at Weybourne and Lutjewad - as opposed to Zweth, of which O_2 data is not yet available. Groningen is located in the north of the Netherlands. Measurement site Lutjewad is located on the coast (shown in Figures 6a and 7), in a more rural area than Rijnmond. The municipality in which the measurement site is located contains about 10 thousand inhabitants over 240 km^2 (CBS 2017). Carbon emissions in the direct surroundings of Lutjewad are limited, with about 0.5 Mt CO_2 per year in the surrounding area about the same size as North Norfolk and Rijnmond (RIVM 2016). Potential emission sources that can influence concentrations at Lutjewad are the city of Groningen and the city of Leeuwarden. Groningen city is located about 40 km southeast of the measurement site, and Leeuwarden is located about 45 km southwest.

North Norfolk is located at the east coast of the UK. The measurement site at Weybourne is situated about 40 km north of the city of Norwich (as showin in Figure 6b). The area is less urbanized compared to Rijnmond, with only about 104 thousand inhabitants (ONS 2016) over 962.5 km^2. Carbon emissions are around 0.7 Mt CO_2 per year (BEIS 2015). There are three gas

production plants in the area, located about 20 km east of Weybourne, which are responsible for about 35% of all CO_2 emissions in the area.

Figure 6: Maps showing a) study area the north of Groningen containing measurement site Lutjewad, and b) study area North Norfolk containing measurement site Weybourne.

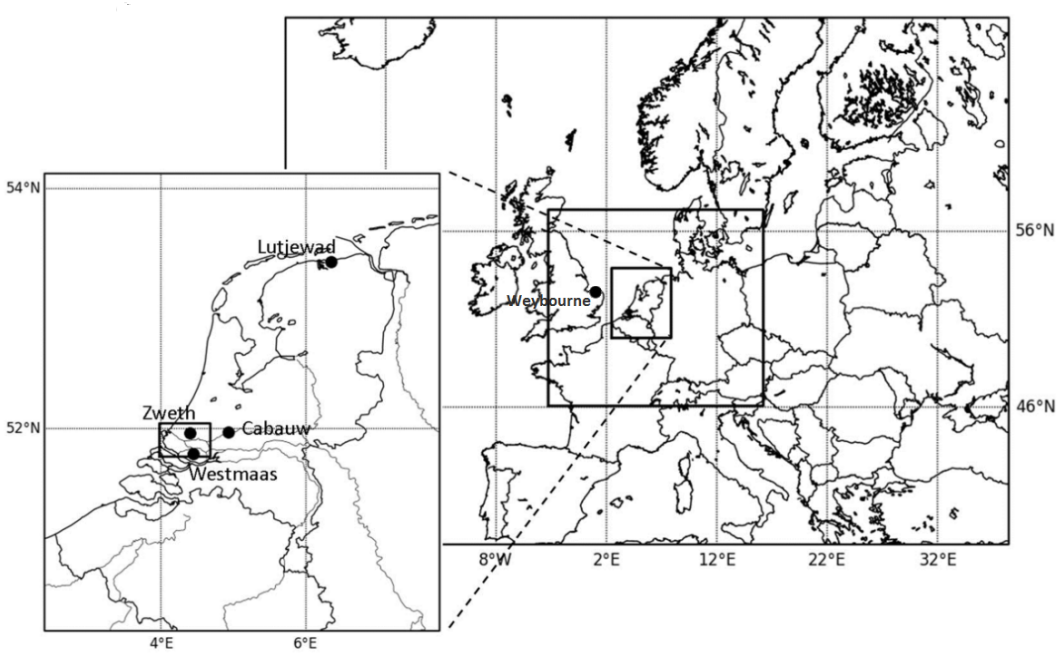

Figure 7: Locations of the domains with horizontal resolutions of 48x48, 12x12, 4x4, and 1x1 km, respectively.

2.2 Modelling framework and settings

As mentioned in Section 1.2, WRF-Chem V3.2.1 is used to simulate CO_2 and O_2 concentrations in the study areas. As initial and boundary conditions in WRF-Chem, meteorological fields from

the National Centers for Environmental Prediction (NCEP) Final (FNL) Operational Global Analysis (National Centers for Environmental Prediction/National Weather Service/NOAA/U.S 2000) are used. These initial and boundary conditions have a horizontal resolution of 1x1° and a temporal resolution of 6 hours. CO_2 initial and boundary conditions are taken from the 3D mole fractions of CarbonTracker Europe (Van Der Laan-Luijkx et al. 2017). These have a horizontal resolution of 1x1° and have 25 vertical levels, and are therefore both horizontally and vertically interpolated onto the WRF-Chem grid.

Four domains are defined as shown in Figure 7. The outer domain is situated over Europe, domain 2 is zoomed into the Netherlands and contains the study area North Norfolk. Domain 3 covers only the Netherlands, and domain 4 is zoomed into the Rijnmond area. These domains have a horizontal resolution of 48x48, 12x12, 4x4 and 1x1 km respectively, and a vertical resolution of 29 eta levels. The lowest model layer is 40 m deep, and the lowest 1 km is divided in 8 levels. The Yonsei University boundary layer scheme (Hong, Noh, and Dudhia 2006) is used as this scheme has proven to be most reliable over the Netherlands (Bozhinova et al. 2014; Daniels et al. 2016; Steeneveld, Ronda, and Holtslag 2014). Furthermore, the Dudhia scheme is used as shortwave radiation scheme (Dudhia 1989), the Rapid Radiation Transfer Model (RRTM) is used as longwave radiation scheme (Mlawer et al. 1997), and the Unified Noah Land-Surface Model is used as surface physics scheme (Ek 2003). An overview of the model settings and schemes used is given in Table A1 in the Appendix.

2.3 Modelling strategy

In order to achieve the first research objective, and model O_2 concentrations in WRF-chem, a few steps are taken to add to the current model setup. These steps are described in Sections 2.3.1 to 2.3.3; the modelling of CO_2 sources and sinks, the implementation of O_2 uptake and release due to these CO_2 sources and sinks, and the implementation of O_2 ocean exchange.

2.3.1 Modelling CO_2 emissions, photosynthesis, and respiration

To model emissions in WRF-chem, several emission databases are used. The TNO-MACC III inventory for 2011 provides fossil fuel and biofuel emissions at a horizontal resolution of

0.123x0.0625°, which are used for the simulations in domain 1 to 3. The emissions for domain 4 are taken from the Dutch Emission Registration, and compiled by the Netherlands Organisation for Applied Scientific Research (TNO) to a 1x1 km resolution emission map. Area sources are added to the lowest surface level, whereas point sources are given a vertical distribution based on plume rise calculations by Bieser et al. (2011). The emissions are categorized using the Standardized Nomenclature for Air Pollutants (SNAP) classification. SNAP distinguishes 10 emission categories (shown in Table 1), which are classified according to the power developed by the combustion processes (mostly categories 01, 02, and 03), the technical characteristics of the process (categories 04 and 05), or the condition of use of the fuel types (mainly the mobile sources, categories 07 and 08) (EUROSTAT 2005). In the model setup by Super et al. (2017), categories 03 and 04, and categories 05, 06, and 09 are combined, since they would separately be too small to distinguish.

Table 1: CO_2 emission categories along with the description of the SNAP classifications. Estimations of the average oxidative ratios for the Netherlands are given for every category.

CO_2 emission category (SNAP and biogenic)	Description	$OR_{O_2:CO_2}$
01	Combustion in energy and transformation industries	-1.762
02	Non-industrial combustion plants	-1.460
03	Combustion in manufacturing industry	-1.460
04	Production processes	-1.460
05	Extraction and distribution of fossil fuels and geothermal energy	-1.4
06	Solvent and other product use	-1.4
07	Road transport	-1.536
08	Other mobile sources and machinery	-1.536
09	Waste treatment and disposal	-1.4
10	Agriculture	-
Biofuel emissions		-1.07
Photosynthesis		-1.1
Respiration		-1.1

Furthermore, biofuels are distinguished as a separate category, as well as uptake and release of CO_2 by the biosphere through photosynthesis and respiration. Photosynthesis and respiration are calculated by the SiBCASA model for nine different land use types at a 1x1° resolution. This is scaled to the land use map, and the modelled short wave radiation and temperature in WRF-chem as described by Super et al. (2017).

2.3.2 Modelling O_2 uptake and release

Within the various categories (as shown in Table 1), exchange between O_2 and CO_2 takes place. Therefore, per (combined) emission category, an average oxidative ratio (OR_{in}) is calculated based on the fuel mix used in the Netherlands and the relevant oxidative process as described in equation 2 (derived from Emissiefactoren, 2017; LNG, 2017; RvO, 2016; Wikipedia, 2017; Wikipedia, 2017a). In this study, processes that consume or emit O_2 in exchange with CO_2 are given a negative OR. This means that the OR for fossil fuel burning, photosynthesis, and respiration are negative. For photosynthesis and respiration an OR_{in} for the biosphere of -1.1 is assumed. The average values for OR_{in} per emission category are shown in Table 1. These are used to calculate the uptake of O_2 as 'negative emissions' per SNAP category in WRF-chem through:

$$\Delta O_2 = \Delta CO_2 \cdot OR_{\text{in}}. \tag{8}$$

This results in negative values for ΔO_2, except for the photosynthesis term. The sum of ΔO_2 per category (i.e. the total fluctuation in O_2 concentration) is therefore often negative. Negative concentrations can however not be modelled in WRF-chem, therefore the background value of O_2 is in first instance set to a constant of 1000 ppm. This way, increases as well as decreases can be simulated, and the background value can easily be corrected for in the analysis. The changes in fossil fuel O_2 concentration, along with the corresponding increases in fossil fuel CO_2 can again be converted to values for OR_{ff} for specific events and at specific locations, which can be studied.

The values for OR_{in} can be assigned using two different methods; either by assigning an OR_{in} to CO_2 emissions per emission category, or by assigning an OR_{in} to each grid cell based on activities in that cell. The differences between the two methods will be elaborated on in the coming paragraph, and the results will be compared in Chapter 6.

As explained above, average OR_{in} values are calculated and assigned per CO_2 category. For the SNAP categories, these values are based on average fuel mixes used in the Netherlands. However, for some point sources in Rijnmond, the specific fuel type that is used is known. With this information, a more accurate OR_{in} value can be established for the grid cell in which the point source is located. Therefore, as a second experiment, OR ratios are firstly based

on the used fuel type of the point sources (if the information is known), and secondly on the SNAP categories. Therefore, the OR_{in} ratio is calculated per grid cell, which is then used to calculate changes in O_2 concentration. O_2 production or consumption through photosynthesis, respiration, and biofuel burning are - similar to the first method - calculated using the calculated average OR as shown in Table 1. The method used in this experiment will only affect O_2 concentrations in the 4^{th} domain, since specific fuel type information is only known over Rijnmond, and thus does not affect simulated O_2 concentrations in North Norfolk or the north of Groningen.

2.3.3 Ocean-atmosphere O_2 exchange

The atmospheric O_2 concentration does not only fluctuate through fossil fuel burning and exchange with the biosphere. The ocean can also act as an O_2 source or sink as described in Section 1.1.1. This exchange is however not directly correlated t CO_2 uptake by the ocean. O_2 uptake by the ocean is implemented in WRF-chem through Atmospheric Potential Oxygen (APO) inversions as modelled by Rödenbeck et al. (2008). APO is used to express the oceanic O_2 uptake or release, and thus exclude all biological processes and most of the fossil fuel influences (Section 1.1.3). APO inversions by Rödenbeck et al. (2008) are implemented as initial condition and boundary condition in WRF-chem, and thus added to the constant 1000 ppm background value as described before. 6-hourly APO inversions are available on a global scale on a 5x3.8° horizontal resolution and 26 vertical levels. For more information about the APO inverse modelling please refer to Rödenbeck et al. (2008).

2.4 Analysis of the results

Once O_2 is implemented into the WRF-chem setup, the model results need to be validated and further analysis can be done. The most important steps applied in the model validation and further analysis are discussed below.

2.4.1 Converting O_2 data to ppm concentrations

In order to validate the model, O_2 simulations are compared to O_2 observations. Due to the relatively small changes in O_2 concentration compared to its background, changes in O_2 con-

centration are expressed as changes in (O_2/N_2) ratio compared to a reference concentration in per meg (as described in Section 1.1.3). In order to compare the simulated and observed values, the observed values thus have to be converted to O_2 concentrations in ppm. Since the changes in O_2 concentrations are assumed to be due to exchange with CO_2, measurement data is converted using:

$$O_2 \quad [ppm] = \frac{O_2/N_2 \quad [permeg]}{4.77}. \tag{9}$$

Before applying this equation, the APO values that represent ocean exchange are converted to O_2/N_2 using (Wilson 2012):

$$\delta(O_2/N_2) = \delta APO = 1.1 \cdot \frac{CO_2 - 350}{X_{O_2}}, \tag{10}$$

in which 1.1 is oxidative ratio typically used for the land biosphere, CO_2 is the simulated CO_2 concentration in ppm, 350 is an arbitrary reference, and X_{O_2} is the standard mole fraction of O_2 in air (i.e. 0.209392).

2.4.2 Calculating and analysing outcoming Oxidative Ratios

Once O_2 fluctuations are modelled, the information can be used to calculate fossil fuel oxidative ratios (OR_{ff}), and identify the dominant fossil fuel sources in the study areas. This analysis can be done for the average over October 2014, as well as for specific times. In order to study a specific CO_2 emission event information is needed about the maximum CO_2 concentration measured during the event, as well as the background CO_2 concentration before the event. If the peak in CO_2 is due to fossil fuel burning, the CO_2 peak will correspond to a low in O_2 concentration. The magnitude of the decrease in ffO_2 along with the magnitude of the increase in $ffCO_2$ concentration yields an OR_{ff} for that specific event following (this is the same principle as rewriting Eq. 8):

$$OR_{\text{ff}} = \frac{\Delta(\text{ff})O_2}{\Delta(\text{ff})CO_2}. \tag{11}$$

The value for OR_{ff} that is found yields information about the important fossil fuel sources in case of the specific emission event. This, in combination with meteorological conditions during the event can identify the origin of the high CO_2 concentrations simulated during the event. An OR_{ff} including influences from the biosphere (and the ocean) can also be generated using Eq.

8. The ΔO_2 and ΔCO_2 that is used is than calculated as changes as opposed to the background value, taken into account uptake and release by the biosphere and ocean.

3 Wind direction - statistical analysis of the model performance

Modelled compound concentrations (i.e. tracers) are greatly influenced by local sources, as well as the transport of compounds emitted elsewhere. In this transport, the modelled wind direction plays an important role. For this research, the WRF-chem setup as developed by Super et al. (2017) will be used as a starting point to model CO_2 mole fractions. Ultimately, O_2 will be added as a tracer to the model setup. Super et al. (2017) found that the main discrepancy in their model performance on simulating CO and CO_2 concentrations around Rotterdam was due to errors in the simulated wind direction. They used a combination of WRF-chem version 3.2.1 and the Gaussian plume model OPS (Operational Priority Substances) to simulate the CO and CO_2 mixing ratios. The analysis in this chapter is a follow up to those conclusions by Super et al. (2017). To gain more insight in the WRF model performance, in the following sections the wind direction simulation of WRF version 3.2.1 will be discussed, the used model version will be compared to a more recent model version (Section 3.1), the performance between various locations within the domain will be compared (Section 3.2), and the model performance using a finer horizontal resolution will be analysed (Section 3.3). Furthermore, observation nudging will be attempted to improve the simulations (Section 3.4).

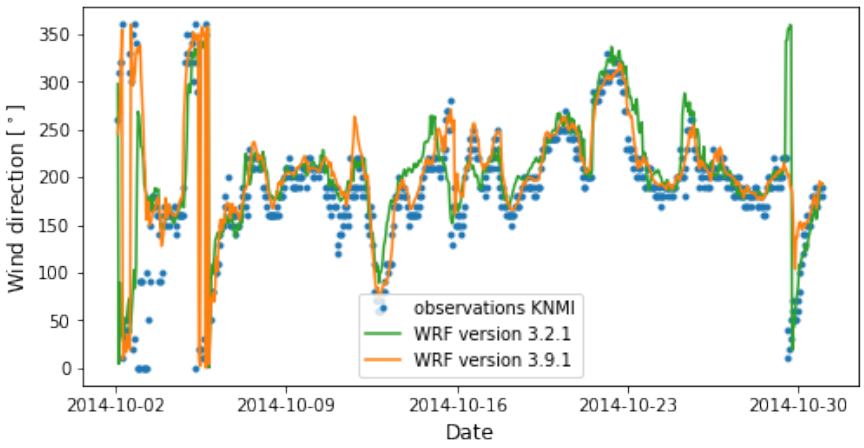

Figure 8: Wind direction for October 2014 at Rotterdam airport as measured by KNMI and simulated by WRF version 3.2.1 and version 3.9.1.

The wind direction for October 2014 simulated by WRF (at a 4x4 km grid size), along with the observations by KNMI at Rotterdam airport are shown in Figure 8. The observations agree with observations done at other KNMI sites in the area, such as Rotterdam Geulhaven and

Table 2: Most important quantitative measures of wind direction model performance for WRF version 3.2.1 and WRF version 3.9.1. Where $\overline{O}$ and $\overline{P}$ is the mean of the observed and simulated values, sd_O and sd_P the standard deviation of the observed and simulated values, RMSE the root mean square error, and d the index of agreement. Terms d and R^2 are dimensionless, the remaining terms have unit $^\circ$.

WRF-chem version	$\overline{O}$	$\overline{P}$	sd_O	sd_P	RMSE	d	R^2
3.2.1	189	204	63.0	57.0	66.3	0.685	0.182
3.9.1	189	206	63.0	56.5	58.2	0.761	0.337

Cabauw; the mean and standard deviation do not vary more than 5° between the surrounding measurement stations. The average simulated wind direction over the month overestimates the wind direction by about 15°, simulating slightly more westerly winds. The trend in the wind direction is similar between the simulations and observations. South-easterly winds (around 130-160°) are sometimes mistaken for more southerly winds, such as on the 10th, and 14th and 15th of October. Wind speed tends to be overestimated by WRF. A statistical analysis of the wind speed is added to the Appendix (Table A2).

Statistical analysis is done on the observed (O) and simulated (P) wind direction values, of which the most important quantitative measures are shown in Table 2. The same tables including the number of values (N), regression parameters (intercept a and slope b of the linear regression), Mean Average Error (MAE), and systematic and unsystematic Root Mean Square Error ($RMSE_s$ and $RMSE_u$, respectively) are added to the Appendix (Table A3). In Table 2 all modelled values are included. In literature it is found, however, that WRF is less successful in simulating wind directions when wind speeds are low (Jimenez and Dudhia 2013; Papanastasiou, Melas, and Lissaridis 2010). This is because low wind speed values can induce errors in the physical parameterization processes during the model application (Papanastasiou, Melas, and Lissaridis 2010). Furthermore, when wind speeds are low, they are often also more difficult to measure accurately, resulting in less reliable observation values. When plotting the difference in simulated and observed wind direction against wind speed for October 2014, a larger disagreement between simulated and observed values can indeed be identified at the lower wind speed range (Figure A.1, Appendix). In Table 3 therefore, similar to the study by Jimenez & Dudhia (2013), all directions simulated at wind speeds lower than 3.0 m/s are excluded and considered 'low wind speeds'. At these times, observed wind speeds are generally also below 3.0 m/s.

To accompany the qualitative indices in Tables 2 and 3, the relation between the simulated

Table 3: Same as Table 2, only here wind direction values simulated with wind speeds larger than 3 m/s are taken into account.

WRF-chem version	$\overline{O}$	$\overline{P}$	sd_O	sd_P	RMSE	d	R^2
3.2.1	197	212	50.6	46.2	48.3	0.752	0.307
3.9.1	201	212	50.8	48.8	41.5	0.827	0.460

and observed wind directions are displayed in Figure 9 (a). The average values $\overline{O}$ and $\overline{P}$ in Tables 2 and 3 show that the average wind direction is overestimated by about 15°. Even though the simulated wind direction becomes more westerly when low wind speeds are excluded, so does the observed wind direction. The general wind direction simulations over the month are thus not improved due to this selection. The standard deviations (sd_O and sd_P) show that the variability is underestimated by the model; the model thus shows less variability in wind direction than the observations. Figures 8 and 2 show the relation between the observed and simulated wind direction. Even though a clear relation is apparent, there are also outliers. A large number of these outliers are simulated at low wind speeds. Furthermore, it is important to notice that the outliers observed around 0-50° and simulated around 330-360° look like they are far from the ideal regression line, but are in fact not necessarily far of. This, since a wind direction simulated at 350° is in reality only 20° from a wind direction observed at 10. The RMSE is sensitive to extreme values, and is therefore generally regarded as a high estimate of the MAE (Table A3 Appendix) (Willmott 1982). The relatively low RMSEs compared to RMSEu (Table A3 Appendix), indicates that the errors in the model simulations are largely unsystematic. Overall, the values for index of agreement (d, ranging from 0 to 1) and R^2 indicate a relatively low model performance. Super et al. (2017) calculated statistics on the daytime (08:00-17:00 LT) average values of a three month period (from October to December). The daytime averages are not analysed here, since this leaves a too low value for N, decreasing the reliability of the quantitative measures. The outcome of the quantitative statistics on wind direction in this study are however in the same order of magnitude as the statistics by Super et al. (2017). The R^2 and RMSE that follow from the wind speed do improve by about 20% as only daily averages are taken into account. This suggests that daily averages in wind speed are captured better by WRF than hourly fluctuations, since individual wind speeds simulated from 8:00 to 17:00 LT do not match observations significantly better than wind speeds simulated for other times.

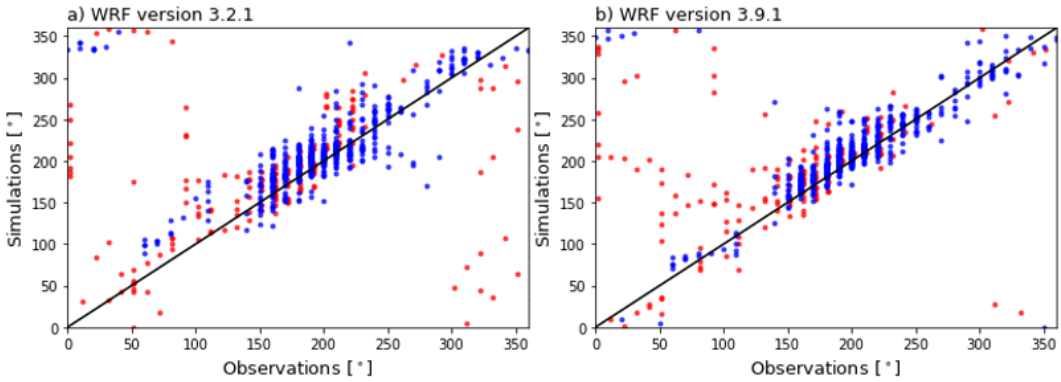

Figure 9: Relation between the simulated and the observed wind direction for WRF model version 3.2.1 (a) and version 3.9.1 (b). The wind directions simulated at wind speeds lower than 3 m/s are shown in red (and shifted slightly), and directions simulated at wind speeds higher than 3 m/s are shown in blue. An ideal regression line is shown in black.

From this, it can indeed be concluded that WRF has some difficulties simulating the correct wind direction, which are most apparent at low wind speeds. On average over the month, simulated wind directions are more westerly than observations. Furthermore, WRF underestimates variations in the wind direction by about 6° on average. The errors are mainly unsystematic, and are therefore difficult to correct for.

3.1 WRF version 3.2.1 vs version 3.9.1

In their research Super et al. (2017) used WRF-chem version 3.2.1, whereas the currently latest available version of WRF is version 3.9.1. We investigate the possible changes and improvements in wind direction simulations between those versions. Again, the simulated wind directions will be compared to observations at Rotterdam airport (Figure 8). Figure 8 does not show striking differences between wind direction as modelled by the two WRF versions: both versions show a similar trend and thus generally follow the KNMI observations. From Figure 8 it is difficult to determine which model version actually performs better in simulating wind direction. The quantitative measures are again shown in Tables 2 and 3 (extended in Appendix Table A3). The average values and standard deviations do not improve significantly as simulations are done by the later model version. The RMSE and MAE do improve by about 12% and 20% respectively as the later model version is used. This improvement increases to about 14% and

26% as wind speeds lower than 3 m/s are excluded. d and R^2 also improve when version 3.9.1 is used, however, this improvement is relatively smaller when low wind speeds are excluded from the model run.

Overall, WRF version 3.9.1 performs better in simulating wind directions than version 3.2.1. Both model versions are less successful in simulating wind directions with relatively low wind speeds. Version 3.2.1, however, seems to have more difficulty in simulating wind directions at low wind speeds than version 3.9.1.

A low model performance at low wind speeds would indicate poorer model performance at stable conditions, for instance during the night. The difference between simulations and observations are however not systematically larger at night. In the update to WRF version 3.7, the Revised MM5 Monin-Obukov scheme, which is used in this study as a surface layer scheme (Table A1, Appendix), is adapted to better represent the roughness length of water bodies (Ucar 2015). This could have its effect on the wind direction simulated above the ocean at low wind speeds. At Rotterdam, the wind often originates from the sea located only about 30 km West. Winds simulated at Rotterdam airport are thus influenced by the winds simulated above the North Sea. This improvement in the surface layer scheme could explain the increased model performance in the later model version.

3.1.1 Update in the Revised MM5 Monin-Obukov scheme

As mentioned in Section 3.1, the Revised MM5 Monin-Obukov scheme was updated with WRF model version 3.7. This could explain the changes in model performance between version 3.2.1 and 3.9.1. In this subsection the changes made in the surface layer scheme will be further explained, and it will be investigated whether these changes are actually responsible for the difference in model results.

During the WRF version 3.7 update, the heat and moisture exchange coefficients over water were adapted; from version 3.7 on, exchange coefficients are calculated using COARE 3.0 instead of Carlson-Boland (UCAR 2014). The adaptation is implemented through the change in determination of the roughness length (z_0) of water surfaces. z_0 is calculated using Charnock's (1955) expression plus a smooth flow limit, following Smith (1988):

$$z_0 = \frac{\alpha u_*^2}{g} + \frac{0.11\nu}{u_*}, \tag{12}$$

in which u_* is the friction velocity, α is Charnock's parameter (with a value of 0.0185 m in the used surface layer scheme), g is the gravitational constant, and ν is the kinematic viscosity. Version 3.2 made use of a constant value for the smooth flow limit of 1.59e^{-5} m in calculation of z_0. In version 3.7, this constant is replaced by a calculation of the flow limit in equation 11 with a value for ν of 1.5^{-5} m^2/s. Because of the dependence of the smooth flow limit on u_*, z_0 increases when $u_* < 0.104$ m/s, and decreases z_0 when $u_* > 0.104$ m/s. This generally results in lower values for z_0, since in practice u_* has values of about 0.2 m/s and larger (Vickers, Mahrt, and Andreas 2015). Due to the surface layer scheme updates, wind speeds close to the surface ocean are thus generally higher. The adaption also has its effect on the heat and moisture exchange coefficients and consequently reduces moisture and heat fluxes over water surfaces.

To investigate whether these changes are responsible for the improvement in wind direction at low wind speeds in version 3.9.1 as opposed to version 3.2.1, the surface layer physics file in WRF version 3.9.1 was adapted so that the calculations of the moisture and heat flux above water surfaces are done according to the equations used in version 3.2.1. The results are added to Table 4 (extended in the Appendix). The model performance parameters show that the wind simulation of version 3.9.1 without the update improve as the wind directions simulated at low wind speed are excluded, similar to version 3.2.1. Furthermore, the number of values excluded due to a simulated wind speed lower than 3.0 m/s increases by 146 values as the update is removed from the model. There are still some differences between the simulations of the adapted version 3.9.1 and version 3.2.1. The remaining differences between the two models are due to other model updates which affect the simulated wind direction, such as e.g. updates in the YSU boundary layer scheme.

Table 4: Most important quantitative measures of wind direction model performance for WRF version 3.9.1 without the surface layer scheme updates from version 3.7. Results of version 3.2.1 are repeated for clarity. The statistics are shown of all values, as well as only the values simulated at wind speeds > 3 m/s. It can be seen that just as is the case with version 3.2.1, the model performance improves as values at low wind directions are excluded.

WRF-chem version	$\overline{O}$	$\overline{P}$	sd_O	sd_P	RMSE	d	R^2
3.2.1	189	204	63.0	57.0	66.3	0.685	0.182
3.9.1	189	206	63.0	56.5	58.2	0.761	0.337
3.9.1 - update	190	202	62.3	51.4	57.9	0.730	0.271

3.2 Location comparison

The statistical analysis as presented in Section 3.1.1 shows the differences in wind direction simulation by WRF version 3.2.1 and version 3.9.1. The simulations are compared to observations conducted at Rotterdam airport. It can be discussed whether the model performance based on observations and simulations conducted for Rotterdam are representative for the entire domain (domain 3 in Figure 7), which covers the Netherlands as a whole. The model performance of version 3.2.1, the version which will be used in this study, at Rotterdam will be compared to the performance at Eindhoven and Lauwersoog (as shown in Figure 10). The observation site at Eindhoven is, similarly to Rotterdam, situated in an urbanized area, but is located more inland in Noord Brabant. Lauwersoog is situated closely to the measurement station at Lutjewad, where O_2 measurements are being conducted which might be useful for further analysis of the model performance of simulating O_2 in this or future research. The observation site is located in Groningen, on the north coast of the Netherlands. In Figure 11, the simulated and observed wind direction for all three locations for October 2014 is shown. A similar trend for the three locations can be seen, although there are also several moments in which the simulated wind direction varies within the domain (also depicted in Figure 10).

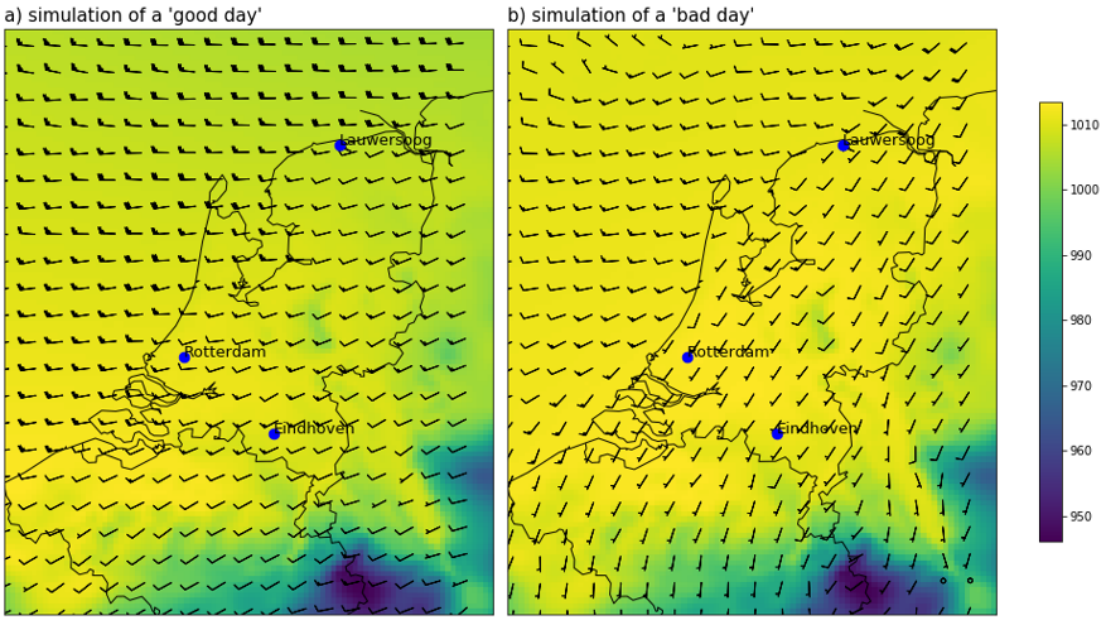

Figure 10: Map of the surface level pressure (hPa) with wind barbs of domain 3 for the 20th (a) and 23th (b) of October 2014. The map shows the location of the three analyzed sites: Rotterdam, Eindhoven, and Lauwersoog. It can be seen that the wind direction can vary within the domain. a) shows a day where the simulations by WRF followed the observations for all three sites, b) shows a day where the simulations did not match observations well at Rotterdam and Eindhoven.

A statistical analysis of the model performance at the three locations is shown in Table 5. At all sites, simulated winds are more westerly than the observed winds, and deviations from the general wind directions are underestimated. The simulations at Lauwersoog statistically match the observations best, whereas the simulations at Eindhoven show the poorest results. In Eindhoven, the simulated mean is the largest (+25° compared to observations), and deviations from the mean are smallest (-10.3° compared to observations). The sd_O and sd_P at Lauwersoog similar those calculated for Rotterdam, suggesting that the poorer model performance at Rotterdam as expressed by d and R^2 are mainly due to the stronger overestimation in the general wind direction (hence winds coming more from the west in the simulations as compared to observations). At Lauwersoog, the sd_P is largest, and RMSE is lower than at the other sites. Furthermore, the amount of simulations with wind speeds lower than 3.0 m/s is limited. The improvement in model performance when low wind speeds are excluded is lower for this station compared to the other stations. This suggests that the better model performance at Lauwersoog is due to the larger wind speeds at the coast. It should be noted that lower wind speeds also make the observations of wind direction less reliable, which can have its effect on the calcu-

lated statistical measures.

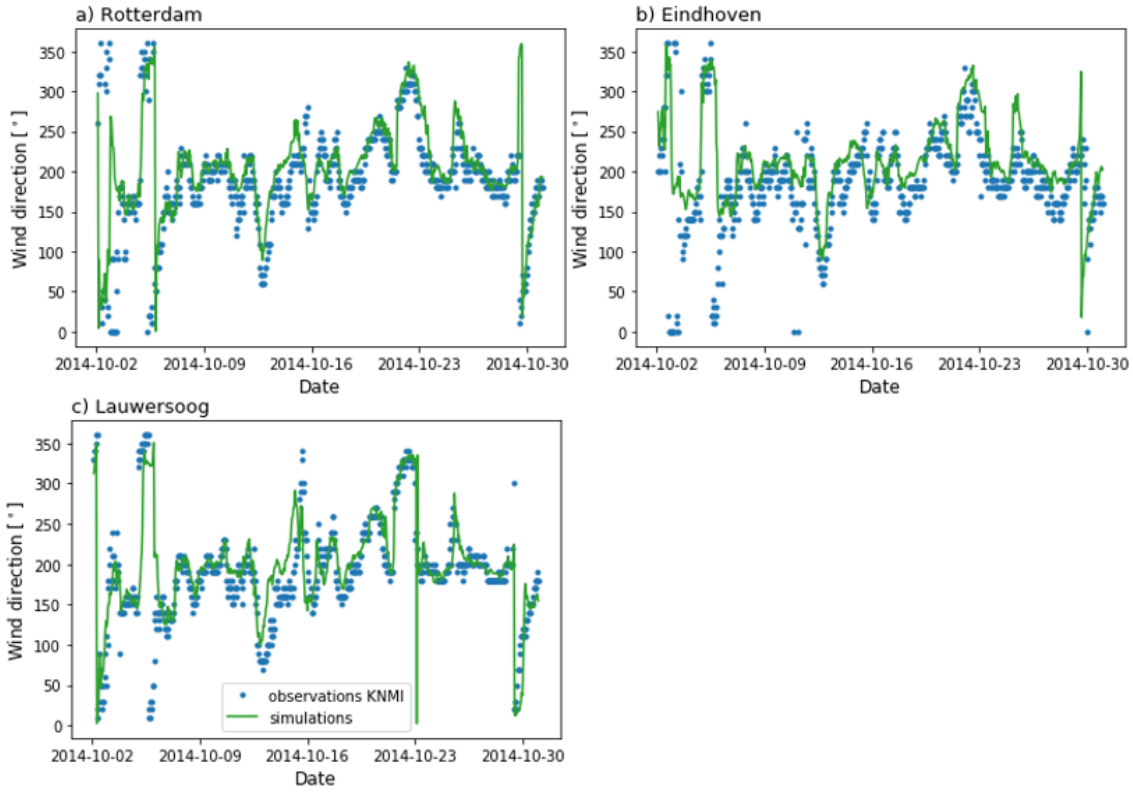

Figure 11: Wind direction for October 2014 as simulated by WRF and observed by the KNMI at Rotterdam (a), Eindhoven (b), and Lauwersoog (c) for October 2014.

Table 5: Most important quantitative measures of wind direction model performance at Rotterdam, Eindhoven, and Lauwersoog.

Location	$\overline{O}$	$\overline{P}$	sd_O	sd_P	RMSE	d	R^2
Rotterdam	189	204	63.0	57.0	66.3	0.685	0.182
Eindhoven	187	212	58.7	48.4	61.1	0.673	0.224
Lauwersoog	190	198	63.6	58.1	50.4	0.820	0.448

Overall, WRF's performance in simulating wind directions, and consequently the transport of compounds, does not show striking differences, but can vary over the third domain. The simulations analyzed so far are done at a 4x4 km horizontal resolution. In Section 3.3, the model performance at this horizontal resolution is compared to simulations done at a 1x1 km horizontal resolution.

3.3 4x4 km vs 1x1 km horizontal resolution

The compound concentrations modelled by (Super et al. 2017), as well as in this study, are finally simulated in a smaller domain covering the Rijnmond area only (domain 4, Figure 7). This domain has a horizontal resolution of 1x1 km. Therefore, the wind directions simulated at this resolution will be compared to the wind directions as previously simulated and analyzed in this chapter. The comparison of simulations is shown in Figure 12. Furthermore, the quantitative statistics are shown in Table A3 in the Appendix. It can be seen that there is very little difference between the simulations at the two resolution sizes. This is the case for wind direction, as well as wind speed (not shown). Studies have shown that a model's performance can be improved by using a finer horizontal resolution, but may also be similar, or even worse (Carvalho et al. 2012). This is due to uncertainties in the performance of the various physical parameterizations and their responses to grid resolution (Pleim et al. 1995; Wu et al. 2008; Y. Zhang et al. 2006). Increasing grid resolution may improve the simulation of fine-scale processes (Mass et al. 2002; Westphal 2001) but does not necessarily correlate to better model accuracy (Gego et al. 2005). Furthermore, computational costs of finer resolutions are often much higher. Therefore it is important to outweigh the improvement of results to the computational costs. In this study, however, even though the simulated wind directions do not improve in domain 4 as opposed to domain 3, it will still be worthwhile to simulate compound emissions at a 1x1 km horizontal resolution. This, as Dekker (2014) shows, that to successfully model compound emissions in an urban area, a horizontal resolutions of 1x1 km is needed.

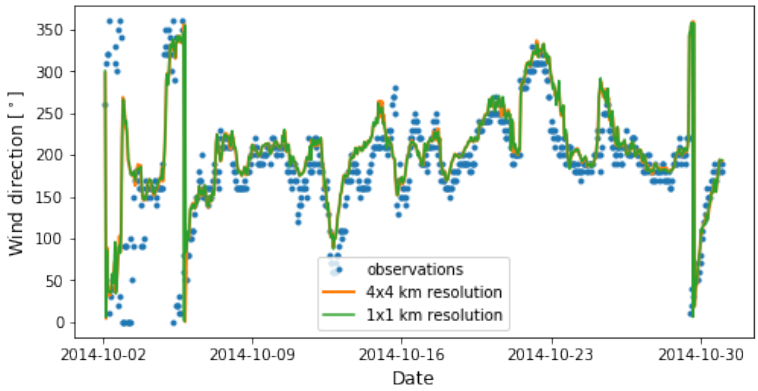

Figure 12: Observations and simulation of the wind direction as modelled by WRF version 3.2.1 at Rotterdam airport in domain 3 (4x4 km horizontal resolution) and domain 4 (1x1 km horizontal resolution). It can be seen that there is almost no difference between the simulations between the two domains.

3.4 Wind direction nudging

From the analyses done in Sections 3.1 to 3.3, it becomes apparent that WRF has issues in simulating the correct wind directions, especially at lower wind speeds. Simulated compound concentrations depend largely on the transport of the compound and thus the wind direction. A potential way to improve the simulated wind direction is by observation nudging. In observation nudging, artificial tendency terms are introduced to gradually 'nudge' the model towards observations (Pettersson 2016). In order to investigate the potential use of observation nudging in this study, observation nudging of the wind direction is implemented in domain 1 (Figure 7). The most important nudging settings are the nudging weight, the horizontal radius of influence, and the time window. A nudging strength of 6.0e^{-4} s^{-1} is used. This effects the strength to which a simulated value is pulled towards an observation in units of inverse seconds (for more information: Pettersson (2016)): the larger the nudging strength, the smaller the error is that remains after a certain amount of time. The horizontal radius of influence is set to 250 km. This means that simulations up until 250 km from an observation point are influenced by that observation. The influence is however larger if the location of the observation is close to the simulated grid cell than if the grid cell were further away. Finally, since observations are hourly, the time window is set to 1 h. This means that the nudging strength is largest at the time of observation, and decreases to 0 up until half an hour before and after the observation. The observational data that is used for the wind direction nudging is obtained from the Integrated Surface Database (ISD) from the National Oceanic and Atmospheric Administration (NOAA). The ISD contains

global hourly and synoptic observations over land and water (NOAA, 2014). Observation nudging using similar datasets have improved forecasts in other experiments, although impacts are not equally positive in various situations (Liu et al. 2007; Macpherson, Deblonde, and Aparicio 2008).

Statistics of the wind nudging data are shown in Table 6 (extended in Appendix Table A3). The observation nudging was conducted only at surface levels and in the 1st domain. This mainly reduces the standard deviation of the simulated values. The time series of the wind direction with and without observation nudging in Figure 13 shows that the model runs are similar, and differences are often difficult to distinguish. The model does not show clear improvements towards the KNMI observations due to the nudging. From this, it can be concluded that, for the used nudging strength, observation nudging is not useful to improve wind direction simulations. There is still discussion in literature on the combination of nudging settings to simulate without over-manipulating the data (Bullock et al. 2014; Li et al. 2016; Liu et al. 2007). In this case, the effect of observation nudging is not significantly positive enough to improve simulations, and a greater nudging weight would increase the chance of losing important mesoscale features created by the model, or creating noise in the model results (Deng et al. 2008). Therefore, observation nudging will not be applied in order to obtain further results in this study.

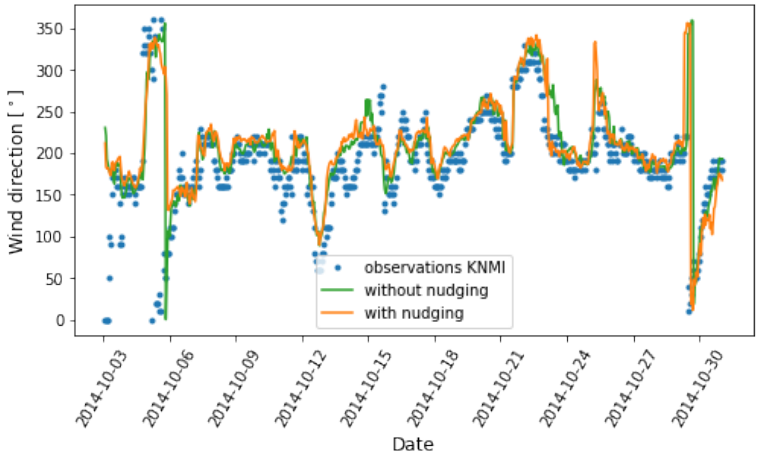

Figure 13: Observations and simulation of the wind direction as modeled by WRF with and without observation nudging applied.

Table 6: Most important quantitative measures of wind direction model performance for WRF version 3.2.1, without and with observation nudging applied.

	$\overline{O}$	$\overline{P}$	sd_O	sd_P	RMSE	d	R^2
Without nudging	190	207	57.5	57.3	57.64	0.720	0.257
With nudging	190	210	57.5	52.3	55.6	0.739	0.310

4 Partitioning fluctuations in atmospheric O_2

The first research objective (as stated in Section 1.3) is to implement O_2 as a tracer for fossil fuel CO_2 ($ffCO_2$) in WRF-chem. To do so, fossil fuel O_2 (ffO_2) is simulated as negative emissions as a result of CO_2 emissions as described in Section 2.3.1. To complete the modelling of O_2, uptake and release as a response to biospheric processes (i.e. respiration and photosynthesis), as well as uptake and release by the ocean (hereafter referred to as $O_{2_{bio}}$ and $O_{2_{oc}}$) are included in the model. To gain an overview of the importance of these O_2 sources and sinks in the modelling of O_2, partitioning of the ocean, biosphere, and fossil fuel components is elaborated on in this chapter (Section 4.1). The total of the modelled fluctuations in O_2 is compared to measurements in Lutjewad (NL) and Weybourne (UK) in order to validate the model results (Section 4.2). After the various O_2 sources and sinks are explored in this chapter, ffO_2 and its use as a tracer for fossil fuel sources are analysed in more detail in Chapters 5 and 6.

4.1 O_2 fluctuation partitioning

O_2 is the second most abundant molecule in the atmosphere, with a relative abundance of about 20.9%. Small scale fluctuations in atmospheric O_2 concentration can be used to partition and quantify the land and ocean carbon sinks in the carbon budget at described in Section 1.1. Since only fluctuations on a scale of ppm appear and are important in this partitioning, the O_2 background concentration is not implemented in the model. The variation in concentration that remains, is due to O_2 uptake or release by the ocean, biosphere, and (fossil) fuel burning.

The fluctuations as modelled per component (i.e. the ocean, biosphere, and fossil fuel burning) vary over the three study areas. The three components as simulated for Zweth (Rijnmond, NL) are shown in Figure 14. Figure 14a shows a time series of the O_2 fluctuations. O_2 is mainly depleted from the atmosphere during October 2014. As can be expected in an urban area, most of the O_2 fluctuations are due to fossil fuel burning (as also shown in Figure 14b). Fossil fuel burning is responsible for 53.7% of all O_2 uptake in Zweth, with a average of -9.6 ppm as opposed to the background concentration. There is however a lot of fluctuation in the importance of the fossil fuel component over time, as it is driven by the $ffCO_2$ emissions in the nearby area.

O_2 fluctuations due to the biosphere is the second largest component at Zweth. The effect

of the biosphere can be divided in uptake of O_2 due to respiration, and release of O_2 due to photosynthesis. The biosphere is a net O_2 sink over the studied month (October 2014). It is responsible for 43.8% of the total O_2 uptake, with an average of -7.8 ppm as opposed to the background. Even though fluctuations in the biospheric uptake and release are not as large as the fluctuations due to the fossil fuel component, they are still easily distinguished in the dataset, indicating that the biosphere is not a constant sink over time. In spring and summer months, this component is expected to act as a O_2 source, due to the increased amount of photosynthesis.

The final component responsible for O_2 variation in the atmosphere is the ocean. In Zweth, the ocean in responsible for 2.4% of the total O_2 uptake, with an average of -0.4 ppm. Not only uptake of O_2 takes place, as on occasion, the ocean acts as a O_2 source in Zweth. This is due to due to the alternation of outgassing and uptake of O_2, dependent on solubility changes in the ocean (Rödenbeck et al. 2008). Relatively slow equilibrium rates in this solubility of O_2 in the ocean cause relatively little variation in the total O_2 concentration due to the ocean over the examined time scale. Over longer time scales, the ocean has a larger influence on atmospheric O_2 as new equilibria are reached with changing climates (R. F. Keeling and A. C. Manning 2014).

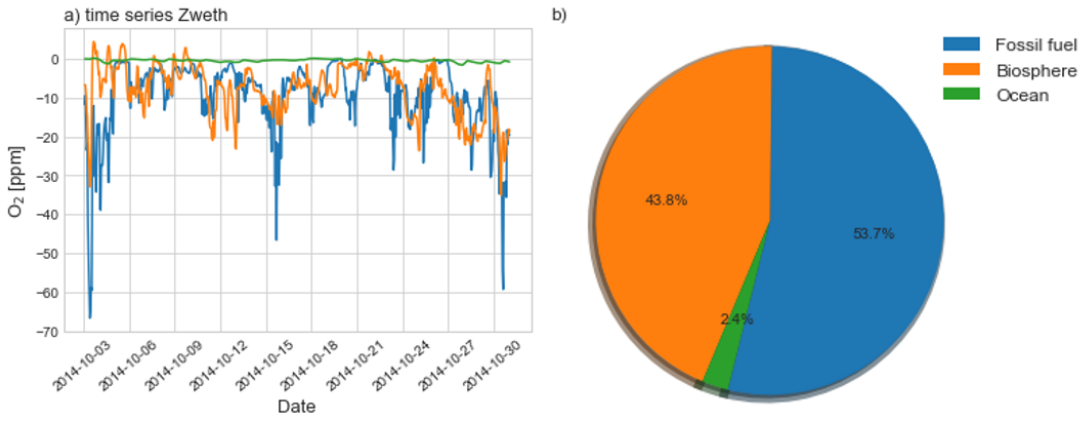

Figure 14: a) Time series of O_2 fluctuations due to fossil fuel burning (blue), land biosphere activity (orange), and the ocean (green), and b) cumulative importance of fossil fuel burning, land biosphere activity, and the ocean for October 2014 at Zweth (Rijnmond, NL).

As a second study area, O_2 fluctuations at Lutjewad are analysed. Lutjewad is a rural station, located on the north coast of Groningen (NL). Even though the modelled total O_2 fluctuations are smaller due to the more remote location, the fossil fuel component is cumulatively still the

largest (49.0%, Figure 15b), with an average O_2 uptake of -5.7 ppm. The fluctuations of the ffO_2 at Lutjewad are smaller than the ffO_2 at Zweth. This is because CO_2 emissions are less severe at Lutjewad, and emission concentrations are more diluted. Furthermore, due to the coastal location of Lutjewad, inversions are less severe. This decreases the trapping of air with low O_2 concentrations.

The biosphere is almost equally important as fossil fuel burning in the total O_2 uptake in Lutjewad, with and average of -5.4 ppm. It is responsible for 46.4% of all O_2 taken up. It is important to note that the prevailing wind direction is southwest. Air modelled at this location has thus travelled over land before reaching Lutjewad, increasing the importance of the fossil fuel and land biosphere components. The ocean is again a relatively small component, responsible for 4.6% of the total O_2 fluctuations. Even though the wind originates from the land, the oceanic component is still larger for Lutjewad than for Zweth (with an average uptake of -0.5 ppm), due to the coastal location of the study area.

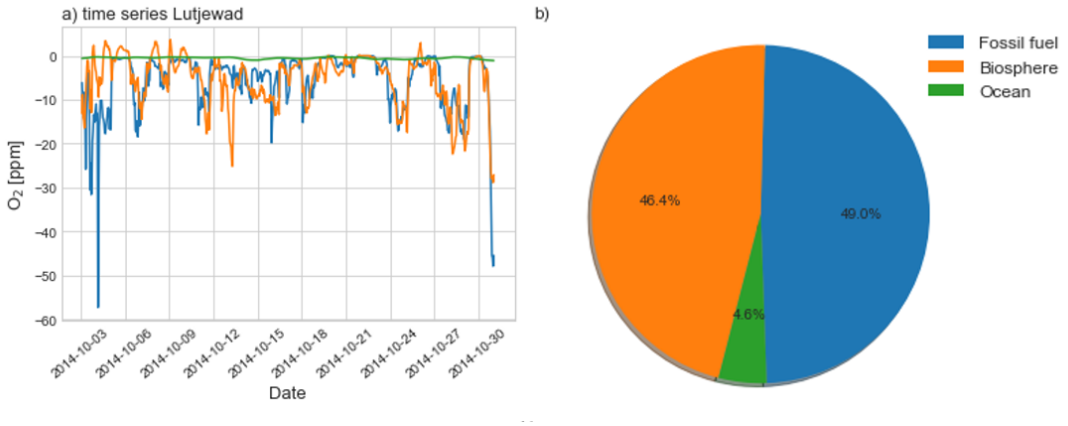

Figure 15: a) Time series of O_2 fluctuations due to fossil fuel burning (blue), land biosphere activity (orange), and the ocean (green), and b) cumulative importance of fossil fuel burning, land biosphere activity, and the ocean for October 2014 at Lutjewad (Groningen, NL).

In Weybourne total O_2 fluctuations are smallest as shown in Figure 16. This is mainly due to the relatively small amount of fossil fuel burning in the area. Weybourne is the only study area in which the biosphere is a more important component than fossil fuel burning (62.5% vs 31.5% of the modelled total O_2 fluctuations). Fossil fuel burning causes an average uptake of -2.9 ppm, whereas the biosphere causes an average net uptake of -5.7 ppm O_2.

The ocean causes an uptake of -0.5 ppm on average. The O_2 fluctuations at Weybourne

due to the biosphere and ocean are thus similar in magnitude to those at Lutjewad, showing the similarities between the two sites (i.e. coastal background stations). O_2 concentrations at Lutjewad are however more influenced by fossil fuel burning than concentrations at Weybourne.

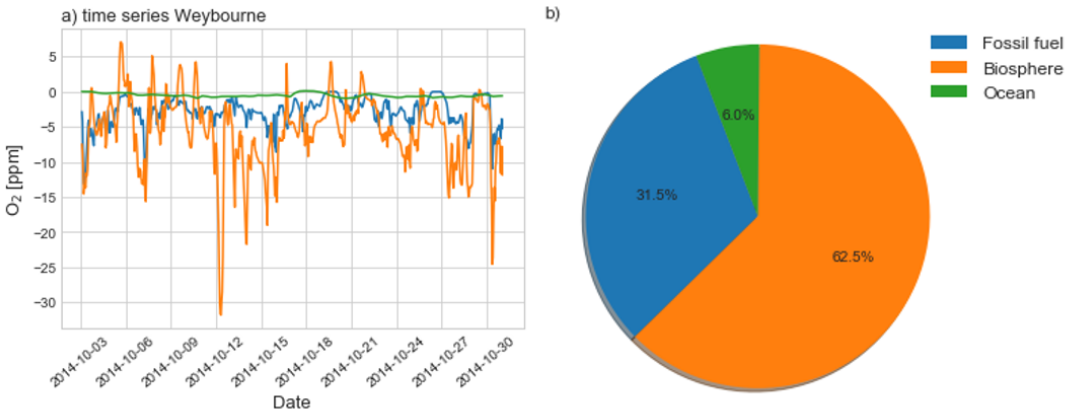

Figure 16: a) Time series of O_2 fluctuations due to fossil fuel burning (blue), land biosphere activity (orange), and the ocean (green), and b) cumulative importance of fossil fuel burning, land biosphere activity, and the ocean for October 2014 at Weybourne (North Norfolk, UK).

Overall it can be stated that during the autumn month of October 2014, all three components act as a net sink of atmospheric O_2. In summer months, the biosphere is likely to turn into a source of atmospheric O_2. The total uptake of O_2 (mainly due to fossil fuel burning) is then expected to be mitigated by the biosphere. In the case of Weybourne, biological activity in summer is even likely to result in a net increase in O_2 concentrations. On the short time scales as modelled here, O_2 fluctuations due to the ocean are relatively small, especially in urban areas. The main difference between the three study areas in O_2 uptake is to be found in the amount of fossil fuel burning in the nearby area upwind.

4.1.1 Diurnal cycles

The times series in Figures 14a to 16a show variation in the amount of O_2 uptake over time. From these figures a clear diurnal cycle is however not easily distinguished. Figure 17 shows the average diurnal cycle of the three components for the three measurement sites over the studied month. ffO_2 is expected to decrease during the day due to increased anthropogenic activity and thus ffCO_2 emissions, and increase again at night. The decrease is mitigated by boundary layer mixing and entrainment with air from the free troposphere with higher concentrations.

This decrease during the day is simulated at Zweth and Weybourne (Figure 17a). In Zweth commuting hours around 8:00 and 18:00 LT can be distinguished. At Weybourne, ffO_2 is larger, with a relatively small average amplitude (0.5 ppm). The diurnal average ffO_2 at Lutjewad does not show the expected cycle: ffO_2 is largest during the day and lower at night with an amplitude of about 2 ppm. The $ffCO_2$ emissions around Lutjewad are smaller than those around Zweth. It could thus be the case that the effect of boundary layer mixing and entrainment at this location overpowers the increase in $ffCO_2$ emissions, causing an increase in ffO_2 during the daytime.

The average diurnal cycle of $O_{2_{bio}}$ is shown in Figure 17b. A clear diurnal cycle can be seen for Zweth and Weybourne, with the lowest concentrations at night and in the morning due to plant respiration at night. During the day, photosynthesis becomes relatively more important, releasing oxygen and causing an increase in $O_{2_{bio}}$. In Zweth, the total effect of the biosphere is larger than in Weybourne (i.e. the lower average $O_{2_{bio}}$). This is likely due to the more inland location of the site. $O_{2_{bio}}$ in Lutjewad also shows a low in the early morning. The amplitude of the cycle is however smaller at this site compared to the other sites. This means that there is less difference between the photosynthesis and respiration term simulated at Lutjewad.

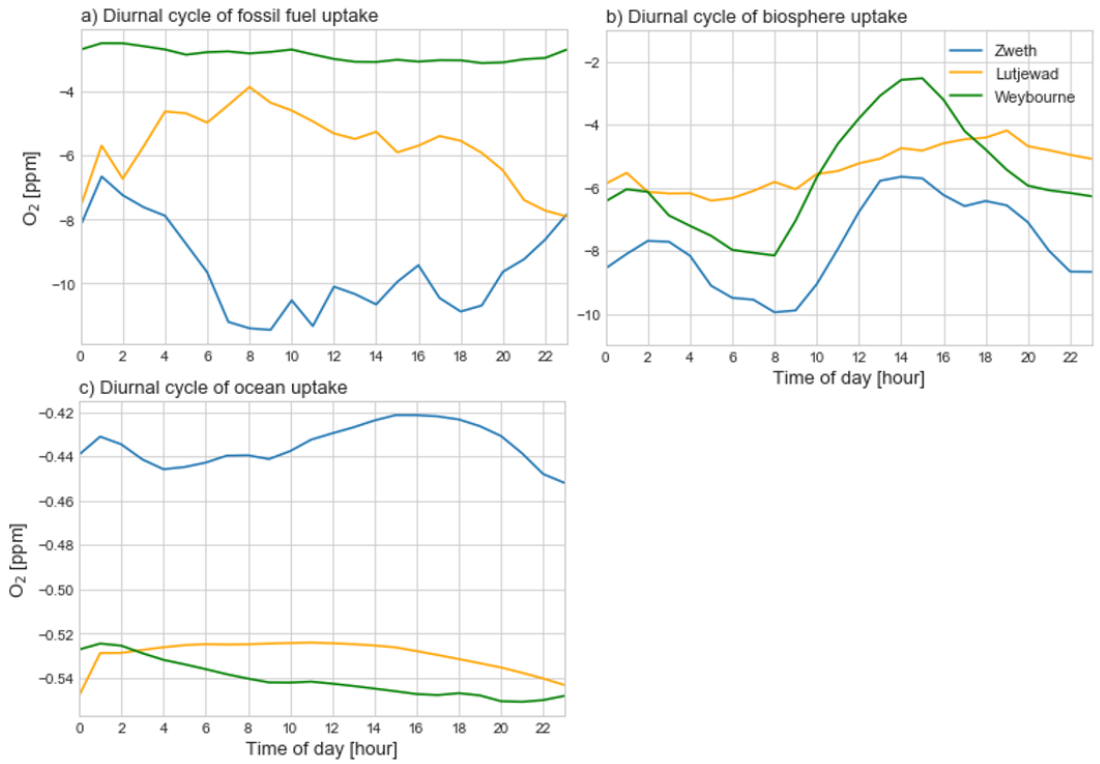

Figure 17: Average diurnal cycles of O_2 uptake due to a) fossil fuel burning (ffO_2), b) biospheric activity ($O_{2_{bio}}$), and c) the ocean ($O_{2_{oc}}$) in Zweth (blue), Lutjewad (orange), and Weybourne (green).

The diurnal variation in $O_{2_{oc}}$ as shown in Figure 17c is minimal for all three sites. A diurnal cycle in ocean uptake/outgassing is however not expected due to its slow response time. The figure does show the similarity in $O_{2_{oc}}$ between coastal sites Lutjewad and Weybourne, and the slightly lower impact in the more inland site Zweth. It should be noted that the uptake and release of O_2 from the ocean is modelled based on the Atmospheric Potential Oxygen (APO) fluxes as modelled by Rödenbeck et al. (2008). This model has a coarse spatial scale of 3.8x5.0°, meaning that the resolution of the ocean O_2 fluxes are not very precise and more regional scale differences between the sites could be missed.

4.2 Total O_2 fluctuation and model validation

The combination of ffO_2, $O_{2_{bio}}$, and $O_{2_{oc}}$ results in a total fluctuation in O_2 concentration as opposed to the background concentration. This total fluctuation over the month, as well as the diurnal averages are analysed for each study area. In case of Lutjewad and Weybourne,

measurements of both atmospheric CO_2 and O_2 concentration are compared to the simulated results in order to asses the model performance.

4.2.1 Zweth, Rijnmond

As is apparent from Section 4.1, fossil fuel burning in the industrial area and harbour nearby has the largest influence on variation in atmospheric O_2 at Zweth. The steep lows shown in Figure 18a can be largely attributed to O_2 uptake due to fossil fuel burning. However, the biosphere does still play a significant role in the total uptake of atmospheric O_2. The average diurnal cycle as shown in Figure 18b shows a low around 8:00 LT, and a high just after midnight. The total O_2 concentration has an average of -17.3 ppm with an amplitude of 3.3 ppm. Again it becomes clear that fossil fuel burning is the most important component at this site, with highs and lows at corresponding times (as depicted in Figure 17a). However, the total concentration is still influenced by the biosphere (see Figure 17b), diminishing the low O_2 concentration in the afternoon and causing a small peak through photosynthesis. The increase in total O_2 in the afternoon is also partly attributed to the effect of boundary layer mixing and entrainment. Air entrained from the free troposphere contains more O_2 than the air within the boundary layer, resulting in an increase in O_2 at the surface.

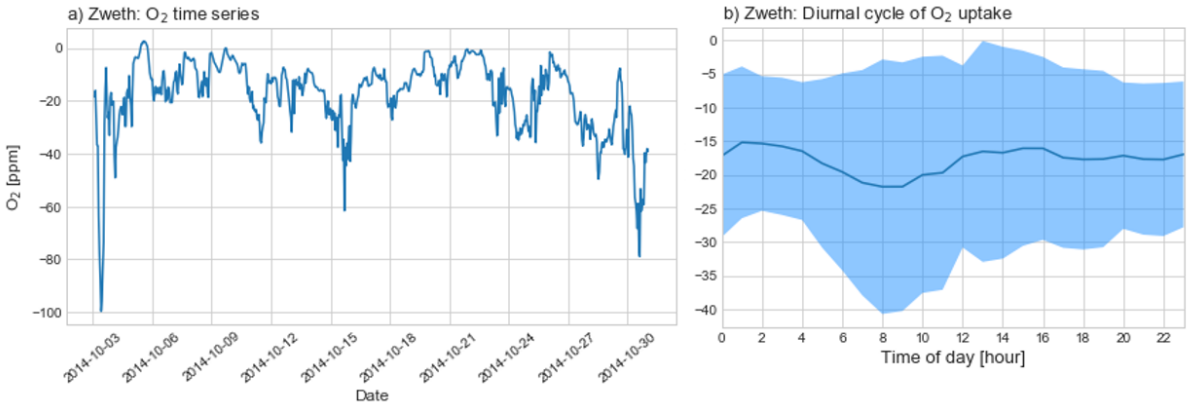

Figure 18: a) Time series of the total O_2 fluctuations and b) diurnal average of total O_2 as opposed to the background, as modelled for Zweth during October 2014. The shading represents the standard deviation of the simulated averages.

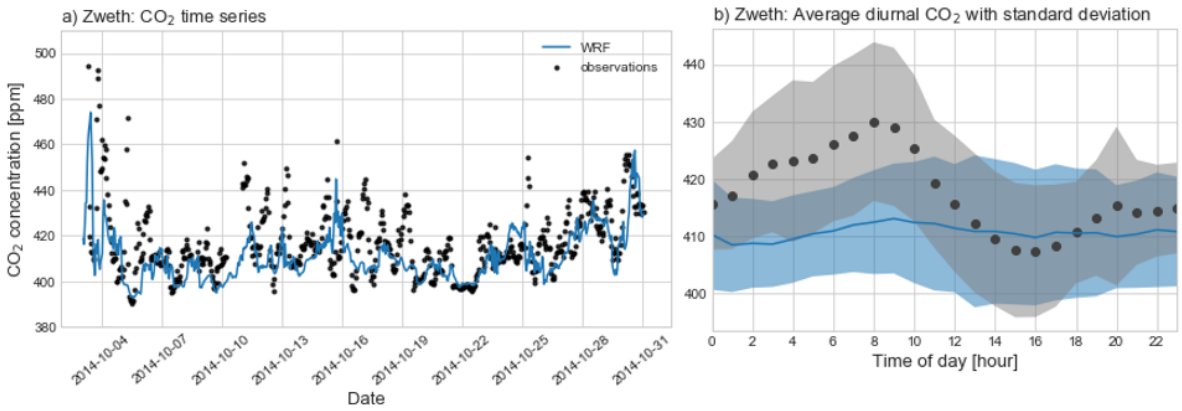

Figure 19: a) Time series of the total CO_2 and b) diurnal average of total CO_2, as modelled and observed at Zweth during October 2014. The shading represents the standard deviation of the simulated and observed averages.

In addition to the O_2 concentrations simulated at Zweth, the CO_2 concentrations are shown in Figure 19. This figure also contains data of hourly observations in Zweth. It can be seen that the model often underestimates CO_2 concentrations. The diurnal cycle simulated at Zweth follows a similar trend as the average diurnal cycle of the observations. The amplitude in the cycle is however underestimated, as becomes especially apparent during the night and (early) morning. This shows the difficulty the model has in representing stable conditions at night. The CO_2 measurements at Zweth are conducted at ground level, resulting in a large influence of local sources and processes. This can influence the measured CO_2 concentration in a way that is not captured by the model simulating on a 1x1 km horizontal resolution. The O_2 concentrations shown in Figure 18 are modelled making use of the CO_2 emissions. Furthermore, the emitted O_2 and CO_2 are transported in a similar way. Errors in simulated CO_2 are therefore translated into the modelled O_2 concentrations. This effect becomes apparent when comparing modelled and observed O_2 and CO_2 concentrations at Lutjewad and Weybourne in Sections 4.2.2 and 4.2.3, respectively.

4.2.2 Lutjewad, Groningen

Changes in simulated O_2 concentration at Lutjewad are analysed and compared to observations in order to validate the model. Figure 20a shows the comparison of the simulated and observed O_2 fluctuations at Lutjewad in October 2014. Observations at Lutjewad are done at the top of the measurement tower, at 60m height (I. T. Van Der Laan-Luijkx et al. 2010). Variation

in O_2 concentration in Lutjewad is limited compared to Zweth due to the smaller amount of fossil fuel burning in the area. O_2 exchange through the biosphere is therefor relatively more important at this site. The fluctuations shown here are also smaller due to the increased height (i.e. 60 m compared to surface concentrations). Further analysis done on concentrations at Lutjewad outside of this Section focuses surface concentrations, in order to make the results corresponding to this site optimally comparable to results from the other sites. The change in O_2 concentration fluctuates between about -75 ppm and 6 ppm compared to the background value during October 2014. At some moments, the simulated O_2 matches the observations quite well (e.g. the 7^{th}, 13^{th}, 20^{th}, 21^{st}, 30^{th}, and 31^{st} of October). At other times, the modelled and observed values vary quite a lot (in the periods from the 12^{th} to 18^{th} and 25^{th} to 28^{th} of October). In this case, hourly observations of O_2 are available, however, the reliability of these values is questionable (I. Van Der Laan-Luijkx 2018). Sample flasks are alternated every 24 hours. Leaking occurred in one of the two flasks causing measurement errors in part of the observations. This means that even though a (statistical) comparison of the observations and simulations possible, solid conclusions cannot be drawn from this. A true validation or rejection of the model is thus not possible based on these figures. Because of the indefinite certainty of the hourly measurements, 3-daily flask data is added to Figure 20a in gray. Even though these measurements are more reliable, only 6 observational values are available from this dataset for October 2014. This makes it impossible to draw hard conclusions about the model performance based on this data. However, the flask data that is available shows similar values as simulated at those moments.

Statistical measures of the model performance in simulating CO_2 and O_2 concentrations based on the hourly observations are shown in Table 7. A discrepancy is shown in CO_2 as well as O_2. The average CO_2 concentration and standard deviation is underestimated by the model by 4.5 and 2.8 ppm, respectively. These differences are expected to translate to the measures for simulated O_2, as those are based on the simulated CO_2 and OR_{in}. This is also displayed in Figure 21a, where the observed CO_2 values are plotted against simulations. At times when the simulated O_2 deviates from observations, simulated CO_2 also does not agree with CO_2 observations. This means that if the errors shown are due to poor model performance, then errors in simulated O_2 would be due to errors in simulated CO_2 rather than faulty values of OR_{in}.

Furthermore (as stated by Super et al. (2017) and further elaborated on in Chapter 3), these discrepancies in CO_2 concentration are often attributed to errors in the simulated wind direction. As a result, the simulated average O_2 is overestimated by 5.4 ppm, and the standard deviation is underestimated by 3.2 ppm. If the these errors have their origin in the simulated CO_2 concentrations, then the amplification in discrepancies can be explained by the multiplication by OR_{in} (with an average value of about -1.5). In this case, however, variations between the modelled and observed values are not necessarily due to mistakes in the model, but could also be due to unreliable observations. With this kept in mind, statistical analysis results in an index of agreement of 0.72 and an R^2 of 0.30 for the modelled O_2 fluctuations and an index of agreement of 0.71 and an R^2 of 0.30 for the modelled CO_2 concentrations.

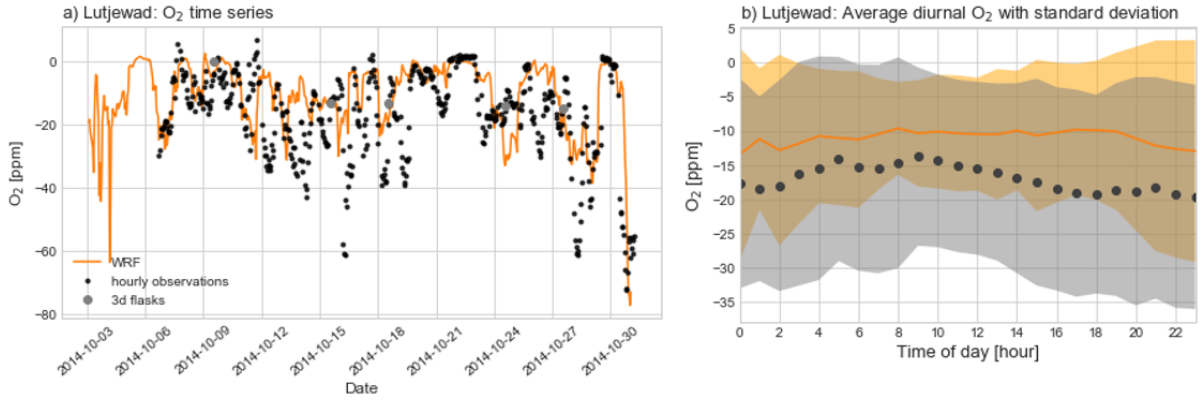

Figure 20: a) Time series of the total O_2 fluctuations and b) diurnal average of total O_2 as opposed to the background, as modelled and observed at Lutjewad during October 2014. The shading represents the standard deviation of the simulated and observed averages.

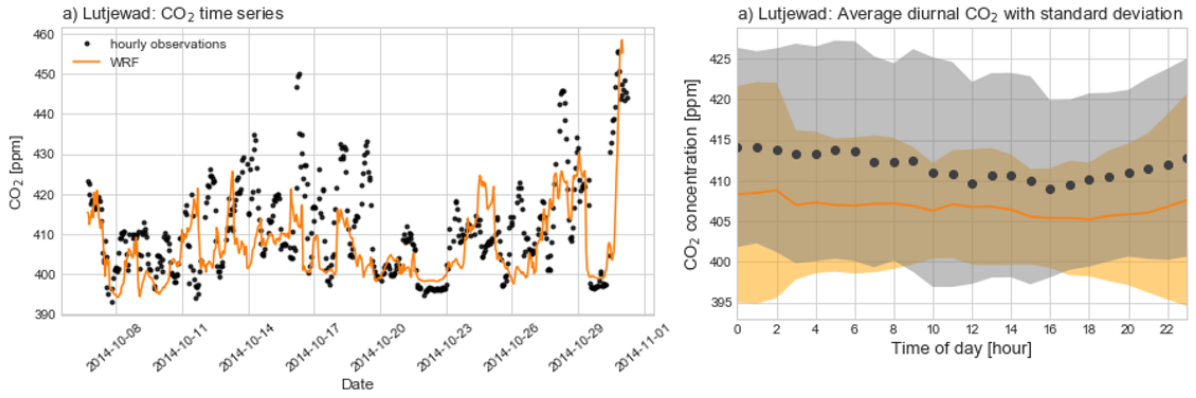

Figure 21: a) Time series of the total CO_2 and b) diurnal average of total CO_2, as modelled and observed at Lutjewad during October 2014. The shading represents the standard deviation of the simulated and observed averages.

Table 7: Most important quantitative measures of CO_2, O_2, and wind direction model performance at Lutjewad.

	$\overline{O}$	$\overline{P}$	sd_O	sd_P	RMSE	d	R^2
CO_2	411.5	407.0	12.2	9.4	11.5	0.71	0.30
O_2	-16.4	-11.0	14.5	11.3	13.5	0.72	0.30
Wind direction	190	198	63.6	58.1	50.4	0.820	0.448

The simulated daily average values of O_2 as shown in Figure 20b do not show a clear diurnal cycle. From midnight on, O_2 concentrations increase by about 3.5 ppm until the afternoon, after which they decrease again. The observed values show a similar trend, with (as mentioned above) average values about 5 ppm lower. This is in line with the observed and simulated CO_2 concentrations (21b), which also display a lack in diurnal trend and slightly higher average concentrations. This consistency between the simulations and the observations does make the trends shown in Figures 21b, and consequently Figures 20b and 17 more likely to represent reality. The lack in diurnal trend suggests a the signal of a station measuring a background signal. Winds originating mainly from the southwest over the analysed period contradict this, resulting in a signal influenced by fossil fuel burning and biosphere exchange in Figures 20a and 21a. The lack in diurnal trends shown in Figures 20 and 21b may be explained by the relatively small amount of $ffCO_2$ emissions, which are mixed and diluted when they reach Lutjewad, combined with a relatively small amount of boundary layer development and entrainment at the coast, leading to quite constant concentrations during the day. Furthermore, the influence of fossil fuel burning is expected to be lower at 60 m height (at which the air is sampled at this station) as compared to the surface. In order to further investigate whether the lack in diurnal cycles shown in Figures 20b and 21b are due to oceanic influences may be studied by using radon as a tracer to gain insight on the air mass origins at coastal locations (Pszenny and Larson 1990).

4.2.3 Weybourne, North Norfolk

Even though the OR_{in} used as model input are averages per SNAP category for the Netherlands, the changes in O_2 concentration in Weybourne (situated in the UK) are also analysed and compared to observations. Figure 22a shows the O_2 fluctuations according to the simulations and observations at Weybourne. Weybourne is, similar to Lutjewad, a more rural station than Zweth located on the coast. As a result, the O_2 signal is more influenced by biological activity.

During autumn and winter, respiration is generally higher than photosynthesis, resulting in a net uptake of O_2 by the land biosphere and therefore amplifying the O_2 signal. Figure 22a shows the modelled changes in O_2 concentration along with O_2 observations at Weybourne, sampled at 10m height (Wilson 2012). The simulations generally follow the same trend as observations, with fluctuations in O_2 concentration varying between about -40 ppm and 8 ppm compared to the background value for October 2014. Most of the fluctuations observed are well captured by the model.

Statistical measures of the model performance in simulating CO_2 and O_2 concentrations are shown in Table 8. The values show that the average concentrations are overestimated by 3.0 ppm by the model. The standard deviation of the modelled O_2 concentrations is slightly low compared to the standard deviation of the observations. These differences are smaller for observed and modelled CO_2 concentrations. Discrepancies in the modelled CO_2 are likely due to the misrepresentation of the wind direction in the model (Chapter 3), whereas the poorer model performance in simulating O_2 as compared to CO_2 are more likely due to the OR_{in} values. Table 8 thus suggests that the values for OR_{in} is slightly high in Weybourne, as lower value for OR_{in} would result in larger fluctuations from the background value. Even though the hourly observations at Weybourne are more reliable than those from Lutjewad, it should be kept in mind that observations of atmospheric O_2 have an uncertainty of about 2 ppm (Barningham 2017).

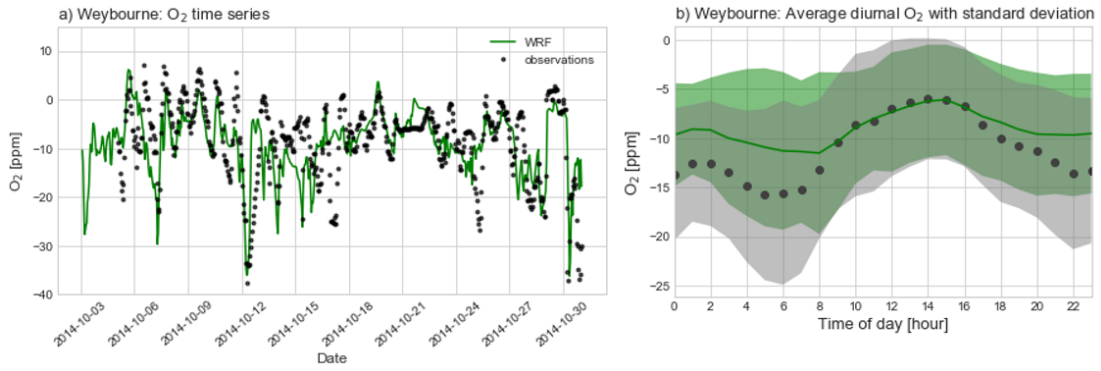

Figure 22: a) Time series of the total O_2 fluctuations and b) diurnal average of total O_2 as opposed to the background, as modelled and observed at Weybourne during October 2014. The shading represents the standard deviation of the simulated and observed averages.

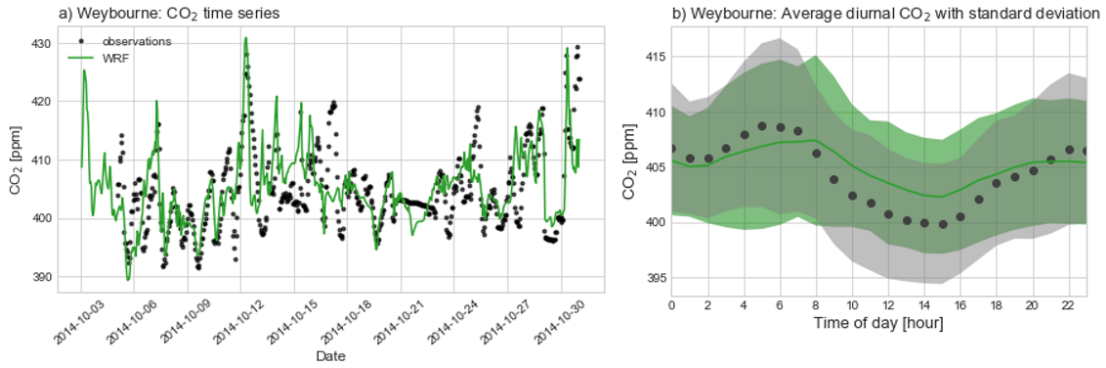

Figure 23: a) Time series of the total CO_2 and b) diurnal average of total CO_2, as modelled and observed at Weybourne during October 2014. The shading represents the standard deviation of the simulated and observed averages.

Table 8: Most important quantitative measures of CO_2, O_2, and wind direction model performance at Weybourne.

	$\overline{O}$	$\overline{P}$	sd_O	sd_P	RMSE	d	R^2
CO_2	404.4	404.8	6.8	6.0	5.63	0.78	0.38
O_2	-11.3	-8.3	7.7	6.4	6.7	0.75	0.34
Wind direction	214	219	58.2	60.3	77.8	0.47	0.02

The simulated average diurnal cycle of O_2 (as shown in Figure 22b) shows a similar trend as the observed average values. However, the simulated average is slightly high and the amplitude of the cycle is underestimated. During the nighttime and early morning, the O_2 uptake is generally underestimated by a maximum of 4.2 ppm on average, whereas the maximum is better captured by the model. The underestimation in O_2 uptake in the average diurnal cycle can have multiple causes. The overestimation of the mean O_2 is likely due to an overestimation in OR_{in}. The underestimation in diurnal fluctuations in O_2 concentration are also shown in the comparison of simulations and observations of the average diurnal cycle of CO_2 at Weybourne, as shown in Figure 23b. This suggests that some of the discrepancies between the observed and simulated average diurnal O_2 are due to misrepresentations in CO_2 concentrations. This could again be due to a poor representation of the wind direction. It could also be that photosynthesis and respiration are underestimated by the model. These processes would mitigate the O_2 decrease during the day and reinforce the O_2 decrease during the night. Other possible causes could be the misrepresentation of anthropogenic CO_2 emissions, or misrepresentation of the boundary layer development at Weybourne. Since Weybourne is located on the coast, boundary layer development is not as pronounced as it would be over land. Larger fluctuations in

boundary layer height would result in larger fluctuations in CO_2 concentration. This means that the underestimations in CO_2 fluctuations would be due to an underestimation of boundary layer development in the model. The average simulated boundary layer height fluctuates between about 600 m at night and 920 m during the day on average. Bannan et al. (2017) measured an average boundary layer height fluctuating between 300 m at night increasing to 1300 m in the morning up until 1800 m in the afternoon in March and April at Weybourne. Even though boundary layer development is expected to be smaller in October as compared to March/April, this comparison to literature does offer a potential explanation as to the underestimation in diurnal variation of the compound concentrations. Furthermore, it is important to note that the simulations in domain 2 are over a 12x12 km domain, whereas the observation data from Weybourne can be influenced by local processes. It could be that the averaging of concentrations over the 12x12 km grid cell smoothens out the simulated compound concentrations, resulting in lower fluctuations.

5 Simulating (fossil fuel) CO_2, fossil fuel O_2, and fossil fuel oxidative ratios

One of the main objectives of this research is to introduce atmospheric oxygen as a tracer for fossil fuel emissions in urban areas. The main processes influencing the oxygen concentration on short time scales are fossil fuel burning, the uptake and release of O_2 through respiration and photosynthesis, and O_2 exchange with the ocean. One of the advantages of modelling O_2 fluctuations as opposed to measuring O_2 concentrations, is that the different processes are introduced as separate tracers and can thus be separately analysed (as shown in Section 4.1). In order to investigate fossil fuel CO_2 sources, variation in O_2 concentrations due to fossil fuel burning (ffO_2) are of interest. The modelled CO_2 and fossil fuel CO_2 ($ffCO_2$) are first discussed. After a general overview of the (fossil fuel) CO_2 concentrations and CO_2 emission sources in the study areas is obtained, the fluctuations in ffO_2 are discussed, as well as the oxidative ratios (OR_{ff}) that follow from this. This is done for Rijnmond (Section 5.1), the north of Groningen (Section 5.2), and North Norfolk (Section 5.3). The applicability of OR_{ff} values during specific emission events to identify $ffCO_2$ emission sources is explored in Section 5.4.

5.1 Fossil fuel CO_2, O_2, and OR_{ff} at Rijnmond

5.1.1 CO_2 concentrations

CO_2 concentrations in Rijnmond vary between about 390 and 480 ppm during October 2014. Figure 24 shows the simulated CO_2 concentrations at Zweth. As depicted in Figure 24b, winds originate mostly from the south southwest. As the wind originates from the south, concentrations are in the higher range; generally above 420 ppm. This is due to the location of the industrial area Botlek situated south to southwest from Zweth, and the city of Rotterdam situated southeast from Zweth (as can be seen in Figure 5). On the occasion the wind originates from the north, concentrations are in the lower range; below 420 ppm.

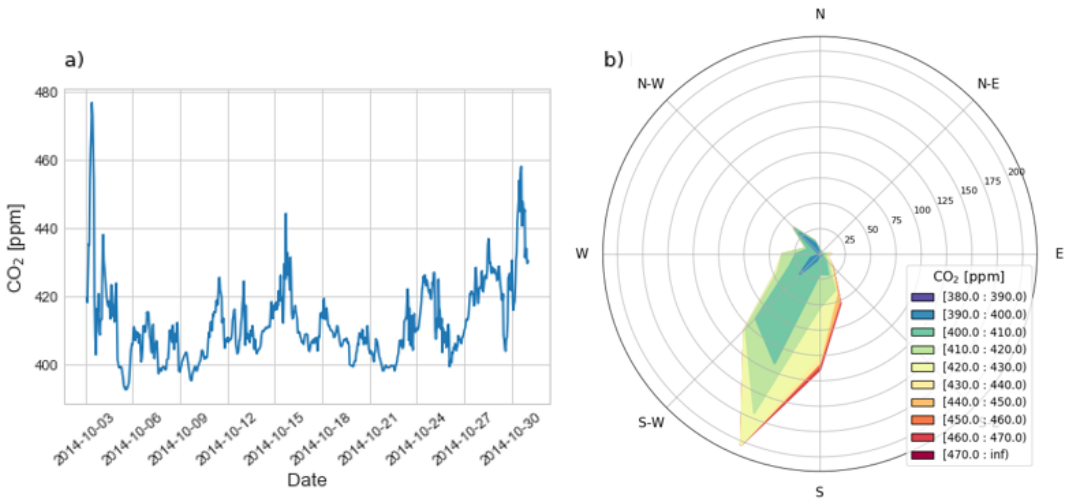

Figure 24: a) Time series of total CO_2 concentration and b) wind rose showing the origin of the CO_2 concentrations, simulated at Zweth.

In section 4.2.1, the average diurnal cycle of CO_2 concentrations at Zweth is discussed. From the time series of the total CO_2 concentration over the entire month in Figure 24a, the diurnal pattern is not easily distinguished. A few moments with exceptionally high atmospheric CO_2 concentrations can be distinguished as 'high CO_2 events' or 'CO_2 peaks'. This is during the 3rd, 15th, and 30th of October. These events will be further analysed in Section 5.4.

5.1.2 Dominant CO_2 emission sources

Most of the fluctuations in CO_2 concentrations at Zweth are due to fossil fuel emissions in the area. The various CO_2 emission sources distinguished in the model are described in Section 1.1.2 and Section 2.3.1. Not all anthropogenic emission sources are equally influential in Zweth, as depicted in Figure 25b. Overall, CO_2 emissions from industrial production processes (SNAP category 03/04) are the largest contributors to fossil fuel CO_2 at the surface. These emissions are on average responsible for more than 38% of the simulated anthropogenic CO_2 at Zweth in October 2014. Non-industrial processes, road transport, and power generation are other large emission sources, contributing to about 20%, 19%, and 12% of all anthropogenic CO_2 simulated at Zweth, respectively. It is expected that the relative importance of the emission sources varies with height, since emissions of certain production processes and power generation plants are stack emissions. The analysis in this chapter is however limited to surface concentrations only.

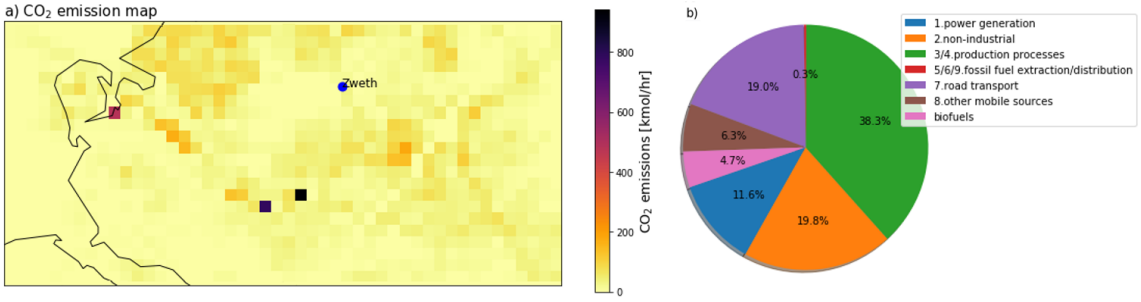

Figure 25: a) Map of the average ffCO_2 emissions in kmol/hr in Rijnmond and b) the relative importance of various ffCO_2 emission sources (per SNAP category) in Zweth (after transport) for October 2014.

5.1.3 Fossil fuel O_2 and $OR_{(ff)}$

The CO_2 emission categories are linked to the uptake of O_2 through the average oxidative ratio (OR_{in}) per category as described in Section 2.3.2 (Table 1). The average ffCO_2 and the consequential O_2 uptake (ffO_2) in Rijnmond are shown in Figure 26a and b. The maps are averages for October 2014 as simulated by WRF. It is apparent that ffO_2 uptake follows the patterns of ffCO_2 emissions. As expected, ffCO_2 is largest around the industrial area and the harbour, and is then transported by the southwesterly winds. From the ffCO_2 emissions and the additional ffO_2 uptake, a time-average OR_{ff} can be calculated as shown in Figure 26c. This value is variable due to the processes of atmospheric transport and mixing, and thus not necessarily equal to the value assigned to the emissions in its particular grid cell. The OR_{ff} shows spatial fluctuations over the area, ranging between -1.49 and -1.56. These values are, as expected, lower than the world average OR of -1.4 for fossil fuel burning due to the above average gas use in the Netherlands. OR_{ff} values closer to -1 can be found in the same areas as the fossil fuel CO_2 plumes of the industrial area and harbour, suggesting that the usage of coal and oil are larger in those regions. In other areas, gas would be a relatively more important fuel source. This is however based on the average OR_{in} per SNAP category in the Netherlands, and thus not specifically for Rijnmond. An attempt to improve on this is presented in Chapter 6.

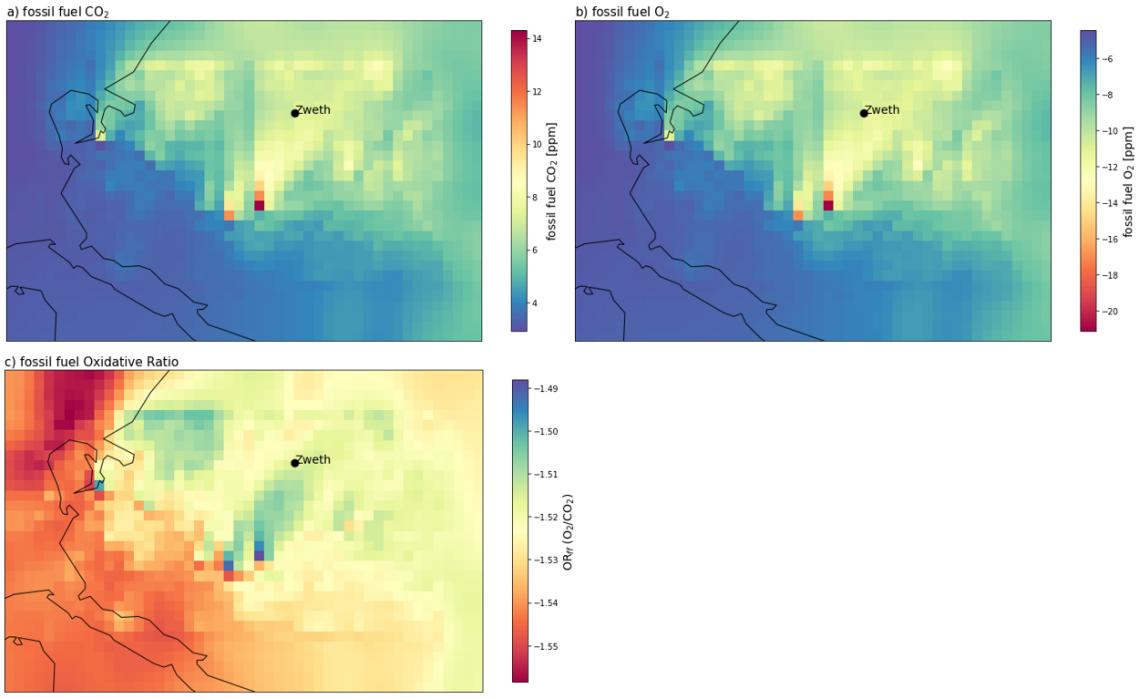

Figure 26: Maps of a) the average fossil fuel CO_2, b) average fossil fuel O_2, and c) average OR_{ff} over Rijnmond for October 2014. The location of the measurement station Zweth is indicated on the maps.

O_2 uptake and release and ORs do not only show spatial variation, but also variation in time. In this study, the model run is limited to one month due to the required simulation time. Because of this, only variations on a relatively short time scale can be studied. Seasonal variations are thus not shown, although they are expected to be apparent as well, with a higher amount of net O_2 uptake in winter due to larger emissions and less biosphere release of O_2. Furthermore, certain fuel types might gain relative importance as the seasons change, resulting in a seasonal variation in OR_{ff}. For instance, increased heating might result in a lower OR_{ff} during wintertime. This seasonal fluctuation is expected to have an amplitude of 0.03 (I. Van Der Laan-Luijkx 2010) to 0.04 (Steinbach et al. 2011) on the northern hemisphere.

The average diurnal $ffCO_2$ concentration as simulated for October 2014 at Zweth shows the highest concentrations at night and in the morning, with a maximum at 8:00 LT and a minimum at 16:00 LT (Figure 27a). The increase in concentrations in the morning are due to the increased anthropogenic activity and the persistence of the nocturnal boundary layer in winter, trapping anthropogenic CO_2 emissions. This causes an increase in $ffCO_2$ of 4 ppm on average.

On a diurnal time scale, ffO_2 concentrations show a low in the morning hours, around 8:00 and 9:00 LT, in line with the increasing CO_2 emissions (Figure 27a). From that time on, the O_2 concentration increases again. This can be attributed to the decrease in CO_2 emissions in between commuting hours and the growth of the atmospheric boundary layer (ABL). As the ABL grows, mixing of the air and entrainment takes places. In the case of oxygen, this entrainment is with air containing higher O_2 concentrations (i.e. closer to the background value, in reality around 20.95%).

The OR_{ff} also shows variation in time. It should be noted that a larger OR_{ff} is not necessarily related to larger CO_2 emissions or O_2 uptake or release. Instead, variations in OR_{ff} are due to temporal factors influencing the relative importance of the different fuel mix types. For instance, during the morning and afternoon commuting hours, transport (SNAP category 07) will have a relatively large contribution to the CO_2 emissions. During these times, OR_{ff} values are pulled more towards about -1.5 (Figure 27b). Other important emission sources in Rijnmond are production processes and energy production (SNAP categories 01 and 03/04). These processes do not have a clear diurnal variation, and are thus relatively more important when other emissions sources are smaller, causing lower than average OR_{ff} values at night and around noon. It should be noted that the average diurnal variation in simulated OR_{ff} is limited, with an average variation of 0.022.

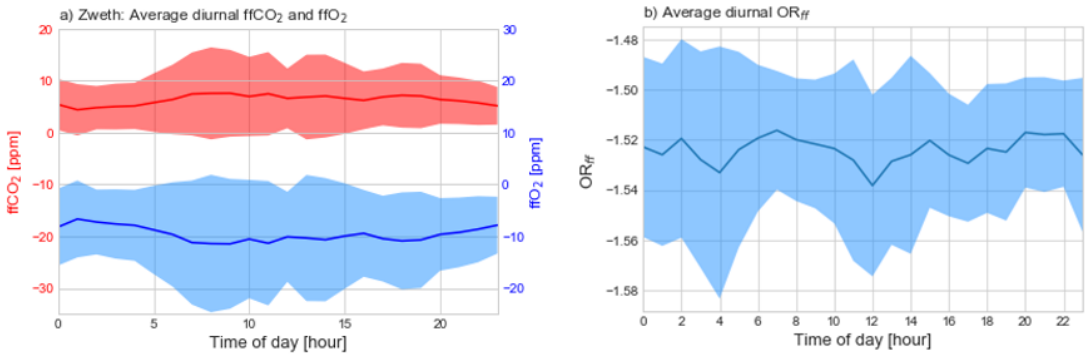

Figure 27: Average diurnal cycle of a) $ffCO_2$ and ffO_2 concentration, and b) OR_{ff} in Zweth for October 2014.

5.2 Fossil fuel CO_2, O_2, and OR_{ff} at the north of Groningen

5.2.1 CO_2 concentrations

As opposed to Rijnmond, the north of Groningen is a more rural area with less CO_2 emissions. As a consequence, the total CO_2 concentration is smaller, showing weaker variations. In Lutjewad total CO_2 concentrations vary between 397 and 441 ppm during October 2014 (Figure 28a), in line with measurements done by I. Van Der Laan-Luijkx (2010) at the site. Just as simulated at Zweth, winds at Lutjewad also generally originate from the south southwest. This means that the air at Lutjewad has traveled over land and is thus expected to be influenced by the biosphere and anthropogenic emissions (south) southwest, causing relatively high fluctuations in CO_2 concentration for a coastal station.

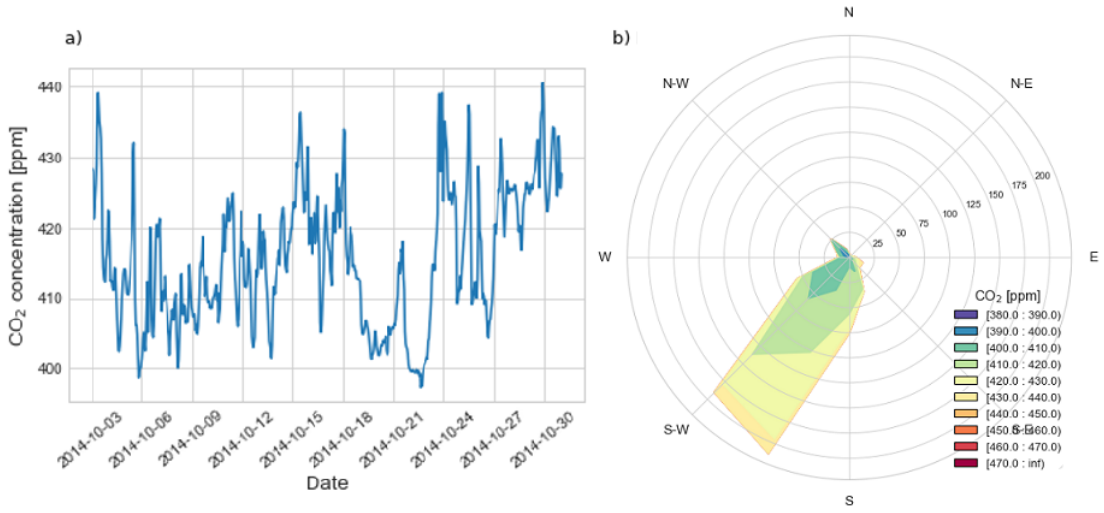

Figure 28: a) Time series of total CO_2 concentration and b) wind rose showing the origin of the CO_2 concentrations, simulated at Lutjewad.

The segregation of emission peaks or high CO_2 events from the time series in Figure 28 is more difficult than for Zweth. This is because the CO_2 peaks are lower, and the signal is relatively more influenced by the biosphere. However, based on the modelled $ffCO_2$ signal (as shown in Section 4.2), three emission events are selected which will be further analysed in Section 5.4.

5.2.2 Dominant CO_2 emission sources

As mentioned in Section 5.2.1, air at Lutjewad is influenced by anthropogenic CO_2 emissions due to the prevailing wind direction during October 2014. Figure 29a shows the average CO_2 emissions as modelled for the model domain in which Lutjewad is located. It can again be seen that emissions in the area around Lutjewad are smaller than those in Rijnmond. Nearby cities Leeuwarden and Groningen can be distinguished from this figure (further described in Section 2.1). Considering the south southwesterly winds during October 2014, air at Lutjewad can be expected to be influenced by emissions from Leeuwarden.

The relative importance of emissions from the city is also portrayed in Figure 29b, as road transport (SNAP category 07) is on average the most important emission source at Lutjewad. Industrial production processes (SNAP category 03/04) are however almost equally influential, responsible for an average of about 23% of all CO_2 emissions. Overall, CO_2 emissions at Lutjewad find their origin in a mix of SNAP categories, all (with the exception of category 05/06/09) of significant importance at the site.

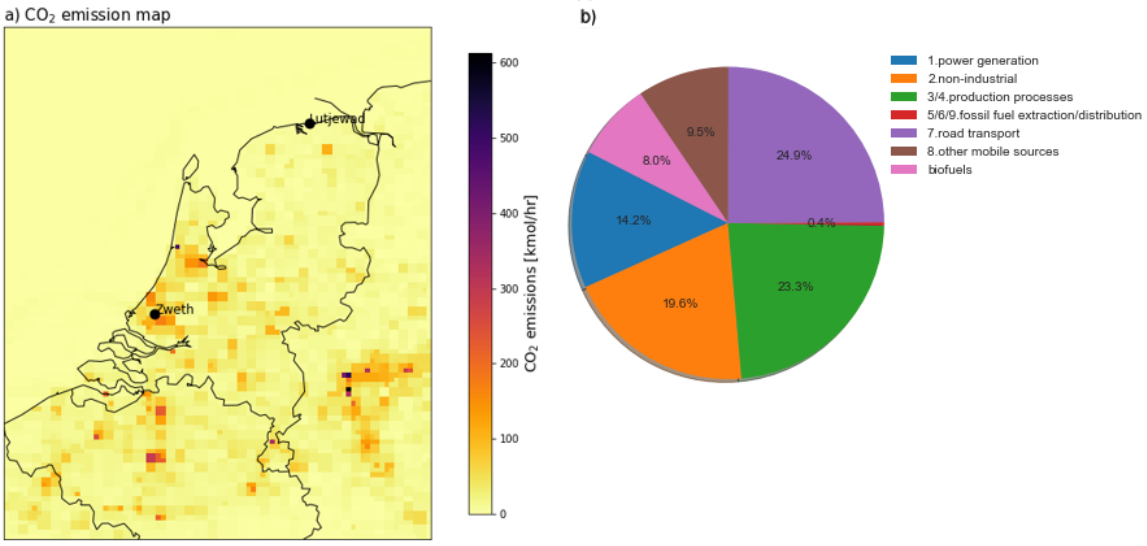

Figure 29: a) Map of the average $ffCO_2$ emissions in kmol/hr in the Netherlands and b) the relative importance of various CO_2 emission sources (per SNAP category) in Lutjewad (after transport) for October 2014.

5.2.3 Fossil fuel O_2 and $OR_{(ff)}$

Maps of the average $ffCO_2$ and consequential ffO_2 over the Netherlands are shown in Figure 30a and b. The location of study sites Zweth and Lutjewad are indicated in the figures. Again,

it can be seen that ffO_2 is lowest where $ffCO_2$ is highest. Some cities can be identified, and transport of the emissions towards the northeast is visible. The average fossil fuel oxidative ratio (OR_{ff}) that follows from Figure 30a and b is shown in Figure 30c. It can be seen that OR_{ff} in Groningen is lower than OR_{ff} in Rijnmond. This suggests a larger amount of gas use in Groningen as opposed to Rijnmond. Figure 30c shows the OR_{ff} values after transport. It can be seen that relatively high OR_{ff} values originating in Belgium are transported and still visible over the southern part of the Netherlands. The Ruhr area in Germany shows interesting results. $ffCO_2$ concentrations are the highest around this area over the entire domain. As a result, O_2 uptake is also largest. The calculated OR_{ff} shows a relatively strong spatial fluctuation over this area, with the highest OR_{ff} value in the domain north of Düsseldorf, and the lowest OR_{ff} in the domain south of Düsseldorf. With a difference in OR_{ff} of almost 0.1, the variation in dominant emission categories are evident. The values for OR_{in} are based on the average OR_{in} per emission category, resulting in a mix of fuel types. If the actual fuel type used at certain locations were to be implemented into the model, these kind of differentiation in emission sources is likely to become even more evident.

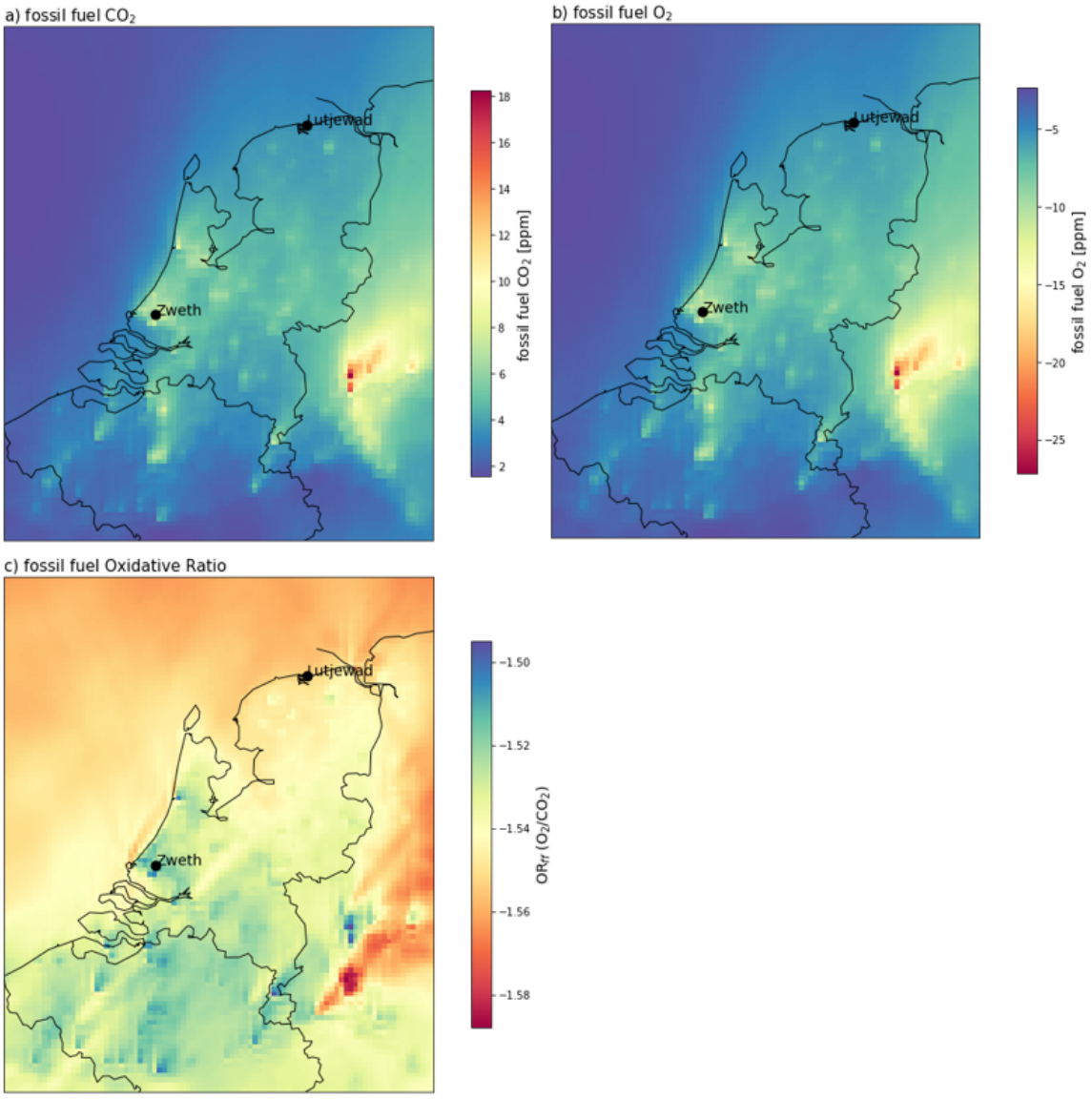

Figure 30: Maps of a) the average fossil fuel CO_2, b) fossil fuel O_2, and c) average OR_{ff} over the Netherlands (model domain 3) for October 2014. The location of the measurement stations Zweth and Lutjewad are indicated on the maps.

The average diurnal cycle of $ffCO_2$ is shown in red in Figure 31a. It can be seen that the $ffCO_2$ concentrations are generally highest at midnight, decrease about 2.5 ppm until 8:00 LT, and then increase again. This is not the diurnal trend which may be expected. The low $ffCO_2$ at 8:00 LT suggests relatively clean air. Around this time, the standard deviation is also smallest, showing a relatively constant concentration around this time. After 8:00 LT $ffCO_2$ concentrations increase due to emissions. On the one hand, the increase is limited due to ABL growth during the day. The relatively large fluctuation in average $ffCO_2$ in Lutjewad compared

to Zweth considering its remote location could be attributed to its limited ABL growth due Lutjewad's location at the coast, causing accumulation of the emissions that do occur or are transported toward the location.

The average diurnal cycle of ffO_2 as shown in Figure 31a follows the inverse trend of $ffCO_2$: Concentrations are highest around 8:00 LT, when the air is less influenced by human activity, after which ffO_2 decreases about 6 ppm until it reaches its low around midnight. The average values for OR_{ff} are shown in Figure 31b. An average OR_{ff} of -1.551 is simulated, with an average variation of 0.017 (0.005 smaller than at Zweth).

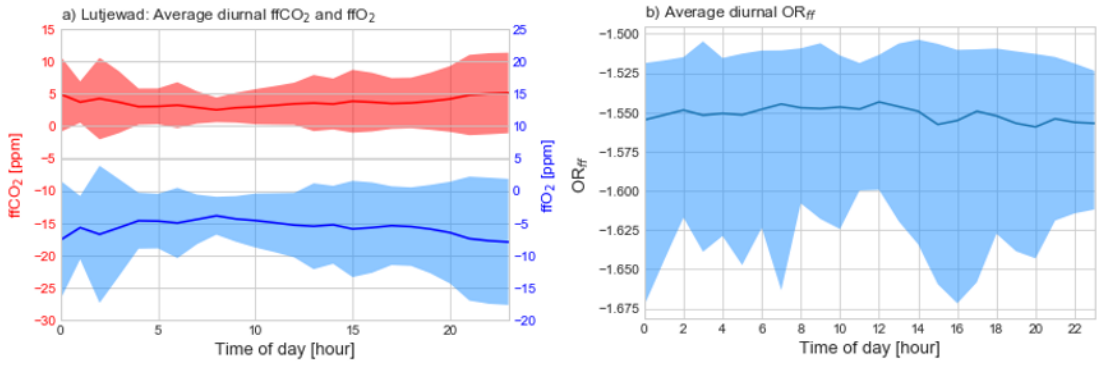

Figure 31: Average diurnal cycle of a) $ffCO_2$ and ffO_2 concentration, and b) OR_{ff} in Lutjewad for October 2014.

5.3 Fossil fuel CO_2, O_2, and OR_{ff} at North Norfolk

5.3.1 CO_2 concentrations

As is apparent in the site descriptions in Section 2.1, North Norfolk is less urbanised than Rijnmond. This results in less CO_2 emissions and consequently smaller total CO_2 concentrations. At Weybourne, CO_2 concentrations vary between about 390 and 430 ppm during October 2014 (Figure 32). Weybourne is a background station. However, due to the prevailing wind direction, CO_2 concentrations still show relatively large fluctuations as compared to concentrations observed at sea in this region by Pickers et al. (2016). These measurements show concentrations more constant around 390 ppm (for September 2014). Figure 32b shows winds originating mainly from the southwest. The largest concentrations originate from the south, potentially from the city of Norwich.

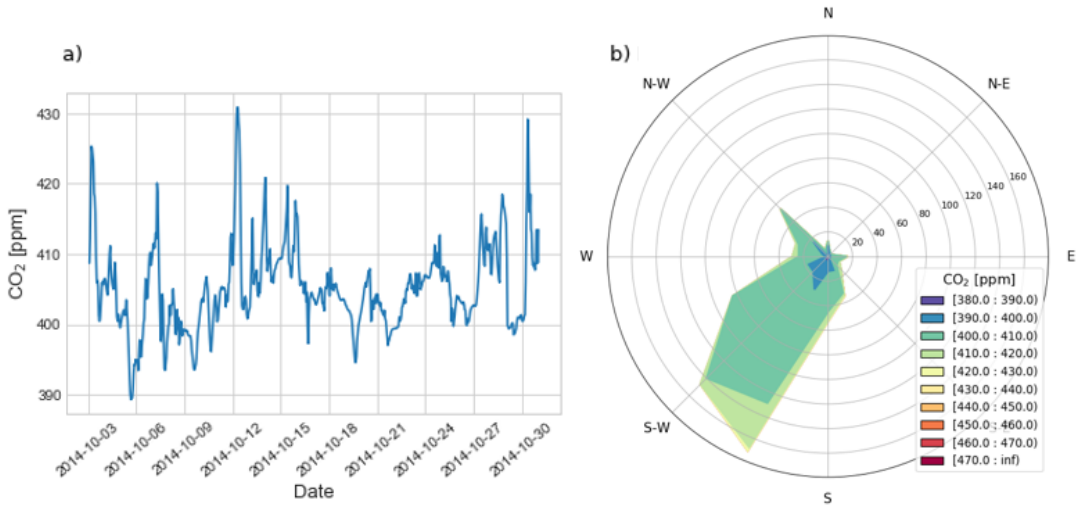

Figure 32: a) Time series of total CO_2 concentration and b) wind rose showing the origin of the CO_2 concentrations, simulated at Weybourne.

The time series for October 2014 in Weybourne shows numerous peaks with higher than average CO_2 concentrations. Even though ffCO_2 emissions are relatively small in Weybourne, some peaks in Figure 23a do coincide with anthropogenic CO_2 emissions in the area. It should be noted that the peaks are of a smaller magnitude than those identified in simulations for Zweth, however, they are still easily identified in the time series. The events of the 7^{th}, 15^{th}, 28^{th}, and 30^{th} are further analysed in Section 5.4.

5.3.2 Dominant CO_2 emission sources

The origin of the emissions at Weybourne differs from those at Rijnmond: Where in Rijnmond most of the fossil fuel CO_2 came from industrial production processes and power generation, in Weybourne the largest fossil fuel CO_2 source is road transport, similar to Lutjewad (SNAP category 07). Next to road transport, non-industrial processes, power generation, and industrial production processes, are large fossil fuel sources, responsible for about 23%, 18%, and 16% of anthropogenic CO_2 in Weybourne, respectively. The relatively large importance of road transport in Weybourne is very likely attributed to the city of Norwich, which is located about 40 km south.

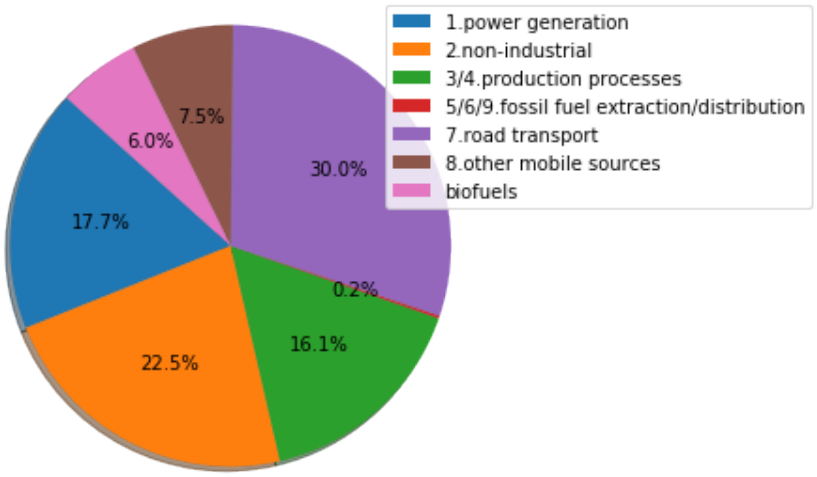

Figure 33: Relative importance of the various $ffCO_2$ emission sources (per SNAP category) in Weybourne after transport for October 2014.

5.3.3 O_2 fluctuations and OR

Average $ffCO_2$ concentrations, ffO_2, and OR_{ff} values are plotted for domain 2 (containing North Norfolk and Weybourne). These maps, shown in Figure 34, identify large cities as CO_2 emitting areas, and consequently the places where ffO_2 uptake is the largest. The average OR_{ff} varies over the domain, ranging between -1.50 and -1.60. Some differences in average OR_{ff} between cities can be identified. For instance, Paris the Ruhr area seem to be two of the largest emitters of fossil fuel CO_2 within the domain. The OR_{ff} around Paris is however higher than in the Ruhr area. This suggests that coal and oil are more important in the fuel mix in Paris than in the Ruhr area. It should however be noted that the values for OR_{in} used in the model are based on the average fuel mix used per SNAP category in the Netherlands. Considering these values, this thus means that power generation is a larger CO_2 source in the Ruhr area compared to Paris. The OR_{ff} may change if more information is known about the actual fuel mix used within the various regions over Europe. Since many of the power plants in the Ruhr area are coal-based power plants (RWE 2016), the actual OR_{ff} is expected to be considerably larger.

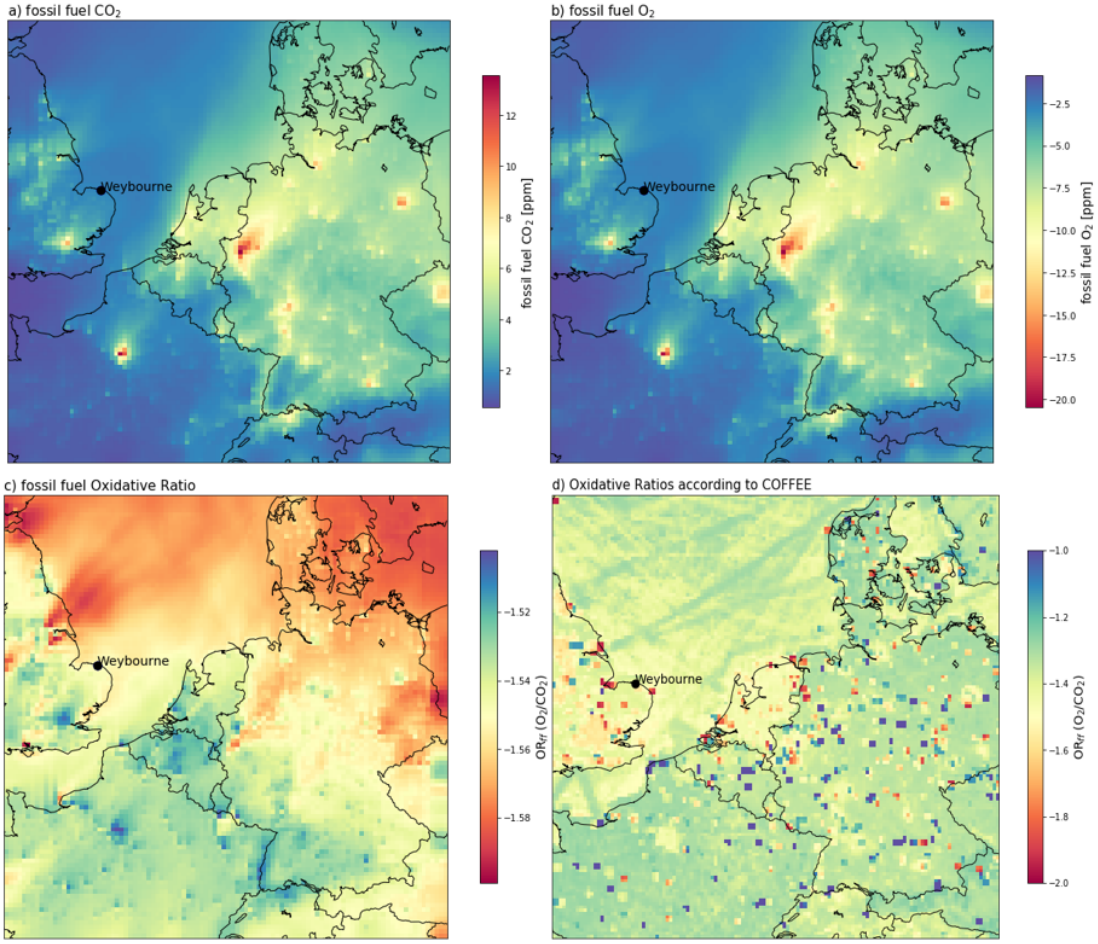

Figure 34: Maps of a) the average ffCO_2, b) average ffO_2, and c) average OR_{ff} over Europe for October 2014 as simulated by WRF. d) shows the OR according to the COFFEE dataset by Steinbach et al. (2011). The location of the measurement station in Weybourne is indicated on the maps.

Figure 34c shows the average OR_{ff} that follows from this study for October 2014 after transport of the compounds. As mentioned, to calculate this, average OR_{in} values per SNAP category are used. In reality however, locations may be more dominated by the use of a specific fuel type. This would result in more spatial variation in OR_{in} and consequently more spatial variation in OR_{ff} over the domain. An example of this is shown in Figure 34d. This figure shows an OR as calculated by the O_2/CO_2 emissions per grid cell according to the CO_2 release and Oxygen uptake from the Fossil Fuel Emissions Estimate (COFFEE) dataset (Steinbach et al., 2011). In COFFEE, CO_2 emissions from the Emission Database for Global Atmospheric Research (EDGAR) at a 1x1° scale were combined with oxidative ratios at the national level. It contains spatial, as well as temporal variation. For more details and information about the

COFFEE dataset, please refer to Steinbach et al. (2011). Figure 34d shows the time-average OR for October 2014 according to this dataset. It can be seen that the spatial variation in OR over the domain is larger, and can vary significantly within relatively small distances. This figure however does not include transport of the emissions over the domain, which would smoothen out some of the strong regional variations in OR_{ff}. A database like COFFEE is likely to offer a more accurate input for OR_{in} compared to the Dutch average ORs per SNAP category to calculate ffO_2 on this (i.e. continental) scale. In the current study, this database was not used with the scale of one of the main objectives in mind; investigating fossil fuel sources in urban areas (i.e. Rijnmond). The 1x1° resolution of COFFEE is thus not appropriate to model O_2 on this regional scale. However, the database may be useful to model ffO_2 in the outer domains in the future.

The average diurnal cycle of $ffCO_2$ concentrations in Weybourne does not show a lot of variation. Concentrations increase during the day and decrease again at night, with an amplitude of only 0.4 ppm. As a consequence, ffO_2 in Weybourne also shows limited diurnal variation, with only slightly increased $ffCO_2$ concentrations on an average day. The average diurnal OR_{ff} does show a pattern, with an average of -1.550 and an amplitude of 0.01. OR_{ff} is relatively low during the night and relatively high during daytime. Road transport is an important emission source at Weybourne. The amount of road transport during the night is however expected to be limited. This would explain the OR_{ff} closer to -1.5 during the day. At night, energy production is a relatively more important source causing a decrease in OR_{ff}.

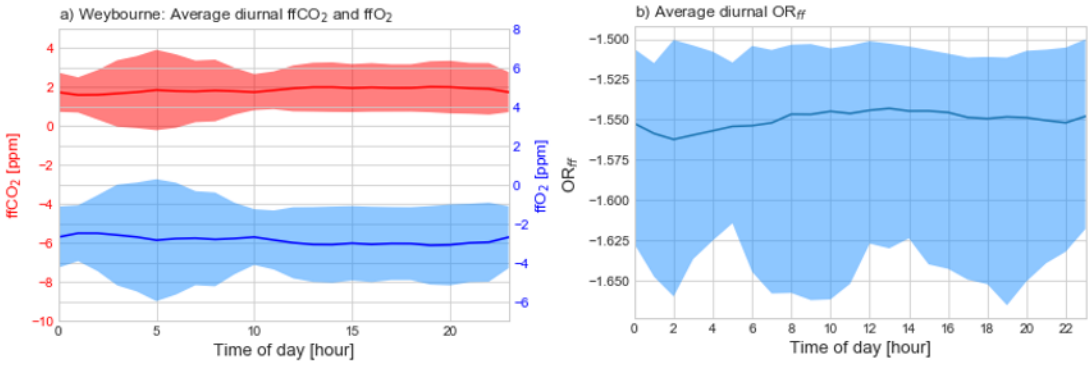

Figure 35: Average diurnal cycle of a) $ffCO_2$ and ffO_2 concentration, and b) OR_{ff} in Weybourne for October 2014.

5.4 CO_2 emission events

As found in Sections 5.1 to 5.3, when looking at a time series of CO_2 concentrations of October 2014, a number of moments with above average CO_2 concentrations can be distinguished. As these peaks are generally due to CO_2 emissions that follow from fossil fuel burning, they are often also accompanied by relatively low O_2 concentrations. From this information, not only average OR_{ff} values can be calculated (as previously done in this chapter), but also OR_{ff} values per specific event. This means that per event, based on the calculated OR_{ff}, suggestions can be done about the main fuel type responsible for and the origins of the high CO_2 concentrations.

5.4.1 CO_2 events at Zweth

The strongest CO_2 peaks simulated at Zweth are identified on the 3rd, 15th, and 30th of October. Information about the minimum and maximum $ffCO_2$ and ffO_2, along with the prevailing wind direction per event, are given in Table 9. The OR_{ff} that follows from this information is also included in this table. It is found that, for the main events at Zweth, the OR_{ff} is in the range between -1.49 and -1.56. This is within the range of the average OR_{ff} of -1.51 in Zweth. The values suggest the usage of a mix of fuel types, and thus no clear top contributor or source as to the CO_2 emission events can be derived from this without considering meteorological circumstances.

The OR_{ff} calculated for the 3rd of October, indicates relatively small contribution of power generation, and larger contribution of (industrial and non-industrial) production processes. Wind during this period generally originates from the south, confirming that the CO_2 simulated at Zweth on this day originates for the industrial area Botlek. The $ffCO_2$ peak simulated on the 15th has an OR_{ff} closer to -2. During this day, winds originate from the southwest, suggesting that the main contributor of the CO_2 concentration measured at Zweth is again Botlek. However, the contribution of a certain CO_2 plume coming from Botlek is more important during this event. This wind direction-OR_{ff} combination could thus be an indication of CO_2 originating from a power plant in the Botlek. The high CO_2 concentration on the 30th of October is marked by an OR_{ff} of -1.50, close to but slightly lower than the event on the 3th. During the 30th, however, winds were freeing from north to south via the east. This means CO_2 concentrations on this day in Zweth originate mainly from outside Rijnmond. The only influential CO_2 source

from within Rijnmond is Rotterdam city. The wind direction during this event results in a mix of CO_2 sources and consequently a rather average value for OR_{ff}.

Table 9: Minimum and maximum $ffCO_2$ and ffO_2, the corresponding OR_{ff}, and prevailing wind direction per CO_2 event at Zweth.

Peak date (day in October)	max $ffCO_2$ [ppm]	min $ffCO_2$ [ppm]	ΔCO_2 [ppm]	max ffO_2 [ppm]	min ffO_2 [ppm]	ΔO_2 [ppm]	OR_{ff}	wind direction
3	45	6	39	67	9	58	-1.49	south
15	31	6	25	47	8	39	-1.56	southwest
30	40	6	34	59	8	51	-1.50	freeing from north to south

5.4.2 CO_2 events at Lutjewad

For Lutjewad, the emission events of the 3rd, 7th, 15th, and 30th of October are chosen to be analysed. The minimum and maximum $ffCO_2$ and ffO_2, along with the OR_{ff} and prevailing wind direction per event are given in Table 10. In general it is more difficult to assign certain sources to the $ffCO_2$ concentrations measured and simulated at Lutjewad. This is because the CO_2 signals found for this location are weaker due to the smaller amount of $ffCO_2$ emissions in the area. Furthermore, the site is located in a remote area, meaning that the $ffCO_2$ emissions that do find their way to Lutjewad are more diluted and mixed with $ffCO_2$ from other sources.

In Lutjewad, more variation in OR_{ff} between the various emission events is found. The average OR_{ff} at the location is -1.55. During the event of the 3rd, the OR_{ff} is relatively close to -1. This suggests strong influences from (non-)industrial production processes (SNAP category 03/04) with origins in the south. During the 15th, the OR_{ff} is closer to the average, with a value of -1.52. The same SNAP categories are however still relatively important, pulling the OR_{ff} towards -1. This time however, the peak is stronger, and the wind direction suggests the source to be located more southeast of Lutjewad. The event on the 15th has a below average OR_{ff} of -1.57. This suggests that power generation (SNAP category 01) is relatively more influential during this emission event. Winds during this event are coming from the southwest. Finally, the event on the 30th has a similar OR_{ff} as the event on the 15th. This suggests similar source types between the two events. The wind at this time is variable, freeing from north to south within a few hours. This increases the difficulty of assigning a source to this emission event.

Table 10: Minimum and maximum $ffCO_2$ and ffO_2, the corresponding OR_{ff}, and prevailing wind direction per CO_2 event at Lutjewad.

Peak date (day in October)	max $ffCO_2$ [ppm]	min $ffCO_2$ [ppm]	$\Delta ffCO_2$ [ppm]	max ffO_2 [ppm]	min ffO_2 [ppm]	ΔffO_2 [ppm]	OR_{ff}	wind direction
3	4.3	1.1	3.3	6.7	1.8	4.9	-1.48	south
7	10.3	1.0	9.3	15.7	1.6	14.1	-1.52	southeast
15	9.8	0.5	9.3	15.2	0.6	14.6	-1.57	southwest
30	30.4	0.1	30.3	47.8	0.2	47.6	-1.57	freeing from north to south

5.4.3 CO_2 events at Weybourne

The events of the 7th, 15th, 28th, and 30th are investigated for Weybourne. Details per event are shown in Table 11. Just as is the case for Lutjewad, identification of the sources responsible for the emission events at Weybourne are more difficult than at Zweth due to its remote location. Furthermore, the concentrations during the events have a smaller magnitude than those analysed for Zweth, again due to the more remote location. The values for OR_{ff} calculated for the events at Weybourne are an indication of a fuel mix, where SNAP categories 02, 03/04, and 07 are important source types. These are substantial emission categories in this region, cumulatively responsible for almost 68% of all CO_2 emissions in Weybourne during the simulation period. Values of OR_{ff} below -1.53 are not found, giving a weaker indication to the importance of SNAP category 01 during the events.

Table 11: Minimum and maximum $ffCO_2$ and ffO_2, the corresponding OR_{ff}, and the prevailing wind direction per CO_2 event at Weybourne.

Peak date (day in October)	max $ffCO_2$ [ppm]	min $ffCO_2$ [ppm]	$\Delta ffCO_2$ [ppm]	max ffO_2 [ppm]	min ffO_2 [ppm]	ΔffO_2 [ppm]	OR_{ff}	wind direction
7	9.2	1.5	7.7	14	2.3	11.7	-1.52	southwest
15	3.4	0.5	2.9	5.1	0.8	4.3	-1.48	southwest
28	5.3	0.0	5.3	8.1	0.0	8.1	-1.53	south southwest
30	7.3	0.2	7.1	11.0	0.5	10.5	-1.48	south southeast

The values for OR_{ff} per event do not vary much between the different dates. This could be due to mixing and dilution of the concentrations before the site is reached. However the 12x12 km grid size on which the values are simulated are also likely to contribute to this lack in variation. This averages out local affects that emission sources might have on the OR_{ff}. The wind directions are similar in all cases, with winds direction generally varying between 180

and 250° during the events on the 7th, 15th, and 28th of October. The last event stands out, with winds originating from the south southeast, where the city of Norwich is located. This is expected to decrease the OR_{ff} due to the relatively large amount of road traffic (SNAP categories 07). This is however not shown through the calculated OR_{ff}, which could again be due to mixing of concentrations. It should however also be mentioned that the OR_{ff} calculated for the events are less accurate due to the lower peaks and lows in CO_2 and O_2 respectively, leading to a larger relative error in the identification in the minimum and maximum concentrations.

6 Source specific OR_{in}

Of some CO_2 point sources in Rijnmond, the exact fuel type that is used is known. This information is used to calculate a more accurate OR_{in} value which can be assigned to the grid cells containing these point sources. The results of this method are shown in Figure 36 and further discussed in Section 6.1. In Section 6.2, the CO_2 emission events at Zweth discussed in Section 5.4 are again analysed and compared to earlier results.

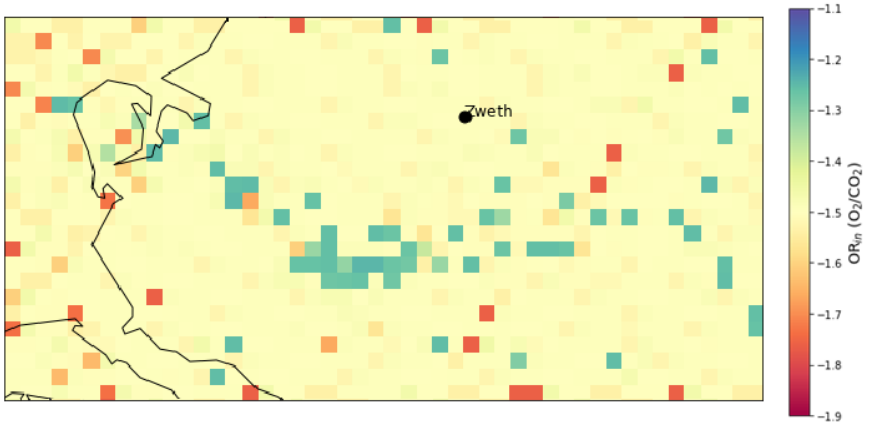

Figure 36: Map of source specific OR_{in} values as model input over Rijnmond.

6.1 O_2 fluctuations and OR_{ff}

The CO_2 point sources in Rijnmond consist of coal, oil, and gas burning industries. The amount of coal and oil usage in Rijnmond are however larger than they are on average over the Netherlands. This results in values for OR_{in} closer to -1 in the study area using this method. This is especially the case around the industrial area, as can be seen in Figure 36. On the borders of the domain, OR_{in} values are generally closer to -2, however, large areas within the domain do not have a distinct fuel type assigned to them and are thus assigned the average SNAP category values of around -1.5 (shown in Table 1). The OR_{in} closer to -1 around the industrial area in Rijnmond results in smaller fluctuations in ffO_2 concentration, and lower values for average OR_{ff} over the entire domain, as can be seen in Figure 37a and b, respectively. OR_{ff} values in Rijnmond fluctuate spatially between -1.37 and -1.51 on average, compared to OR_{ff} varying spatially between -1.49 and -1.56 in the analysis in Chapter 5. This is due to the increased

importance of coal (and oil) as fuel sources in Rijnmond in this method. OR_{ff} values are lowest around the industrial area in both cases. The values are however pulled more towards -1 compared to the surrounding areas when fuel types of point sources are specifically identified: The areas closer to the harbour and industry undergo a change in OR_{ff} of 0.12, whereas the area south of the industries undergo a change in OR_{ff} of 0.04.

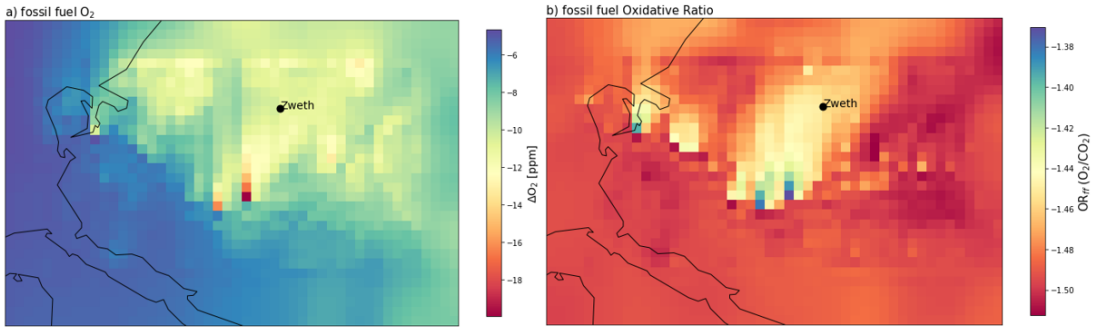

Figure 37: Map of a) average ffO_2 and b) average OR_{ff} in Rijnmond for October 2014, calculated using the source specific OR_{in}.

The average diurnal $ffCO_2$ is not influenced by the introduction of the source specific OR_{in}, and is thus the same as the discussed in Chapter 5. The ffO_2 at Zweth that follows from this does however deviate slightly through the introduction of the source specific OR_{in}. On average, ffO_2 concentrations are slightly higher, with an average of -8.7 ppm compared to -9.6 ppm, and an average diurnal variation of 4.4 ppm compared to 4.9 ppm when using the source specific OR_{in} compared to the average OR_{in} per SNAP category. The shape of the diurnal cycle in ffO_2 is not affected when switching between the two methods.

The average diurnal OR_{ff} shows some notable deviations from the diurnal cycle shown in Chapter 5. When the source specific OR_{in} is used to simulate O_2 concentrations, the average diurnal OR_{ff} is closer to -1, more variable, and shows peaks and lows at different times of the day. The average OR_{ff} in Zweth is -1.452, with a variation of 0.033 (compared to the average of -1.524 with a variation of 0.022 using the SNAP average OR_{in}). Using the current method, OR_{ff} in Zweth is lowest around 8:00 and 17:00 LT, and in the (late) evening. The OR_{ff} is around -1.47 during commuting times, and increases around noon and in the late night. The increased OR_{ff} at these times could be due to the relative importance of the point sources burning coal and oil. Many of the point sources included in this method are power generation plants and oil refineries

(SNAP category 01) which actually decreased the OR_{ff} calculated in Chapter 5. These changes in OR_{in} are the main contributor to the differences in average diurnal OR_{ff} between the two methods. The simulated oxygen in Rijnmond cannot yet be validated due to the current lack of observations in this area. However, the method described in this Chapter is more in agreement with earlier research done by Steinbach et al. (2011). In this research, a similar diurnal cycle in OR_{ff} is found, with variations of 0.04.

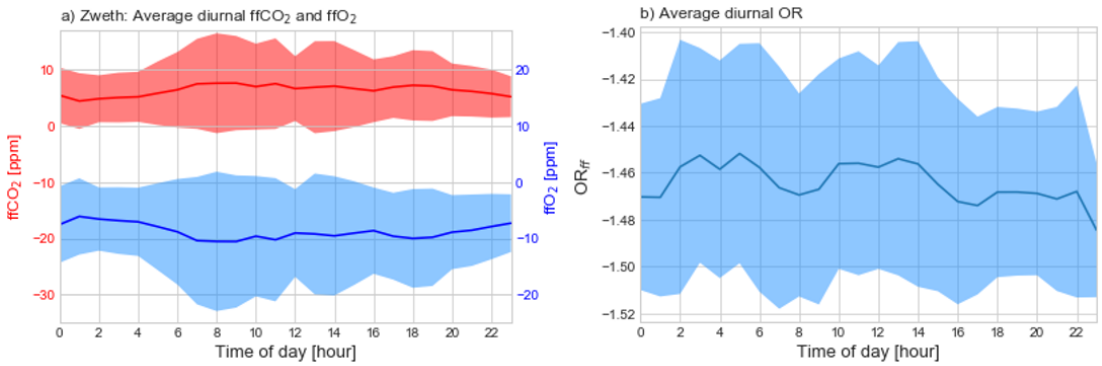

Figure 38: Average diurnal cycle of a) $ffCO_2$ and ffO_2 concentration, and b) OR_{ff} in Zweth in October 2014 simulated using source specific OR_{in}.

Whether the simulated ffO_2 concentrations and the values for OR_{ff} that follow from the method using the source specific OR_{in} values are more accurate than those calculated using the method using the SNAP average OR_{in} cannot be validated, since measurements of atmospheric O_2 concentrations are not yet being conducted at Zweth at this moment. It is expected that the source specific OR_{in} values are closer to reality and will therefore yield more accurate results. However, the actual amount of emission sources for which a specific fuel type is known is still limited. This method could therefore only be applied to Rijnmond at this moment. Furthermore, it is found in Chapter 4 that the largest discrepancy in the simulation of atmospheric O_2 concentrations is also found in the simulated CO_2 concentration. The modelled O_2 concentrations depends on the (negative) O_2 emissions, which are linked to CO_2 emissions. From this it follows that the errors are due to the simulation of the wind direction, rather than the values for OR_{in} that are used. Some recommendations on how the modelling of O_2 can be further improved will be discussed in Chapter 7.

6.2 CO_2 emission events

The emission events in Zweth described in Section 5.4 are again analysed, this time simulated using the source specific OR_{in}. Information about the minimum and maximum $ffCO_2$ and ffO_2, along with OR_{ff} per event are given in Table 12. The values for OR_{ff} found are closer to -1 than those found in Section 5.4, again indicating the relative importance of coal and oil as a fuel source in Rijnmond. The OR_{ff} found for the events vary around the average of -1.45, ranging between -1.50 and -1.32. The deviation from the average is the largest for the event on the 15th.

Table 12: Minimum and maximum $ffCO_2$ and ffO_2, corresponding $\Delta ffCO_2$ and ΔffO_2, and the corresponding OR_{ff} per CO_2 emission event at Zweth, simulated using the source specific OR_{in}.

Peak date (day in October)	max $ffCO_2$ [ppm]	min $ffCO_2$ [ppm]	$\Delta ffCO_2$ [ppm]	max ffO_2 [ppm]	min ffO_2 [ppm]	ΔffO_2 [ppm]	OR_{ff}	wind direction
3	45	6	39	64	8	56	-1.43	south
15	31	6	25	40	7	33	-1.32	southwest
30	40	6	34	57	6	51	-1.50	freeing from north to south

On October 3rd, a $ffCO_2$ peak is simulated with a OR_{ff} of -1.43. During this time, winds originate from the south. This means air is coming from the industrial area Botlek and the city of Rotterdam. The OR_{ff} suggests relatively strong influences of coal and oil burning. During this event, Zweth is not directly affected by the major point sources in Rijnmond as indicated in Figure 25a. The ffO_2:$ffCO_2$ signal is thus expected to be a result of the mixing of various emission sources with their origin mainly in Botlek. The method described in Section 5.4 resulted in an OR_{ff} of -1.49 during this event. This shows the influence of the higher OR_{in} as a result of the relatively large amount of coal and oil use in Botlek.

The event on the 15th of October occurs during southwesterly winds. During this time, Zweth is downwind of two of the strong point sources in Rijmond. These point sources are easily distinguished in the map showing the average $ffCO_2$ emissions over Rijnmond in Figure 25a. The point sources are a power generation plant (SNAP category 01), and a manufacturing/production process factory (SNAP category 03/04). These two point sources use coal and oil as a power source, respectively. This is indeed reflected in the relatively low OR_{ff}, suggesting a mix of mainly coal and oil during the event. Furthermore, the OR_{ff} of -1.56 as calculated in Section 5.4 can be assigned to the importance of power generation plant using coal. In this

method the OR_{in} as modelled for this plant is set to -1.762 (1).

The wind directions during the emission event on the 30th already suggest that the $ffCO_2$ concentrations during this event do not originate from within Rijnmond to the same extent as they do during the other emission events. This is also reflected in the OR_{ff}, which is 0.05 below the average of -1.45. This means that gas and oil usage are more important during this emission event. The wind originates largely from outside the domain, where the OR_{in} is again more influenced by the average OR_{in} per SNAP category for the Netherlands. The only main source within the range upwind of Zweth during this emission event is Rotterdam city, from which emissions are expected to find their origin mainly in oil and gas, resulting in a relatively low OR_{ff} after transport at Zweth. As a result of the wind originating from outside of the industrial area, the OR_{ff} as modelled here and in Section 5.4 shows no difference.

7 Discussion

Oxygen was introduced into the regional model WRF-chem in order to study the importance of the various fossil fuel types (i.e. coal, oil, and gas) and improve fossil fuel carbon dioxide estimates in urban areas. Until now, O_2 had not been included in WRF-chem or similar, regional models. This means that this 'new' compound had to be introduced from scratch. Therefore, along with the time restrains of this research, there is still a considerable amount of research that can be done to improve the model results. Likewise, an extension of the analysis on the current results is recommended to fully reach the objectives posed in this research. In the following sections, some important modelling methods and results are discussed in order to give insight in potential points of improvement in the currently used methods. Based on this, recommendations are done in order to improve on modelling of O_2 and answer the posed research questions with more certainty.

7.1 Model uncertainties and recommendations

O_2 is modelled based on uptake through fossil fuel burning, exchange with the land biosphere, and exchange with the ocean. Considering the general aim of this research, O_2 fluctuations due to fossil fuel burning are most important. However, in order to complete the modelling and compare the model outcome to measurements, land biosphere and ocean exchange are also implemented.

7.1.1 Ocean exchange

O_2 exchange from the ocean is introduced in the model based on the Atmospheric Potential Oxygen (APO) inversion modelling as done by Rödenbeck et al. (2008). This is however a global model with a coarse resolution as compared to the WRF-chem regional model resolutions. There is thus some uncertainty in the precision of the ocean O_2 exchange as implemented on this regional scale. The ocean exchange is found to have a relatively small influence on the O_2 concentration on the time scales as studied in this research, especially in urban areas. The potential for improvement of the overall O_2 fluctuation modelling is thus relatively small here.

7.1.2 Biosphere exchange

The fossil fuel and land biosphere exchange is based on the exchange of CO_2 from these components, and the Oxidative Ratio (OR) coupled to the process. The OR used as model input (OR_{in}) for the land biosphere is set to -1.1. This value is debated in literature, and is found to vary within different vegetation and soil types (Worrall et al. 2013; Masiello et al. 2008; Hockaday et al. 2009). According to this literature, the OR_{in} for the land biosphere can range from -0.96 to -1.22, which could considerably alter the modelled O_2 fluctuations resulting from this biosphere exchange, especially in more rural areas where the biosphere tends to dominate as an O_2 source or sink.

7.1.3 Fossil fuel burning

The OR_{in} used for fossil fuel burning may be a larger factor in model uncertainty, especially in urban areas. At first instance, OR_{in} is based on the average OR per SNAP category in the Netherlands (see Section 2.3.2 and Table 1). This is done because of the implementation of CO_2 emissions according to the same SNAP categories in the model setup. The averaging of the fuel mix within the categories results in a small amount of spatial variation in OR_{in} over the domains, and make the modelling of O_2 in theory strictly applicable to the Netherlands only. This is shown in the OR according to the COFFEE dataset in Figure 34d as developed by Steinbach et al. (2011). Steinbach et al. (2011) find more variation in OR_{in}, however, due to the coarse spatial resolution of COFFEE, the dataset is not useful for modelling in urban areas. The OR as presented by Steinbach et al. (2011) could however be useful as model input for the outer domains. The use of source specific information (i.e. what fuel types are used in a certain process at a specific location) is expected to be more reliable model input for OR_{in}. An attempt to implement this is shown in Chapter 6. This method requires very detailed and high resolution information. This makes it challenging to apply, especially on a large scale.

7.1.4 Uncertainties in advection

As mentioned, the modelling of fossil fuel and land biosphere exchange of O_2 is based on CO_2 and OR_{in}. In the comparison of the model results to observations, it is found that the majority of the errors in modelled O_2 fluctuations are also found in the modelled CO_2 con-

centrations. Therefore, improvement in the modelling of compound concentrations in general yield the largest potential for improvement in the modelled O_2 concentrations as well. Statistical measures found in this study for the modelling of CO_2 concentrations are similar to those found by Super et al. (2017). They found that these discrepancies are largely due to faults in the simulation of the wind direction in the model. This is further elaborated on in Chapter 3 of this research. The wind field - and therefore compound concentrations - simulation in the urban areas may be improved on by the introduction of a plume model, as done by Super et al. (2017).

7.1.5 Initial conditions, boundary conditions, and entrainment

The initial and boundary conditions as currently modelled only include ocean O_2 exchange (as following from Rödenbeck et al. (2008), see Section 2.3.3). O_2 exchange though fossil fuel burning and land biosphere processes are thus not included. O_2 fluctuations at the edge of the outer domain may be simulated more accurately, either by integrating atmospheric O_2/N_2 data from Rödenbeck et al. (2008), or by converting CO_2 fluctuations into O_2 fluctuations using a world average value for OR. These are however fluctuations that in the end would not directly contribute to the objective of identifying fossil fuel emission sources in certain urban areas.

The amount of entrainment involved in the O_2 modelling depends on the difference in O_2 concentration between the air within the boundary layer and the air in the free troposphere. Fitting of O_2 data from a forest in the Netherlands to an idealised model resulted in an O_2 jump of 19ppm (Bindels 2018). This is in the same range as the fluctuations from the background concentration found at the currently researched study areas. The O_2 concentration in the free troposphere in first instance depends on the initial and boundary conditions set in the model, which only include ocean exchange. The concentration difference between the air within the boundary layer and the free troposphere is therefore equal to the O_2 fluctuation modelled within the boundary layer at that time, minus fluctuations due to the ocean exchange at the top of the boundary layer.

Research done on the effect of O_2 exchange from the three sources and sinks on the O_2 concentration at various heights and in the free troposphere is limited. Popa (2008) found that the amplitude of the diurnal cycle in O_2 concentration diminished with height, and even becomes

indistinguishable during wintertime. This is based on measurements done over a rural area in Poland, which reached a maximum height of 300 m. Evidence of a diurnal cycle in the free troposphere is thus not found based on this. A seasonal variation in O_2 concentration was more clearly found in the study by Popa (2008). The amplitude again decreases with height. The oceanic contribution of this variation, however, increases with height. This result agrees with research by Van Der Laan et al. (2014), who found a decreased seasonal O_2 cycle at 3000 m height compared to the cycle at 100 m height, with increased importance of the oceanic component with height. At 300 m height, Popa (2008) found the ocean to be responsible for 32 % of the of the seasonal variation, whereas at 3000 m height, Van Der Laan et al. (2014) found the ocean to be responsible for 30 % of the seasonal variation. Based on this, the boundary conditions as in WRF-chem are assumed to cover about 30-32 % of the seasonal variation in O_2 in the free troposphere. The seasonal variation due to other sources and sinks are thus not yet implemented in the model. Even though the lack of sophistication in the modelled initial and boundary conditions - and therefore entrained concentrations - is not expected to have a large influence on the (diurnal) time scale modelled and analysed in this study, it is part of the model that may be improved for future use.

7.2 Recommendations for future analysis

Apart from the potential points of improvement in the modelling of O_2 fluctuations discussed above, there is analysis still to be done on the results that follow from the model as it is. First of, study area Rijnmond was chosen to contribute to the RINGO project (ICOS n.d.) and improve fossil fuel CO_2 estimates. O_2 measurements are planned to start at Zweth (located in Rijnmond) related this project. These measurements are currently not yet being conducted, however, the data that follows from this will be useful to validate the model. Observations at Zweth will not only give insight in the O_2 modelling in the finest horizontal resolution (1x1 km), but will also give insight in the modelling of O_2 in an urban area as opposed to the more rural (coastal) locations which are currently used to validate the model. Furthermore, the O_2 fluctuations that follow from the method using the average OR_{in} per SNAP category (Chapters 4 and 5) and the method using the source specific OR_{in} (Chapter 6) can be compared to measurement values.

O_2 fluctuations as analysed and discussed in this study are limited to surface concentrations only. Super et al. (2017) modelled CO_2 emissions at the surface, as well as stack emissions. Due to variability of the importance of various emission sources with height, the O_2 concentration is also expected to have a vertical gradient subject to these emissions. The O_2 gradients that follow from this are however not shown in the results or further analysed. It was decided not to do this based on the time limit of this research, the fact that there are no O_2 measurements at various heights within the finer domains, and the uncertainties in the entrainment discussed in Section 8.1.5. The latter has an increased influence on modelled concentrations with height.

8 Conclusion

Oxygen is implemented in the regional model WRF-chem, in order to use as a tracer for fossil fuel CO_2 emission sources. Fluctuations in atmospheric O_2 concentration are modelled based on O_2 exchange with the ocean, the land biosphere, and fossil fuel burning. The partitioning of O_2 from these three components shows that fossil fuel burning and exchange with the biosphere are the dominant O_2 sinks during autumn and wintertime (in this case October). The ocean is relatively neglectable in the total O_2 fluctuations on a diurnal time scale as modelled here.

The total O_2 fluctuations are validated using measurements conducted at coastal stations Weybourne in North Norfolk (UK) and Lutjewad in the north of Groningen (NL). The modelled fluctuations at Weybourne follow the trend of the observations well, resulting in a statistical index of agreement of 0.75. The index of agreement at Lutjewad is slightly lower, with a value of 0.71. For Lutjewad, the modelled fluctuations deviate from the observations at times. The cause of this is however uncertain, due to unreliability in the O_2 measurements conducted at this station. Overall, errors in the modelled O_2 fluctuations are also found in the modelled CO_2 concentration to which the O_2 fluctuations are linked. It is found that errors in modelled compound concentrations can be largely attributed to misrepresentation of the wind direction.

Fluctuations in O_2 concentration due to fossil fuel burning (ffO_2) are further analysed for the study areas North Norfolk, the north of Groningen, and Rijnmond. The OR that follows from the ffO_2 and $ffCO_2$ yields information about the source of the $ffCO_2$, which varies spatially as well as a temporally. ffO_2 uptake is mainly found in areas with large amounts of $ffCO_2$ emittance. Through the analysis of the corresponding fossil fuel oxidative ratio (OR_{ff}), distinct $ffCO_2$ sources can be distinguished within these areas. Moreover, the diurnal cycle in OR_{ff} shows the relative importance of emission sources during the day. The OR_{ff} can also yield information about dominant emission sources during specific moments with high CO_2 concentrations (i.e. emission events).

The distinction of actual fuel types (i.e. coal, oil, and gas) are only recognised if the OR_{in} is modelled using source specific information. However, this method requires high resolution information, making the actual implementation challenging on larger scales. Values for source specific OR_{in} are implemented for point sources in Rijnmond. Though this method cannot yet

be validated, it is expected to produce more accurate ffO_2 concentrations with more spatial and temporal variation.

Overall, the modelling of O_2 proofs to contribute to the fossil fuel CO_2 estimate. There is still room for improvement in the modelling of O_2, though the largest potential for improvement is found in the representation of meteorological circumstances and wind direction, affecting all compound concentrations. There is also analysis still to be done on the current model outcomes, mainly in validating the model results in urban areas. O_2 observations at measurement site Zweth (Rijnmond) in the near future will allow for this.

9 Research outlook

This study on modelling oxygen can serve as a contribution to the Readiness of Integrated Carbon Observation (ICOS) for the Necessities of Integrated Global Observations (RINGO) project. The aim of RINGO is to develop ICOS readiness to provide information on fossil fuel emissions. Amongst others, this is attempted through emission estimates for anthropogenic CO_2 and co-emitted tracers, such as CO and NO_2, and independent $^{14}CO_2$-based fossil fuel CO_2 emission estimates. Therefore, $^{14}CO_2$ and other tracers are sampled in test regions Rijnmond, the Rhine Valley, and Paris (Hammer and Levin 2017). In addition, O_2 can be used as a consumed tracer to increase the temporal resolution of the fossil fuel CO_2 estimates. Solid understanding of tracer-to-fossil fuel CO_2 ratios are key to derive reliable fossil fuel CO_2 estimates. The addition of information from emission models such as presented in this study can contribute to the project and provide a framework to interpret the measurements that are to be conducted in the study areas.

References

Bannan, Thomas J. et al. (2017). "Ground and Airborne U.K. Measurements of Nitryl Chloride: An Investigation of the Role of Cl Atom Oxidation at Weybourne Atmospheric Observatory". In: *Journal of Geophysical Research: Atmospheres*, pp. 154–165. ISSN: 21698996. DOI: 10.1002/2017JD026624.

Barningham, T. (2017). "DETECTION AND ATTRIBUTION OF CARBON CYCLE PROCESSES FROM ATMOSPHERIC O2 AND CO 2 MEASUREMENTS AT HALLEY RESEARCH STATION , ANTARCTICA AND AND WEYBOURNE ATMOSPHERIC OBSERVATORY, U.K." PhD thesis.

BEIS (2015). *National Atmospheric Emissions Inventory*. URL: http://naei.beis.gov.uk/data/gis-mapping.

Bindels, Michelle (2018). *To entrain or not to entrain - Modelling forest carbon and oxygen exchange in CLASS*.

Bozhinova, D. et al. (2014). "Simulating the integrated summertime δ14CO2 signature from anthropogenic emissions over Western Europe". In: *Atmospheric Chemistry and Physics* 14.14, pp. 7273–7290. ISSN: 16807324. DOI: 10.5194/acp-14-7273-2014.

Bullock, O. Russell et al. (2014). "An observation-based investigation of nudging in WRF for downscaling surface climate information to 12-km grid spacing". In: *Journal of Applied Meteorology and Climatology* 53.1, pp. 20–33. ISSN: 15588424. DOI: 10.1175/JAMC-D-13-030.1.

Carvalho, David et al. (2012). "A sensitivity study of the WRF model in wind simulation for an area of high wind energy". In: *Environmental Modelling and Software* 33, pp. 23–34. ISSN: 13648152. DOI: 10.1016/j.envsoft.2012.01.019. URL: http://dx.doi.org/10.1016/j.envsoft.2012.01.019.

CBS (2017). *No Title*. Tech. rep. Den Haag/Heerlen: Centraal Bureau voor de Statistiek. URL: http://statline.cbs.nl/Statweb/publication/?DM=SLNL&PA=37230ned&D1=0,17,21&D2=45,65,137,210,255,298,335,379,443,454,524,556&D3=182-193,195-202&HDR=G2&STB=G1,T&VW=T.

Chevillard, A et al. (2002). "Simulation of atmospheric CO 2 over Europe and western Siberia using the regional scale model REMO". In: *Tellus Series B-Chemical And Physical Meteorology*, pp. 872–894. ISSN: 0280-6509. DOI: 10.1034/j.1600-0889.2002.01340.x. URL: http://www.blackwell-synergy.com/doi/abs/10.1034/j.1600-0889.2002.01340.x%5Cnpapers2://publication/uuid/ED812918-A2DF-4081-9291-A033A42F5DB2.

Cook, J. et al. (2013). "Quantifying the consensus on anthropogenic global warming in the scientific literature". In: *Environmental Research Letters* 8.

Daniels, Emma et al. (2016). *Relative impacts of land use and climate change on summer precipitation in the Netherlands*. DOI: 10.5194/hess-20-4129-2016.

Deng, Aijun et al. (2008). "WRF-ARW Analysis nudging update and future development plan". In: 1, pp. 1–8.

Djuricin, Sonja, Diane E. Pataki, and Xiaomei Xu (2010). "A comparison of tracer methods for quantifying CO2 sources in an urban region". In: *Journal of Geophysical Research: Atmospheres* 115.11, pp. 1–13. ISSN: 01480227. DOI: 10.1029/2009JD012236.

Dudhia, Jimy (1989). "Numerical Study of Convection Observed during the Winter Monsoon Experiment Using a Mesoscale Two-Dimensional Model". In: *Journal of the Atmospheric Sciences* 46.20, pp. 3077–3107. ISSN: 0022-4928. DOI: 10.1175/1520-0469(1989)046<3077:NSOCOD>2.0.CO;2. URL: http://journals.ametsoc.org/doi/abs/10.1175/1520-0469%281989%29046%3C3077%3ANSOCOD%3E2.0.CO%3B2.

Ek, M. B. (2003). "Implementation of Noah land surface model advances in the National Centers for Environmental Prediction operational mesoscale Eta model". In: *Journal of Geophysical Research* 108.D22, p. 8851. ISSN: 0148-0227. DOI: 10.1029/2002JD003296. URL: http://doi.wiley.com/10.1029/2002JD003296.

EUROSTAT (2005). "Emission Inventory Guidebook". In: 39.2, S32–S36. ISSN: 02726386. DOI: 10.1053/ajkd.2002.30941.

Gego, E. et al. (2005). "Examination of model predictions at different horizontal grid resolutions". In: *Environmental Fluid Mechanics* 5, pp. 63–85.

Hammer, Samuel and Ingeborg Levin (2017). *14 C and other tracers for fossil fuel CO 2*. URL: http://www.icos-infrastruktur.de/fileadmin/icos/wiss_vers/2017/impulsref/06_Hammer_Levin_ffCO2_ICOS-D_2017.pdf.

Hockaday, C et al. (2009). "Measurement of soil carbon oxidation state and oxidative ratio by 13 C nuclear magnetic resonance w." In: *Journal of Geophysical Research* 114.January, pp. 1–14. ISSN: 0148-0227. DOI: 10.1029/2008JG000803.

Hong, Song-You, Yign Noh, and Jimy Dudhia (2006). "A New Vertical Diffusion Package with an Explicit Treatment of Entrainment Processes". In: *Monthly Weather Review* 134.9, pp. 2318–2341. ISSN: 0027-0644. DOI: 10.1175/MWR3199.1. URL: http://journals.ametsoc.org/doi/abs/10.1175/MWR3199.1.

Huszar, P., M. Belda, and T. Halenka (2016). "On the long-term impact of emissions from central European cities on regional air quality". In: *Atmospheric Chemistry and Physics* 16.3, pp. 1331–1352. ISSN: 16807324. DOI: 10.5194/acp-16-1331-2016.

ICOS. *READINESS OF ICOS FOR NECESSITIES OF INTEGRATED GLOBAL OBSERVATIONS*. URL: https://www.icos-ri.eu/ringo.

IPCC - Intergovernmental Panel on Climate Change (2013). *Climate Change 2013: The Physical Science Basis; Summary for Policy Makers*. Tech. rep.

Jimenez, Pedro A. and Jimy Dudhia (2013). "On the ability of the WRF model to reproduce the surface wind direction over complex terrain". In: *Journal of Applied Meteorology and Climatology* 52.7, pp. 1610–1617. ISSN: 15588424. DOI: 10.1175/JAMC-D-12-0266.1.

Keeling, R. F. (1988). "Measuring correlations between atmospheric oxygen and carbondioxide mole fractions - a preliminary study in urban air". In: *Journal of Atmospheric Chemistry* 7, pp. 153–176.

Keeling, R. F. and A. C. Manning (2014). *Studies of Recent Changes in Atmospheric O2 Content*. 2nd ed. Vol. 5. Elsevier Ltd., pp. 385–404. ISBN: 9780080983004. DOI: 10.1016/

B978-0-08-095975-7.00420-4. URL: http://dx.doi.org/10.1016/B978-0-08-095975-7.00420-4.

Keeling, R. F., A. C. Manning, et al. (1998). "Methods for measuring changes in atmospheric O2 concentration and their application in southern hemisphere airJournal of Geophysical Research-Atmospheres". In: *Journal of Geophysical Research-Atmospheres* 103, pp. 3381–3397.

Keeling, R. F. and S. R. Shertz (1992). "Seasonal and interannual variations in atmospheric oxygen and implications for the global carbon cycle". In: *Nature* 358, pp. 723–727.

Laan, S. van der et al. (2014). "Atmospheric CO2, δ(O2/N2), APO and oxidative ratios from aircraft flask samples over Fyodorovskoye, Western Russia". In: *Atmospheric Environment* 97, pp. 174–181. ISSN: 18732844. DOI: 10.1016/j.atmosenv.2014.08.022.

Le Quéré, Corinne et al. (2016). "Global Carbon Budget 2016". In: *Earth System Science Data* 8.2, pp. 605–649. ISSN: 18663516. DOI: 10.5194/essd-8-605-2016.

Li, Xiangshang et al. (2016). "The impact of observation nudging on simulated meteorology and ozone concentrations during DISCOVER-AQ 2013 Texas campaign". In: *Atmospheric Chemistry and Physics* 16.5, pp. 3127–3144. ISSN: 16807324. DOI: 10.5194/acp-16-3127-2016.

Liu, Yubao et al. (2007). "An "observation-nudging"-based fdda scheme for wrf-arw for mesoscale data assimilation and forecasting". In: *Fourth Symposium on Space Weather*, pp. 1–6. URL: http://ams.confex.com/ams/87ANNUAL/techprogram/paper_118226.htm.

Lopez, M. et al. (2013). "CO, NO<inf>x</inf> and ¹³CO<inf>2</inf> as tracers for fossil fuel CO<inf>2</inf>: Results from a pilot study in Paris during winter 2010". In: *Atmospheric Chemistry and Physics* 13.15. ISSN: 16807316 16807324. DOI: 10.5194/acp-13-7343-2013.

Macpherson, S R, G Deblonde, and J M Aparicio (2008). "Impact of NOAA ground-based GPS observations on the Canadian regional analysis and forecast system". In: *Monthly Weather Review* 136.7, pp. 2727–2746. ISSN: 0027-0644. DOI: 10.1175/2007mwr2263.1.

Manning, A. C. and R. F. Keeling (2006). "Global oceanic and land biotic carbon sinks from the scripps atmospheric oxygen flask sampling network, Tellus, Series B". In: *Chemical and Physical Meteorology* 85, pp. 95–116.

Manning, Andrew C. and Ralph F. Keeling (2006). "Global oceanic and land biotic carbon sinks from the scripps atmospheric oxygen flask sampling network". In: *Tellus, Series B: Chemical and Physical Meteorology* 58.2, pp. 95–116. ISSN: 02806509. DOI: 10.1111/j.1600-0889.2006.00175.x.

Masiello, C. A. et al. (2008). "Evaluating two experimental approaches for measuring ecosystem carbon oxidation state and oxidative ratio". In: *Journal of Geophysical Research: Biogeosciences* 113.3, pp. 1–9. ISSN: 01480227. DOI: 10.1029/2007JG000534.

Mass, C.F. et al. (2002). "Does increasing horizontal resolution produce more skillful forecasts?" In: *Bull. Amer. Meteor. Soc*, pp. 407–430.

Mlawer, Eli J. et al. (1997). "Radiative transfer for inhomogeneous atmospheres: RRTM, a validated correlated-k model for the longwave". In: *Journal of Geophysical Research: At-*

mospheres 102.D14, pp. 16663–16682. ISSN: 01480227. DOI: 10.1029/97JD00237. URL: http://doi.wiley.com/10.1029/97JD00237.

National Centers for Environmental Prediction/National Weather Service/NOAA/U.S (2000). *Department of Commerce: NCEP FNL Operational Model Global Tropospheric Analyses, continuing from July 1999, updated daily, in, Research Data Archive at the National Center for Atmospheric Research, Computational and Information Systems Laboratory*.

Nicole, JF (2010). "International Energy Agency. World Energy Outlook". In:

Olivier, J.G.J. and J.J.M. Berdowski (2001). "Global Emissions Sources and Sinks". In: *The Climate System*, pp. 33–78.

ONS (2016). *Local Authority District population 2016*. URL: https://www.ons.gov.uk/peoplepopulationandcommunity/populationandmigration/populationestimates.

Papanastasiou, D. K., D. Melas, and I. Lissaridis (2010). "Study of wind field under sea breeze conditions; an application of WRF model". In: *Atmospheric Research* 98.1, pp. 102–117. ISSN: 01698095. DOI: 10.1016/j.atmosres.2010.06.005.

Pettersson, Jens (2016). "A Brief Guide to Observation Nudging in WRF". In: 2, pp. 2–5. ISSN: 01416359. DOI: 10.1002/pssb.201300062.

Pickers, Penelope (2016). "New applications of continuous atmospheric O2 measurements : meridional transects across the Atlantic Ocean , and improved quantification of fossil fuel-derived CO2". In: *School of Environmental Sciences*.

Pleim, J.C. et al. (1995). "Sensitivity of ozone to model grid Resolution: part I Application of high-resolution regional acid deposition model". In: *Atmospheric Environment1* 29, pp. 3085–3100.

Popa, von Maria Elena (2008). "Continuous tall tower multispecies measurements in Europe for quantifying and understanding land-atmosphere carbon exchange". In:

PRTR (2015). *Netherlands Pollutant Release & Transfer Register*. URL: http://www.emissieregistratie.nl/.

Pszenny, A A P and R E Larson (1990). "AEROSOL BLACK CARBON AND RADON AS TRACERS FOR AIR MASS ORIGIN OVER THE NORTH ATLANTIC OCEAN". In: 4.2.

Randerson, James T. et al. (2006). "Is carbon within the global terrestrial biosphere becoming more oxidized? Implications for trends in atmospheric O2". In: *Global Change Biology* 12.2, pp. 260–271. ISSN: 13541013. DOI: 10.1111/j.1365-2486.2006.01099.x.

RIVM (2016). *Klimaatmonitor - CO2 uitstoot*. URL: https://klimaatmonitor.databank.nl/dashboard/CO2-Uitstoot/.

Rödenbeck, Christian et al. (2008). "Interannual variability in oceanic biogeochemical processes inferred by inversion of atmospheric O2/N2 and CO2 data". In: *Tellus, Series B: Chemical and Physical Meteorology* 60 B.5, pp. 685–705. ISSN: 02806509. DOI: 10.1111/j.1600-0889.2008.00375.x.

RWE (2016). *Overzicht Centrales Duitsland*. URL: http://www.rwe.com/web/cms/nl/1756472/rwe-generation-se/brandstoffen/overzicht-locaties/duitsland/.

Seibt, U. et al. (2004). "Observations of O2: CO2 exchange ratios during ecosystem gas exchange". In: *Global Biogeochemical Cycles* 18.4, pp. 1–18. ISSN: 08866236. DOI: 10.1029/2004GB002242.

Severinghaus, J. P. (1995). "Studies of the terrestrial O2 and carbon cycles in sand dunes gases and in Biosphere 2, Ph.D. thesis". In: *Columbia University*.

Sirignano, C. et al. (2010). "Atmospheric oxygen and carbon dioxide observations from two European coastal stations 2000–2005: continental influence, trend changes and APO climatology". In: *Atmos. Chem. Phys* 10, pp. 1599–1615. DOI: 10.5194/acp-10-1599-2010.

Skamarock, W. C. et al. (2008). "A description of the Advanced Research WRF version 3, Mesoscale and Microscale Meteorology Division". In: *National Center for Atmospheric Research*.

Steeneveld, G.J., R.J. Ronda, and A.A.M. Holtslag (2014). "The challenge of forecasting the onset and development of radiation fog using mesoscale atmospheric models". In: *Boudary Layer Meteorology* 8.154, pp. 265–289. DOI: 10.1007/s10546-014-9973-8.

Steinbach, J. et al. (2011). "The CO2 release and Oxygen uptake from Fossil Fuel Emission Estimate (COFFEE) dataset: Effects from varying oxidative ratios". In: *Atmospheric Chemistry and Physics*. ISSN: 16807316. DOI: 10.5194/acp-11-6855-2011.

Stephens, B. B. et al. (1998). "Testing global ocean carbon cycle models using measurements of atmospheric O2 and CO2 concentration". In: *Global Biogeochemical Cycles* 12.2, pp. 213–230.

Super, I. et al. (2016). "Interpreting continuous in-situ observations of carbon dioxide and carbon monoxide in the urban port area of Rotterdam". In: *Atmospheric Pollution Research* 8.1, pp. 174–187. ISSN: 13091042. DOI: 10.1016/j.apr.2016.08.008.

— (2017). "Interpreting continuous in-situ observations of carbon dioxide and carbon monoxide in the urban port area of Rotterdam". In: *Atmospheric Pollution Research* 8.1, pp. 174–187. ISSN: 13091042. DOI: 10.1016/j.apr.2016.08.008. URL: http://dx.doi.org/10.1016/j.apr.2016.08.008.

UCAR (2014). *NCEP ADP Global Surface Observational Weather Data*. URL: https://rda.ucar.edu/datasets/ds461.0/index.html#access.

Ucar (2015). *WRF Model Version 3.7: UPDATES*. URL: http://www2.mmm.ucar.edu/wrf/users/wrfv3.7/updates-3.7.html.

Van Der Laan-Luijkx, I. T. et al. (2010). "CO2, δo2/N2 and APO: Observations from the Lutjewad, Mace Head and F3 platform flask sampling network". In: *Atmospheric Chemistry and Physics* 10.21, pp. 10691–10704. ISSN: 16807316. DOI: 10.5194/acp-10-10691-2010.

Van Der Laan-Luijkx, I.T. (2010). "Atmospheric oxygen and the global carbon cycle. Observations from the new F3 North Sea platform monitoring station and 6 additional locations in Europe and Siberia Groningen: s.n." In:

— (2018). *No Title*. Wageningen.

Vickers, Dean, Larry Mahrt, and Edgar L. Andreas (2015). "Formulation of the sea surface friction velocity in terms of the mean wind and bulk stability". In: *Journal of Applied Meteorology and Climatology* 54.3, pp. 691–703. ISSN: 15588432. DOI: 10.1175/JAMC-D-14-0099.1.

Westphal, M. Liu; D.L. (2001). "A study of the sensitivity of simulated mineral dust production to model resolution". In: *Journal of Geophysical Research* 106.18, pp. 99–112.

Willmott, Cj (1982). *Some comments on the evaluation of model performance*. DOI: 10.1175/1520-0477(1982)063<1309:SCOTEO>2.0.CO;2. URL: http://journals.ametsoc.org/doi/abs/10.1175/1520-0477(1982)063%3C1309:SCOTEO%3E2.0.CO;2.

Wilson, Philip (2012). "Insight into the Carbon Cycle from Continuous Measurements of Oxygen and Carbon Dioxide at Weybourne Atmospheric Observatory , UK". In: October.

Worrall, Fred et al. (2013). "Estimating the oxidative ratio of the global terrestrial biosphere carbon". In: *Biogeochemistry* 115.1-3, pp. 23–32. ISSN: 01682563. DOI: 10.1007/s10533-013-9877-6.

Wu, Shiang Yuh et al. (2008). "Modeling atmospheric transport and fate of ammonia in North Carolina-Part I: Evaluation of meteorological and chemical predictions". In: *Atmospheric Environment* 42.14, pp. 3419–3436. ISSN: 13522310. DOI: 10.1016/j.atmosenv.2007.04.031.

Zhang, Q. J. et al. (2015). "Formation of secondary organic aerosol in the Paris pollution plume and its impact on surrounding regions". In: *Atmospheric Chemistry and Physics* 15.24, pp. 13973–13992. ISSN: 16807324. DOI: 10.5194/acp-15-13973-2015.

Zhang, Yang et al. (2006). "A comprehensive performance evaluation of MM5-CMAQ for the Summer 1999 Southern Oxidants Study episode-Part II: Gas and aerosol predictions". In: *Atmospheric Environment* 40.26, pp. 4839–4855. ISSN: 13522310. DOI: 10.1016/j.atmosenv.2005.12.048.

Zondervan, Albert and Harro A J Meijer (1996). "Isotopic characterisation of CO2 sources during regional pollution events using isotopic and radiocarbon analysis". In: *Tellus, Series B: Chemical and Physical Meteorology* 48.4, pp. 601–612. ISSN: 02806509. DOI: 10.1034/j.1600-0889.1996.00013.x.

Appendix I

Table A1: Overview of the model parameterisation settings.

Grid resolution	48x48, 12x12, 4x4, 1x1 km
Boundary-Layer scheme	1: YSU scheme
Surface Layer scheme	1: MM5 Monin-Obukov scheme
Land surface scheme	2: Unified Noah land surface model
Cumulus scheme	3: Grell-Feitas ensemble scheme
Microphysics	4: WSM 5-class scheme
Shortwave radiation	1: Dudhia scheme
Longwave radiation	1: RRTM scheme
Chemical option	15: Ensemble tracer option using individual tracers and an ensemble tracer array
Emission option	15: Emissions analogue to chemical option 15

Table A2: Statistical analysis of wind speed for WRF version 3.2.1 at Rotterdam. The inclusion of all values are compared to daytime average values only as calculated by Super et al. (2017). Terms N, b, d, and R2 are dimensionless, the remaining terms have unit m/s.

Wind speed	$\overline{O}$	$\overline{P}$	sd_O	sd_P	N	a	b	MAE	RMSE	$RMSE_s$	$RMSE_u$	d	R^2
All values	4.7	4.5	2.2	2.0	697	0.84	0.85	0.63	1.5	0.18	1.5	0.87	0.59
Daytime averages by Super et al. (2017)		$\overline{O}$ - 0.1			90			1.2				0.72	

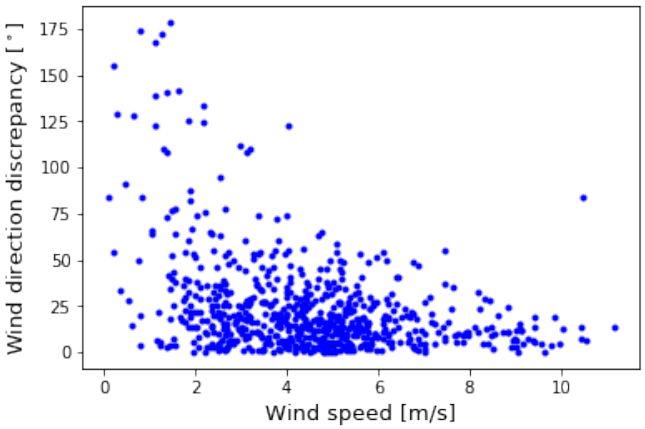

Figure A1: Differences between the modelled and observed wind direction against wind speed for WRF version 3.2.1 at Rotterdam airport. It can be seen that most of the largest discrepancies are simulated along with relatively low wind speeds.

Table A3: Most important quantitative measures of wind direction model performance for the various model versions with and without updates, locations, horizontal resolutions, and nudging as described in Chapter 3. The default settings are WRF-chem version 3.2.1. at Rotterdam with a horizontal resolution of 4x4 km, without nudging applied. Terms d and R^2 are dimensionless, the remaining terms have unit $^\circ$.

version/location/ horizontal resolution/ nudging applied	$\overline{O}$	$\overline{P}$	sd_O	sd_P	N	a	b	MAE	RMSE	$RMSE_s$	$RMSE_u$	d	R^2
Model version comparison													
3.2.1	189	204	63.0	57.0	697	92.3	0.471	32.2	66.3	7.14	65.9	0.685	0.182
3.9.1	190	206	62.3	55.7	721	57.2	0.642	25.2	57.3	7.06	56.9	0.762	0.329
3.9.1 – update	190	202	62.3	51.4	721	61.8	0.632	28.1	57.9	7.06	57.4	0.730	0.271
3.2.1 (u>3 m/s)	197	212	50.6	46.2	526	68.2	0.607	23.0	48.4	8.60	47.5	0.752	0.307
3.9.1 (u>3 m/s)	202	212	50.6	48.4	562	51.0	0.709	17.0	41.2	8.50	40.3	0.827	0.459
3.9.1 – update (u>3 m/s)	205	215	54.2	46.4	416	43.4	0.748	19.9	44.6	10.0	43.4	0.804	0.411
Location comparison													
Rotterdam	189	204	63.0	57.0	697	92.3	0.471	32.2	66.3	7.14	65.9	0.685	0.182
Eindhoven	187	212	58.7	48.4	697	65.2	0.575	36.0	61.1	7.94	60.8	0.673	0.224
Lauwersoog	190	198	63.6	58.1	697	44.8	0.733	26.6	50.4	7.18	49.8	0.820	0.448
Rotterdam (u>3 m/s)	197	212	50.6	46.2	526	68.2	0.607	23.0	48.4	8.60	47.5	0.752	0.307
Eindhoven (u>3 m/s)	190	210	49.3	43.6	612	36.6	0.775	27.6	42.7	7.68	43.9	0.792	0.469
Lauwersoog (u>3 m/s)	190	197	62.3	56.5	681	41.7	0.752	25.5	48.1	7.29	47.5	0.827	0.467
Horizontal resolution comparison													
4x4 km	189	204	63.0	57.0	697	92.3	0.471	32.2	66.3	7.14	65.9	0.685	0.182
1x1 km	189	204	29.4	57.2	697	198	0.0493	39.6	61.9	7.90	61.4	0.382	$9.20e^{-3}$
4x4 km (u>3 m/s)	197	212	50.6	46.2	526	68.2	0.607	23.0	48.4	8.60	47.5	0.752	0.307
1x1 km (u>3 m/s)	197	212	24.5	46.5	548	166	0.200	28.2	43.6	8.92	42.7	0.560	0.145
Nudging option comparison													
Nudging	190	210	57.5	52.3	673	61.3	0.612	28.5	55.6	8.67	43.0	0.739	0.310
Nudging (u>3 m/s)	198	214	51.4	46.2	576	68.1	0.604	26.1	49.8	37.3	31.5	0.739	0.295

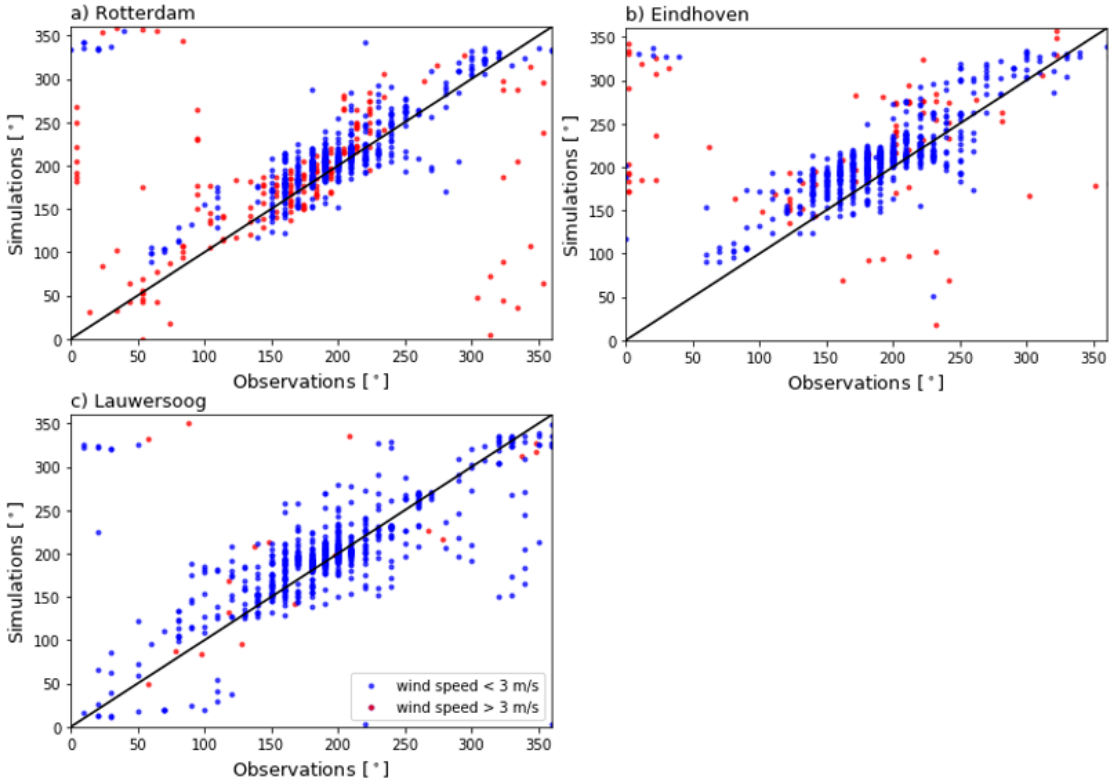

Figure A2: Relation between the simulated and the observed wind direction for WRF model version 3.2.1 at Rotterdam (a) and Lauwersoog (b). Wind directions simulated at wind speeds below 3 m/s are shown in red and directions simulated at wind speeds above 3 m/s are shown in blue. An ideal regression line is shown in black.

Table A4: Most important quantitative measures of O_2, CO_2, and wind direction model performance for the Zweth (Rijnmond), Lutjewad (the north of Groningen), and Weybourne (North Norfolk). Terms d and R^2 are dimensionless, the remaining terms have unit ppm for O_2 and CO_2 and unit $^\circ$ for wind direction.

	$\overline{O}$	$\overline{P}$	sd_O	sd_P	N	a	b	MAE	RMSE	$RMSE_s$	$RMSE_u$	d	R^2
Zweth, Rijnmond													
O_2		204		57.0	697								
CO_2	418	410	15.2	11.4	697	2.32	0.841	5.921	13.5	2.61	12.9	0.697	0.283
Wind direction	189	204	63.0	57.0	697	92.3	0.471	32.2	66.3	7.14	65.9	0.685	0.182
Lutjewad, north of Groningen													
O_2	-16.4	-11.0	14.5	11.3	574	1.94	0.881	6.23	13.5	2.82	13.1	0.714	0.301
CO_2	412	407	12.2	9.42	697	1.63	0.891	5.33	11.5	2.53	10.9	0.712	0.303
Wind direction	190	198	63.6	58.1	697	44.8	0.733	26.6	50.4	7.18	49.8	0.820	0.448
Weybourne, North Norfolk													
O_2	-11.3	-8.3	7.72	6.43	697	1.01	0.913	2.92	6.70	3.03	5.92	0.752	0.344
CO_2	404	405	6.83	6.01	697	0.834	0.943	2.23	5.63	2.12	4.18	0.778	0.381
Wind direction	214	219	58.2	60.3	697	61.8	0.632	28.1	77.8	7.06	74.4	0.471	0.019

Appendix II: WRF-chem O_2 manual

This manual contains information about the changes made to the files and scripts needed to run WRF-chem in order to implement oxygen. An overview of the model runs conducted in this research and the adapted files and scripts corresponding to those runs is given in Table A5.

Table A5: Overview of the files and scripts that were adapted and used in the model runs for method 1 and method 2.

O_2 - average OR_{in}	O_2 - source specific OR_{in}
registry.chem.O2	registry.chem.OR2
emissions_driver.O2.F	emissions_driver.OR2.F
wrf_ibcs_O2_1000ppm.py	wrf_ibcsO21000ppm_OR.py
ibc_O2.ipynb	ibc_O2.ipynb
apo97_v1.5_mix_2014.nc	apo97_v1.5_mix_2014.nc
Chemi_Rijnm.py	Chemi_Rijnm_OR.py
Rijnmond_EI.txt	Rijnmond_EI_OR.txt
MACC_chemi.py	MACC_chemi_OR.py

The runs conducted in this research are based on the WRF-chem model setup as created by Super et al. (2017), covering four domains that zoom in on Rijnmond, the Netherlands. O_2 is added to this setup, resulting in the use of two different methods. In the first method O_2 is calculated based on the average oxidative ratio (OR_{in}) per emission category and the CO_2 emissions from that emission category. In the second method, O_2 is calculated based on the OR_{in} of the actual fuel type used at the emission source and the corresponding CO_2 emissions from that source. More information about the two different methods is given in Section 2.3. The differentiation between the two methods resulted in the following main model runs:

1. O_2 - average OR_{in}
2. O_2 - source specific OR_{in}

In both runs O_2 is added as separate tracers per emission category in registry.chem as follows: `state real e_tracer_xx i+jf emis_ant 1 - i5 "E_O2yyy" "NEG EMISSIONS O2_yyy" "mol km^-2 hr^-1"`, in which xx is the number of the tracer variable and yyy a number corresponding to a certain emission category. The added tracers are then added to: `package etracer_ens emiss_opt==15`. Once the tracers are added to the registry.chem file, O_2 concentrations are calculated in the

emissions_driver.F file. In method 1, this is done as such: `chem(i,k,j,p_tracer_xx) = chem(i,k,j,p_tracer_xx) + emis_ant(i,k,j,p_e_tracer_zz) * conv * OR_in * RME1(MNTH) * RWE1(DAYW) * RDE1(HR)`. In this, zz is the number of the CO_2 tracer corresponding to the same emission category as the O_2 tracer_xx. OR_{in} can be replaced by the value for the average OR_{in} corresponding to the emission category to which tracer_xx corresponds. The value for OR_{in} is negative, however, this would result in a negative value for tracer_xx as well. Negative concentrations can however not be modelled in WRF-chem. Therefore, the separate O_2 tracers are modelled as positive which are subtracted in the final calculation of the total O_2. The background concentration of the total O_2 is then set to a value of 1000 ppm. This is done in the wrf_ibcs.py script, which writes the initial and boundary conditions for the tracers in the wrfinput and wrfbdy files. Other tracers are set to 0 ppm, whereas O_2 is set to 1000 ppm. This value is later subtracted in analysis. In order to model ocean exchange, APO data by Rödenbeck et al. (2008) is added to the initial and boundary conditions. The data is imported from the apo97_v1.5_mix_2014.nc file, and is used in both model runs. In method 2, the values for OR_{in} are added as an extra tracer in the registry.chem file: `state real e_tracer_OR i+jf emis_ant 1 - i5 "OR" "oxidative ratio" "O2/CO2 [-]"`. Again, this tracer is also added to `package etracer_ens emiss_opt==15`. In the emissions_driver.F file, concentrations per tracer are now calculated as: `chem(i,k,j,p_tracer_xx) = chem(i,k,j,p_tracer_xx) + emis_ant(i,k,j,p_e_tracer_zz) * conv * (emis_ant(i,k,j,p_e_tracer_OR)) * RME1(MNTH) * RWE1(DAYW) * RDE1(HR)`. The actual values for OR_{in} are added to Rijnmond_EI.txt, and loaded to the wrf_chemi files for domain 4 using Chemi_Rijnm.py.